12-2012

DEVELOPMENT OF A BEAM-SPECIFIC PLANNING TARGET VOLUME AND A ROBUST PLAN ANALYSIS TOOL FOR PROTON THERAPY

Peter Park

DEVELOPMENT OF A BEAM-SPECIFIC PLANNING TARGET VOLUME AND A ROBUST PLAN ANALYSIS TOOL FOR PROTON THERAPY

by

Peter C. Park, B.S.

APPROVED:

_____
X. Ronald Zhu, Ph.D.
Supervisory Professor

_____
Lei Dong, Ph.D.

_____
Narayan Sahoo, Ph.D.

_____
Laurence E. Court, Ph.D.

_____
Susan L. Tucker, Ph.D.

_____
Andrew K. Lee, M.D.

APPROVED:

_____
Dean, The University of Texas Graduate School of Biomedical Sciences at Houston

DEVELOPMENT OF BEAM-SPECIFIC PLANNING TARGET VOLUME AND ROBUST PLAN ANALYSIS TOOL FOR PROTON THERAPY

A

DISSERTATION

Presented to the Faculty of
The University of Texas Health Science Center at Houston

and

The University of Texas M.D. Anderson Cancer Center
Graduate School of Biomedical Sciences

In Partial Fulfillment
of the Requirements for the Degree of

DOCTOR OF PHILOSOPHY

by

Peter C. Park, B.S.

Houston, Texas

December, 2012

DEDICATIONS

I would like to dedicate this work to: my wife, Yi-Pei Chen, for her support and encouragement, my mother and father, for the never-ending sacrifice for her sons and a daughter, and my son, Ron Park, for making everything worthwhile.

ACKNOWLEDGEMENTS

This research was supported financially by grant PO1CA021239 from the National Cancer Institute.

I would like to express my sincere gratitude to:

- Dr. X. Ronald Zhu, for taking the role of supervisory committee chair after Dr. Lei Dong accepted a new position at Scripps. I am truly grateful for his kindness of including me in many exciting discussions and projects at the Houston Proton Therapy Center. It's been a real privilege studying under him.
- My supervisory committee members, Dr. Narayan Sahoo, for providing me with in-depth discussions of physics, Dr. Susan Tucker, for advice related to statistics, Dr. Andrew Lee, for useful clinical discussions, and Dr. Laurence Court, for steering and guiding many research projects and developments.
- Computational scientist, Dr.Lifei (Joy) Zhang, for helping me in coding and packaging the software. She went the extra mile to help me succeeded in this research.
- Fellow students, Dr. Yoshikazu (Yoshi) Tsunashima, Joey Cheung, Henry Yu, Adam Yock, Luke Hunter, Dr. Adam Melancon, Dr. Ming Yang, Jason Matney, and Yi-Pei Chen for many helpful collaborations.
- PO1 Grant project leader Dr. Radhe Mohan for pioneering the basis of this dissertation work and Dr. Wei Liu for providing me with in-depth physics discussion.
- Tutorial mentor, Dr. TinsuPan, for his encouragements and advice.

- Most importantly, I would like to thank Dr. Lei Dong, for his kind guidance and teaching and for helping me stay on track with this research. His mentorship has been the greatest source of my success during my doctoral study. His time and effort in editing my writing, providing well thought out criticisms and encouragements became the integral part of this work. Dr. Dong has been a mentor who is respectful, responsible, and caring for his students and has set an exemplary model for me to follow.

ABSTRACT

DEVELOPMENT OF A BEAM-SPECIFIC PLANNING TARGET VOLUME AND A ROBUST PLAN ANALYSIS TOOLS FOR PROTON THERAPY

Publication No._____

Peter C. Park, B.S.

Supervisory Professor: X. Ronald Zhu, Ph.D

Proton therapy is growing increasingly popular due to its superior dose characteristics compared to conventional photon therapy. Protons travel a finite range in the patient body and stop, thereby delivering no dose beyond their range. However, because the range of a proton beam is heavily dependent on the tissue density along its beam path, uncertainties in patient setup position and inherent range calculation can degrade thedose distribution significantly. Despite these challenges that are unique to proton therapy, current management of the uncertainties during treatment planning of proton therapy has been similar to that of conventional photon therapy. **The goal of this dissertation research was to develop a treatment planning method and a planevaluation method that address proton-specific issues regarding setup and range uncertainties.**

Treatment plan designing method adapted to proton therapy: Currently, for proton therapy using a scanning beam delivery system, setup uncertainties are largely accounted for by geometrically expanding a clinical target volume (CTV) to a planning

target volume (PTV). However, a PTV alone cannot adequately account for range uncertainties coupled to misaligned patient anatomy in the beam path since it does not account for the change in tissue density. In order to remedy this problem, we proposed a beam-specific PTV (bsPTV) that accounts for the change in tissue density along the beam path due to the uncertainties. Our proposed method was successfully implemented, and its superiority over the conventional PTV was shown through a controlled experiment.. Furthermore, we have shown that the bsPTV concept can be incorporated into beam angle optimization for better target coverage and normal tissue sparing for a selected lung cancer patient.

Treatment plan evaluation method adapted to proton therapy: The dose-volume histogram of the clinical target volume (CTV) or any other volumes of interest at the time of planning does not represent the most probable dosimetric outcome of a given plan as it does not include the uncertainties mentioned earlier. Currently, the PTV is used as a surrogate of the CTV's worst case scenario for target dose estimation. However, because proton dose distributions are subject to change under these uncertainties, the validity of the PTV analysis method is questionable. In order to remedy this problem, we proposed the use of statistical parameters to quantify uncertainties on both the dose-volume histogram and dose distribution directly. The robust plan analysis tool was successfully implemented to compute both the expectation value and its standard deviation of dosimetric parameters of a treatment plan under the uncertainties. For 15 lung cancer patients, the proposed method was used to quantify the dosimetric difference between the nominal situation and its expected value under the uncertainties.

TABLE OF CONTENTS

Acknowledgements ..... **iv**

Abstract ..... **vi**

Table of Content ..... **viii**

List of Figures ..... **xi**

List of Tables ..... **xvi**

Chapter 1. Introduction to Proton Therapy and Its Uncertainties **1**

A. Background 1

B. Objectives 19

C. Hypotheses 20

D. Specific Aims 20

Chapter 2. Beam-Specific Planning Target Volume **21**

A. Introduction 21

B. Methods 23

C. Results 30

D. Discussion 33

E. Conclusion 36

F. Appendix 36

Chapter 3.Application of Beam-Specific PTV in Beam Angle Optimization **40**

A. Introduction 40

B. Methods 46

C. Results 47

D. Discussion 53

E. Conclusion 53

Chapter 4.Fast Proton Dose Approximation for Robust Plan Evaluation..... 55

A. Introduction 55

B. Methods 57

C. Results 61

D. Discussion 68

E. Conclusion 70

Chapter 5.Statistical Robust Plan Evaluation..... 71

A. Introduction 71

B. Methods 73

C. Results 78

D. Discussion 85

E. Conclusion..... 90

Chapter 6. Plan Robustness Comparison: Proton Therapy vs. IMRT 91

A. Introduction 91

B. Methods 92

C. Results 96

D. Discussion 102

E. Conclusion 102

Chapter 7. Conclusion of Dissertation **103**

A. Conclusion of Hypothesis 1 103

B. Conclusion of Hypothesis 2 104

References **105**

Vita **122**

LIST OF FIGURES

Chapter 1: Introduction to proton therapy and its uncertainties

Figure 1-1 A concept art of the depth dose profile of a proton pencil beam …….1

Figure 1-2 SOBP formation using many Bragg peaks ……...……6

Figure 1-3 An example of range modulator wheel …….6

Figure 1-4 A concept art of beam specific hardware ……..8

Figure 1-5 A relative stopping power ratio to CT HU calibration curve ……..…10

Figure 1-6 The effect of setup error on proton dose distribution in lung tissue …..…14

Figure 1-7 Schematic of geometrical target volume expansions …….16

Figure 1-8 An aperture and a compensator ……..17

Chapter 2: Beam-specific planning target volume

Figure 2-1 Comparing dose distribution under breathing phase between IMRT and proton therapy ……22

Figure 2-2 A schematic illustration of the method used to calculate the range matrix and relevant margin of a ray ……25

Figure 2-3 An illustration of the four essential steps in creating the bsPTV from a CTV ……26

Figure 2-4 Final implementation of bsPTV software ……28

Figure 2-5 Dose distributions when conforming dose to the CTV (inner circular contour) using plans based on the PTV and bsPTV ……30

Figure 2-6 The minimum percentage ofprescribeddoseto the CTV comparison between bsPTV and PTV ……32

Figure 2-7 Clinical example of bsPTV in a prostate and a lung case ……..34

Figure 2-8 The DVHs of the CTV under simulated setup error and motion ……..35

Chapter 3: Application of Beam-Specific PTV to Beam Angle Optimization

Figure 3-1 An example of typical field arrangement for IMRT and proton therapy of lung cancer ……41

Figure 3-2 Proximal dose as a function of target depth and varying width of SOBP ...43

Figure 3-3 An example of bsPTV for the selected beam angle ……44

Figure 3-4 A comparison between the bsPTV and planned dose distribution …….45

Figure 3-5 bsPTVs for different beam angles computed to account for 5mm setup and 3% inherent range uncertainties ……48

Figure 3-6 Figure of merit showing the variation of the volume of bsPTV over the span of beam angles ……...……49

Figure 3-7 The volume of intersection and the volume of union of two bsPTVs are shown for a few selected beam angle configurations ……...….50

Figure 3-8 The color map of values representing linear sum of the volume intersection and the volume of union of a bsPTV pair ……..51

Figure 3-9 A comparison of dose distribution of the clinical plan and the beam angle optimized plan ……..52

Figure 3-10 The resulted DVHs of clinical plan (solid line) and optimized plan ….52

Chapter 4: Fast proton dose approximation for robust plan evaluation

Figure 4-1 An oval shaped heterogeneity was inserted in the beam path to simulate anatomical changes ……57

Figure 4-2 The dose distributions for the lung case ……...63

Figure 4-3 The percent dose difference map on the lung week6 CT between dose distribution using full calculation and dose distribution using static dose approximation, and range corrected approximation ……64

Figure 4-4 A comparison of the dose calculation results in the presence of inter-fraction anatomical changes ……66

Figure 4-5 The cDVHs of the CTV and other organs at risks ……67

Chapter 5: Statistical robust plan evaluation

Figure 5-1 A selected case was pre-evaluated to determine the appropriate number of courses andfractions ……76

Figure 5-2 The scattered plot of randomly generated random and systematic setup error shift points and randomly generated systematic range error calibration curves..…...77

Figure 5-3 Overall robustness of the treatment plan under uncertainty visualized with DVH color bands ……...79

Figure 5-4 See the legend from figure 4-3. Shown here are the two lungs ……80

Figure 5-5 See the legend from figure 4-3. Shown here are the esophagus, spinal cord, and heart ……81

Figure 5-6 The effect of uncertainties on the planning parameters (i.e., constraints) visualized using box plots ……..82

Figure 5-7 Dose distribution under the nominal setting and the probability map of risk of the ITV ……..…85

Figure 5-8 The ICTV coverage difference between the nominal plan and its expectation value under uncertaintieswas plotted against the original PTV coverage… ……...87

Figure 5-9 Nominal dose distribution of a two-field IMPT plan in which the CTV is adjacent to the brainstem ……...89

Chapter 6: Plan robustness comparison: proton therapy vs. IMRT

Figure 6-1 Schematics of patient simulation method. Both IMRT and proton plans were created and approved for a selected patient ……95

Figure 6-2 The target coverage in terms of percent volume of PTV and ITV receiving the prescription dose of 74Gy under nominal setting ……97

Figure 6-3 Comparison of the boxplot of the difference in ITV V74Gy coverage between the nominal setting and its expectation value sampled from over 600 dose approximations of all 15 patients ……98

Figure 6-4 See the legend of figure 6-3. Shown here is for Lung V20Gy ……98

Figure 6-5 See the legend of figure 6-3. Shown here is for Lung MLDGy ……...99

Figure 6-6 See the legend of figure 6-3. Shown here is for Esophagus V65Gy ……99

Figure 6-7 See the legend of figure 6-3. Shown here is for Esophagus V45Gy…100

Figure 6-8 See the legend of figure 6-3. Shown here is for Heart V30Gy …….100

Figure 6-9 See the legend of figure 6-3. Shown here is for max Spinal cord dose …101

LIST OF TABLES

Chapter 1: Introduction to proton therapy and its uncertainties

Table 1-1 Proton therapy facilities as in the United States ……2

Table 1-2 Sources of error contributing to the inherent proton range uncertainty ..…12

Table 1-3 A summary of systematic and random setup errors reported in recent studies ……13

Chapter 4: Statistical robust plan evaluation

Table 4-1 The measured volume change of the target volumes of interest observed in the weekly CT images for the lung case ……62

Table 4-2 The result of the 3D gamma analysis on both the ranged-corrected approximation and static dose approximation with respect to the full dose (TPS) calculation under setup error and weekly CT simulations ……..65

Table 4-3 The root mean square (RMS) deviations between the cumulative DVHs derived using a full dose (TPS) calculation and range-corrected dose approximation method under various simulations ……..…68

Chapter 5: Fast proton dose approximation for robust plan evaluation

Table 5-1 Statistical Analysis of Plan Robustness on 15 Lung Cancer Proton Treatment Plans ……84

CHAPTER I: INTRODUCTION TO PROTON THERAPY AND ITS UNCERTAINTIES

A. Background

A.1. Introduction to proton therapy

The concept of treating a tumor using protons was first proposed by Robert R. Wilson at the Harvard Cyclotron Laboratory in 1946 (1). Wilson pointed out that because of the relatively heavier mass of a proton, its track in tissue would be straighter than an electron and its finite range could be utilized to deliver most of its dose at the end of the range. This would produce a clinically desired dose distribution. The depth dose curve of mono-energetic protons is often described using the Bragg curve. When protons interact with a medium, it deposits relatively low dose in the entrance region; however, as it reaches the end of its range, a substantial amount of dose is deposited before the dose quickly falls to zero. (See figure 1-1).

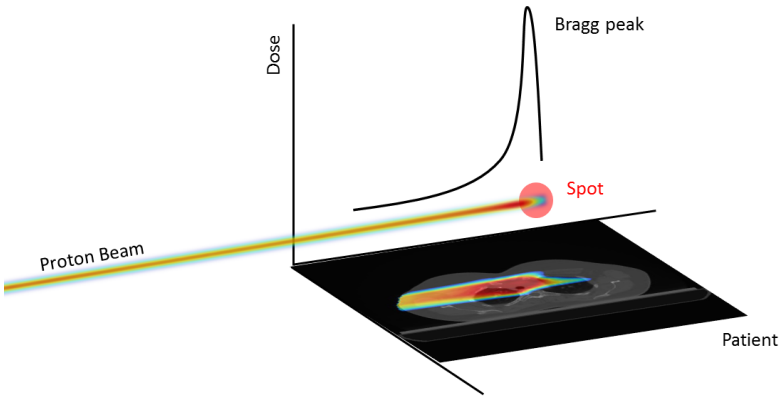

Figure 1-1 Concept art depicting the depth dose profile of a proton pencil beam (the Bragg curve). The Bragg curve shows a relatively low entrance dose and reaches its maximum dose at the end of its range (the Bragg peak).

Soon after Wilson's proposal, the first proton patient was treated in 1950 (2). Following this, the clinical use of protons began to spread across the high energy physics facilities (3). With the advancement of technology in manufacturing particle accelerators, hospital-based proton therapy facilities began to be implemented in the early 1990s (4). Since then, the number of hospital-based proton therapy facilities in the world grew exponentially. As of 2012, there are 33 proton facilities world-wide and 10 proton facilities in the United States with many more facilities planned to be in operation soon (5).

Table 1-1 Proton therapy facilities as in the United States:

Institution	Location	Start Year
Loma Linda	CA	1990
Indiana University	IN	2004
Massachusetts General Hospital	MA	2001
MD Anderson Cancer Center, Houston	TX	2006
University of Florida Proton Therapy Institute	FL	2006
ProCure, OK	OK	2009
University of Pennsylvania	PA	2010
Procure/Central Dupage Hospital	IL	2010
Hampton University	VA	2010
ProCure, NJ	NJ	2012
ProCure, WA	WA	Planned (2013)
St. Jude Children's Research Hospital	TN	Planned (2015)
Provision Center for Proton Therapy	TN	Planned (2014)
MD Anderson Cancer Center, Orlando	FL	Planned (2014)
Barnes Jewish Hospital	MO	Planned (2013)
University Hospital Case Medical Center	OH	Planned (2014)
Scripps Health	CA	Planned (2013)
Mayo Clinics	AZ	Planned (2014)
Mayo Clinics	MN	Planned (2014)
Mclaren Health Care	MI	Planned (2013)

*This list is not exhaustive.

Unlike photons, protons are charged particles that interact with matter through Coulomb electric force with the electrons and nucleus of the medium they traverse. Protons with high kinetic energy (i.e. 100 MeV or higher) may undergo nuclear interactions with contribution of up to 5%of the total dose on the proximal region of the Bragg curve and up to 1% at the distal end (6). The energy of protons passing through the medium is lost through successive collisions by transferring fractions of its initial kinetic energy until it loses all of its initial energy. The expectation value of the rate of energy loss per unit path length x is called stopping power $\left(\frac{dE}{dx}\right)$ and has units of $\left[\frac{MeV}{cm}\right]$. In general, the stopping power of protons depends on the electron density and mean-excitation energy of the medium and the velocity of the protons. The relativistic description of the stopping power is given by the Bethe formula:

$$-\frac{dE}{dx} = \frac{4\pi}{m_p c^2} \cdot \frac{ne^2}{\beta^2} \cdot \left(\frac{e^2}{4\pi\varepsilon_o}\right)^2 \left[ln\left(\frac{2m_p c^2 \beta^2}{I(1-\beta^2)}\right) - \beta^2\right] \qquad \text{(Eq.1)}$$

where, β is the fraction of proton's velocity over the constant speed of light, E is the energy of the proton, x is the distance travelled by the proton, e is the charge of the proton, m_p is the rest mass of the proton, n is the electron density of the medium, I is mean excitation potential of the medium, and ε_o is the permittivity. The shape of the Bragg curve (i.e. sharp increase in dose at the end of range) is a consequence of the fact that the stopping power is inversely proportional to the 2nd power of velocity of protons ($\propto \beta^{-2} = \left(\frac{c}{v}\right)^2$) (7). The precise value of stopping powers for various tissue materials is of significant value to proton therapy as it is closely related to the proton range. It should be noted that the range of protons is a stochastic quantity. The precise range of

each proton in a beam of mono-energetic protons is not easy to determine and is not necessary for the purpose of radiation therapy. However, the mean path length of the proton beam must be precisely determined in order to place the Bragg peak at the intended position within the patient. The range of the proton beam can be formally defined as the expectation value of path length of protons of same initial energy. In practice, the range of protons of a mono-energetic beam is closely approximated using the continuously slowing down approximation (CSDA), which assumes the rate of energy loss at every point along the track is equal to the total stopping power. The range based on CDSA (R_{CSDA}) can be computed as follows:

$$R_{CSDA} = \int_0^{T_o} \left(\frac{dE}{\rho\, dx}\right)^{-1} dE \qquad \text{(Eq.2)}$$

where ρ is the density of medium and T_o is the initial energy of the protons. The expected difference between the formal definition of proton range and R_{CSDA} is less than 0.2% for protons. For practical purposes of dose calculation and other uses, the formal definition of proton range is replaced by the R_{CSDA} (8).

The theoretical advantage of having the depth dose profile of Bragg curve is that when protons are precisely targeted to a tumor, it delivers majority of its dose to the tumor while sparing normal tissue proximal to the target and delivers no dose beyond the target. However, a single Bragg curve cannot cover a typical target size. In order to deliver a uniform dose to a large target volume, the range of protons are modulated to smear the Bragg peak in the depth direction just enough to cover the extent of the target width (9). This so called the spread-out Bragg peak (SOBP) is simply the sum of many mono-energetic Bragg peaks of different energies and intensities entering patient body

(See figure 1-2). There are two distinct types of beam delivery methods in proton therapy: passively-scattered beam and active-scanning beam. For passively-scattered beam delivery, the proton beam is broadened laterally using a scattering system and the SOBP can be obtained by employing a device called a range modulator wheel (RMW) (See figure 1-3). Protons with the maximum energy required to penetrate the maximum depth are forced to pass through the rotating RMW, which has varying segment thickness, thereby pulling some of the protons range proximally (10). For active-scanning beam delivery, magnets are used to steer a narrow proton beam laterally and the SOBP can be obtained by varying the initial energy of protons exiting accelerator directly (11). The details of the difference between passively-scattered and active-scanning beam delivery methods will be discussed in section A.3.Regardless of the beam delivery method, it is of great importance in proton therapy to precisely place the SOBP on a target. Particularly the distal fall off of SOBP must conform to the distal surface of the target to deliver intended dose and to ensure no unnecessary dose is delivered beyond the target. The advantage of protons having a sharp distal fall off dose profile can also be a problem since it is less forgiving when the range of proton beam does not match the range of the distal target volume. Many uncertainties exist related to the proton beam delivery process that needs to be taken into account and evaluated carefully in order to achieve the desired clinical outcomes.

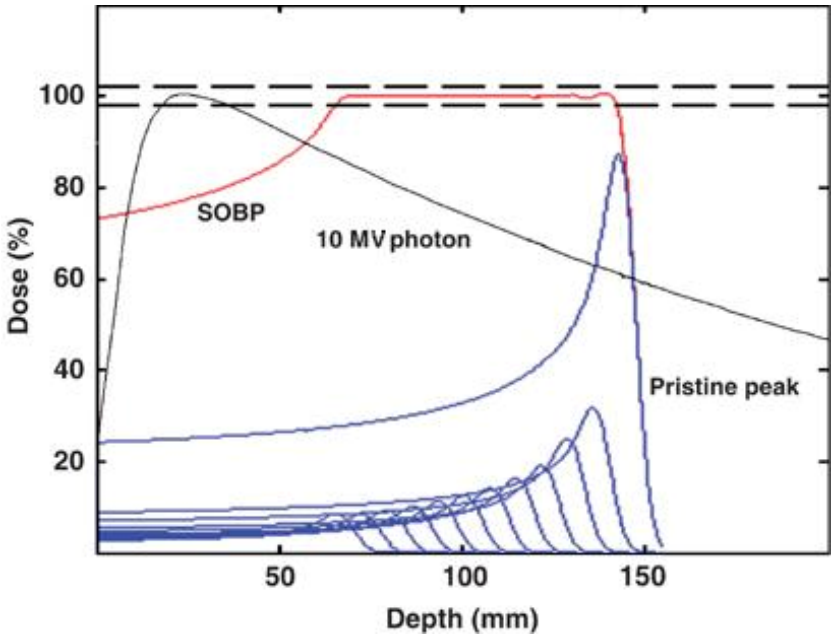

Figure 1-2 SOBP (red) is simply the sum of many mono-exegetic Bragg peaks (blue). Due to the summation of proximal dose from many Bragg peaks, the entrance dose given by the SOBP is significantly higher than a pristine peak. However, the comparison with the depth dose profile of 10MV photon (black) still shows the clear advantage of proton beams.

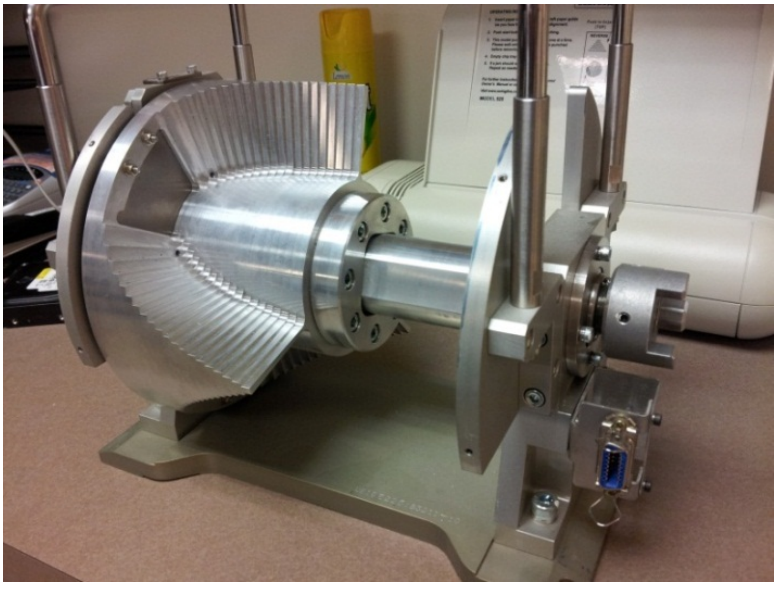

Figure 1-3 An example of a range modulator wheel (RMW) for passively-scattered proton therapy.

A.2. Source of uncertainties in proton therapy

Radiotherapy is a complicated process involving many procedures ranging from delineation of the target volume to beam delivery on the treatment couch. Each of these procedures carries sources of uncertainty. The most prominent sources of uncertainty are from target delineation (12), geometric miss of the target due to patient setup and internal motion error (13, 14), anatomical deformation due to tumor shape change and patient weight loss (15), and the inability to calculate and deliver dose accurately (16). All of these sources of uncertainty are common in all types of external beam radiotherapy. However, the impact of these uncertainties on the delivered dose distribution to a patient is likely to be greater for proton therapy than conventional photon therapy for two major reasons. First, as discussed earlier, the chief advantage of proton therapy is its ability to conform to the target closely. However, this also means that it is less forgiving if the target is missed. Secondly, the range of protons heavily depends on the density of the medium it traverses. Any errors that alter the tissue density of patient with respect to the original setting can significantly deteriorate the intended dose distribution because the range of proton is a function of the stopping power ratio of the tissue it travels through (17). Understanding and reducing each of these uncertainties are the major forefronts of current research effort in the medical physics community. In this research, our focus will be limited to using existing knowledge to deal with setup and proton range uncertainties practically.

A.2.1 Range uncertainty

In order to fully utilize the advantage of proton therapy, a precise determination of the required proton range to the target is crucial. The proton range in any medium can be converted to its equivalent range in water. For the convenience of relating proton ranges in different materials, and because most of beam commissioning data collection is done in water, it is useful to speak of the proton range as water-equivalent thickness (WET). For example, protons with same initial energy will have different ranges in materials of different densities but their WET will be the same. Once the WET is calculated, the initial energy of protons required to penetrate the depth of a target can be determined. To calculate WET, we need to know all of the materials that the proton beam passes through in order to reach the required depth in the patient (see figure 1-4). Depending on the beam delivery method, the correct combination of beam modifying devices such as RMW, aperture, compensator and energy absorber of known density needs to be included.

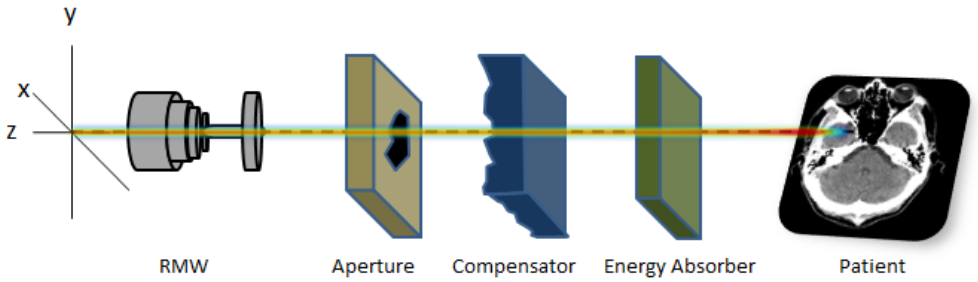

Figure 1-4 The initial energy of proton beam or WET is calculated based on the depth required to penetrate the beam modifying devices and patient tissue density.

A WET corresponding to a specific line segment that extends from a source to a specific point in a target volume can be calculated from a line integral of relative stopping power ratio (rsp) (18) as follow:

$$WET_{x,y} = \int_{Source}^{Depth} rsp\ (x, y, z)dz \qquad \text{(Eq.3)}$$

where the $rsp(x, y, z)$ is defined by:

$$rsp(x, y, z) = \frac{\rho_m}{\rho_w}\frac{\bar{S}_m}{\bar{S}_w}\Big|_{x,y,z} \qquad \text{(Eq.4)}$$

with ρ_m, ρ_w are the mass density and $\bar{S}_m$, $\bar{S}_w$are the mean proton mass stopping power at (x, y, z) of the medium and water respectively (19). In order to determine the rsp of a given medium at a particular point in space, it is necessary to determine $\bar{S}$. In theory, $\bar{S}$ can be derived using the Bethe formula (Eq.1) if the complete information regarding the material's electron density, elemental composition, and mean excitation energy are known. However, currently there is no straight forward way to obtain this information for any given tissue element in the patient. In practice, for the purpose of treatment planning and dose calculation, the rsp of the patient body is approximated from the patient's planning CT images by using a calibration curve that establishes a one-to-one relationship between CT Hounsfield Unit (HU) numbers to the rsp (See figure 1-5).

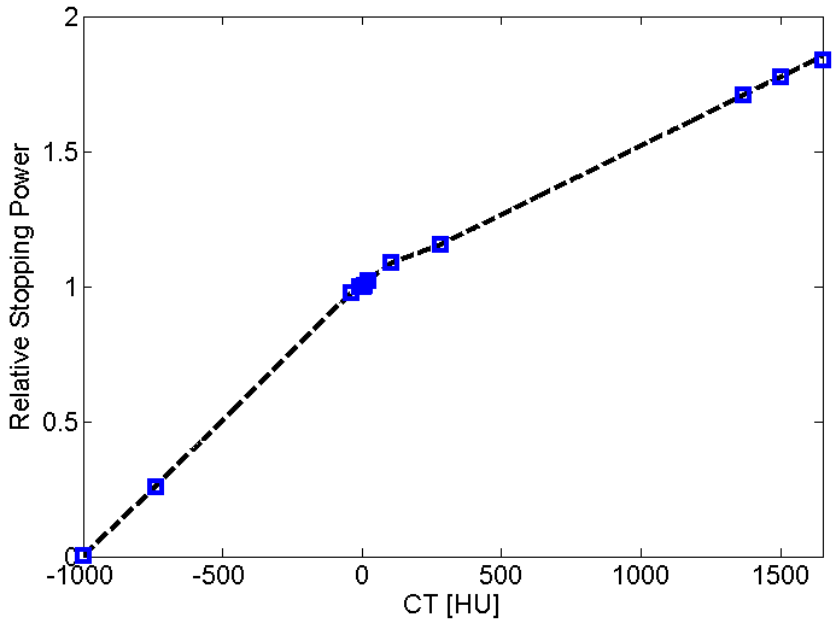

Figure 1-5 An example of calibration curve that maps CT HU numbers to relative stopping power ratio (rsp) of a planning CT images.

The CT HU number is defined as:

$$HU = \frac{\overline{\mu_m} - \overline{\mu_w}}{\overline{\mu_w}} \times 1000 \qquad \text{(Eq.5)}$$

where $\overline{\mu_m}$ and $\overline{\mu_w}$ are the mean photon linear attenuation coefficients of the medium and water averaged over the x-ray spectrum of CT. $\overline{\mu_m}$ is in turn a function of electron density (ρ_e) and effective atomic numbers of the material ($\tilde{z}$ for photo electric interaction and $\hat{z}$ for coherent scattering). For example, Schneider *et al* 1997 suggested following model to be used:

$$\overline{\mu_m} = \rho_e(K^{ph}\tilde{z}^{3.62} + K^{coh}\hat{z}^{1.86} + K^{KN}) \qquad \text{(Eq.6)}$$

where$K^{ph}, K^{ph}, and\ K^{ph}$are constants describing the photoelectric interaction, coherent scattering, and Compton scattering (20). The most widely used method of generating a calibration curve is called the stoichiometric method proposed by Schneider *et al* in 1996 (21). In this stoichiometric method, CT HU number of selected tissue human substitutes are calculated based on CT HU modeling parameters (i.e. rather than directly measuring them) that are uniquely determined for the CT scanner. Although both CT HU number and the rsp are predominantly governed by the electron density of the material, from Eq.2 it is clear that there are other variables governing the value of rsp that are missing from Eq.6. This results in degeneracy of the rsp values for a given CT HU number. In other words, human tissues with different proton stopping power can have the same CT HU number. Furthermore, there are many uncertainties in the values used to model or calculate both the rsp and the CT HU numbers of human tissue substitutes, resulting in overall inherent uncertainty in our ability to calculate the proton range in the patient (22).

Recently, Yang*et al.* (23) performed a comprehensive uncertainty analysis of calibration curves generated using the stoichiometric method and found that the uncertainties in rsp values for different tissue type ranges from 5%, 1.6%, and 2.4% for lung-like, soft, and bone-like tissues. In this study, the authors concluded that when considering a typical patient of mixed tissue types, the overall proton range error is 3.0-3.4% (See Table 1-2). In this work, we will assume that most of all range error due to the inherent uncertainties in the calibration curve to be within 3% to 3.5% of the total proton range in WET.

Table 1-2 Sources of error contributing to the inherent proton range uncertainty.

Sources of error	Lung (%)	Soft (%)	Bone (%)
CT Image	3.3	0.6	1.5
Stoichiometric Formulation	3.8	0.8	0.5
Tissue composition data	0.2	1.2	1.6
Mean excitation energies	0.2	0.2	0.6
Energy spectra of scanner	0.2	0.2	0.4
Total (RMS)	5	1.6	2.4
Total (RMS) for composite tissue	**3.0-3.4**		

A.2.2 Setup uncertainty

Another type of uncertainty that will be considered in this research is setup uncertainty. Patient setup error results in a geographic miss of some fraction of the target volume that can occur during registration of the external surface markers attached to the patient or during registration of soft-tissue or bony landmark under image-guidance. During the treatment planning process, the beam's isocenter is defined relative tothe position of the target volume. Based on this geographical configuration, the beam is shaped and dose distribution is optimized. Therefore, it is crucial that the position of the target volume remains identical throughout the course of a multi-fractionated treatment (24). Setup error can be divided into two sub-categories: systematic and random setup error. In this work, a systematic setup error is defined as the error that is committed during treatment simulation and therefore gets carried over the entire course of a multi-fractionated treatment. Some examples of sources of systematic changes include a change in landmark position in patient, change in treatment room, and change in patient positioning devices. Random setup error,

however, is not committed consistently over the course of treatment, but its value varies from fraction-to-fraction. Because of this, random error cannot be avoided as it is similar to the natural uncertainty that arises from repeated measurements. However, random setup errors can be minimized by implementing processes to ensure a more consistent setup in between fractions. In general, the magnitude of setup error depends on many factors such as the image-guidance modality in use (25), treatment site (26), patient positioning device (27), and other human errors. In recent years, researchers have reported both systematic and random errors that are measured using kV-radiograph using onboard imaging system and kV cone-beam CT (kV-CBCT) (See Table 1-3). Overall, the average systematic and random errors reported are roughly 2mm (27, 28, 29, 30).

Table 1-3 A summary of systematic and random setup errors reported in recent studies. Because not every author uses the same terminology to report patient setup errors, some results in this table were re-interpreted or estimated from the original studies. Overall, the average systematic and random errors are roughly 2mm.

Authors	Site	Modality	Systematic (σ)	Random (Σ)
Huang *et al*. (28)	Prostate	kV-CBCT	2.2mm	1.5mm
Letourneau *et al*.(29)	Prostate	kV-CBCT	1.0mm	2.4mm
Arjomandy*et al*.(30)	Lung	kV-radiograph	2.7mm	2.5mm
Li *et al*. (27)	Lung	kV-CBCT	1.4mm	1.5mm
Average			**1.8mm**	**2.0mm**

Although the magnitude of setup error is not necessarily larger for proton therapy than the conventional photon therapy (i.e. assuming identical beam delivery process) the impact of setup error on delivered dose distribution for proton therapy can be more deteriorating. In order to estimate the effect of setup errors on the cumulative proton

dose to a lung motion, Engelsman*et al*. demonstrated the perturbation of dose distribution due to the change in position of target volume (i.e. soft tissue) surrounded by lung tissue (See figure 1-6) (31). In this study it was clearly demonstrated that the conventional PTV does not guarantee target coverage for proton therapy.

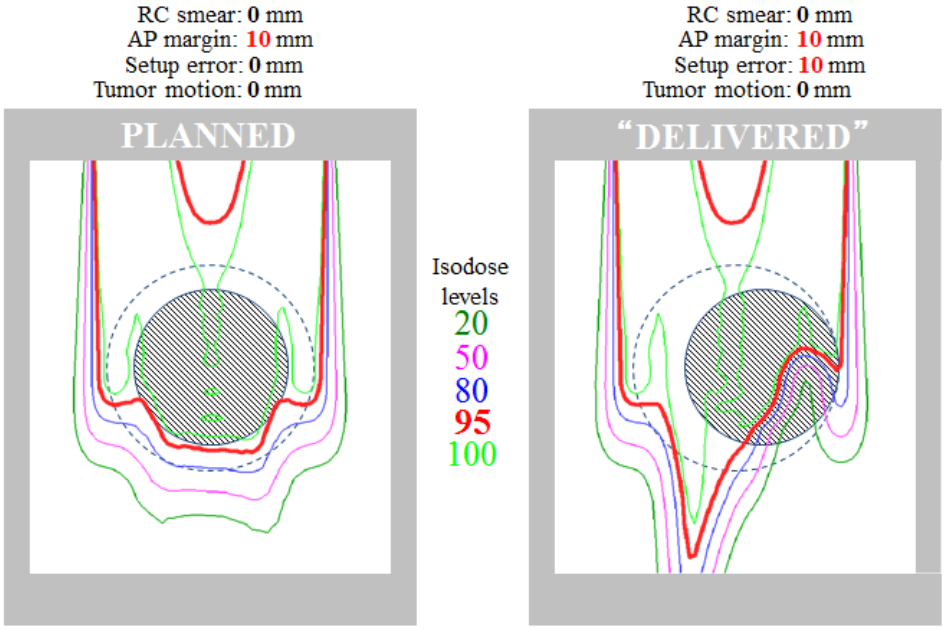

Figure 1-6 When there is no setup error, the planned proton dose shows good conformity to the target volume. However, when 10mm setup error is introduced by shifting the target volume perpendicular to the incoming beam direction, a significant under dosage and over-shoot of dose distribution occurs along the beam direction (This figure is courtesy of MartijinEngelsman from Holland PTC).

In general, patient anatomy is a complicated mixture of different tissue types and different lines of beam paths inside the patient can have significantly different tissue densities. When a setup error occurs, a line of beam path whose proton range was pre-calculated is no longer correct which can cause further range error in addition to the inherent range uncertainty. In other words, for proton therapy, setup error is coupled to range error. A misalignment of target volume in the direction perpendicular to the beam path not only causes a partial geometric miss, but it can further cause over or under-shoot of the proton beam in the direction parallel to the beam path.

A.3 Treatment planning and plan evaluation methods in proton therapy

In this section we briefly introduce the current treatment planning and treatment plan evaluation methods with emphasis on how range and setup uncertainties are handled. Passively scattered beam proton therapy treatment planning is significantly different from treatment planning using photon external beam radiotherapy. One of the most important differences is in the role of the planning target volume (PTV). International Commission on Radiation Units and Measurements (ICRU) report No. 83 defines a set of geometrical volumes that can be used during treatment planning procedures and these conventions are well adopted in the conventional photon external beam therapy treatment planning practice (32). In this convention, the gross tumor volume (GTV) defines tumor volume that is visually evident from imaging (such as CT or PET). The clinical target volume (CTV) is the tumor volume defined by the GTV plus a sub-volume that includes possible extent of the primary tumor volume or microscopic spread of diseases. The planning target volume (PTV) is the volume that extends further from the CTV to include geometrical uncertainties in the CTV position. If time resolved

4DCT is available, the extent of internal motion of the CTV through different breathing phase can be combined to give the internal target volume (ITV) which is then expanded further to the PTV (See figure 1-7).

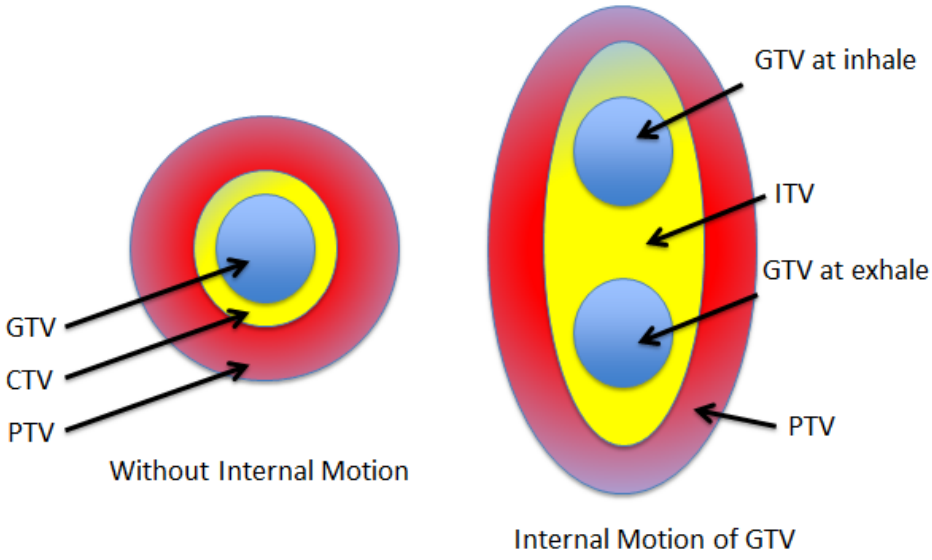

Figure 1-7 Schematic of geometrical target volume expansions from GTV (gross tumor volume) to CTV (clinical target volume) to ITV (internal target volume) to PTV (planning target volume) according to the ICRU definition.

It should be noted that while the determination of GTV, CTV, and ITV are primarily clinical in nature, the PTV is concerned more with the physical process of beam delivery and its uncertainties. In other words, the PTV should be created differently for different beam delivery methods and choice of therapy type. Previously, researchers

have shown that the concept of PTV alone cannot ensure target coverage sufficiently for proton therapy as it did for the conventional photon therapy (31, 33). The conventional PTV is purely a geometrical concept and it does not account for the change in tissue density due to setup or internal motion error in heterogeneous medium. In other words, unlike dose distributions found in conventional photon therapy, proton dose distributions can be perturbed as a result of both setup and internal motion error. For this reason, the proton therapy community has instead developed treatment planning methods for passively scattered proton therapy that focus on delivering dose to CTV itself (rather than PTV) and deal with uncertainties through the design of beam-specific hardware such as apertures and compensators. The aperture is a block that is cut-out to have a shape of CTV in beam's eye view in order to completely block the dose to normal tissue outside of CTV laterally. The compensator is a block made out of Lucite (or other material type with density similar to that of water) with variable thickness to match the proton beam's range to the distal surface of CTV (See figure 1-8).

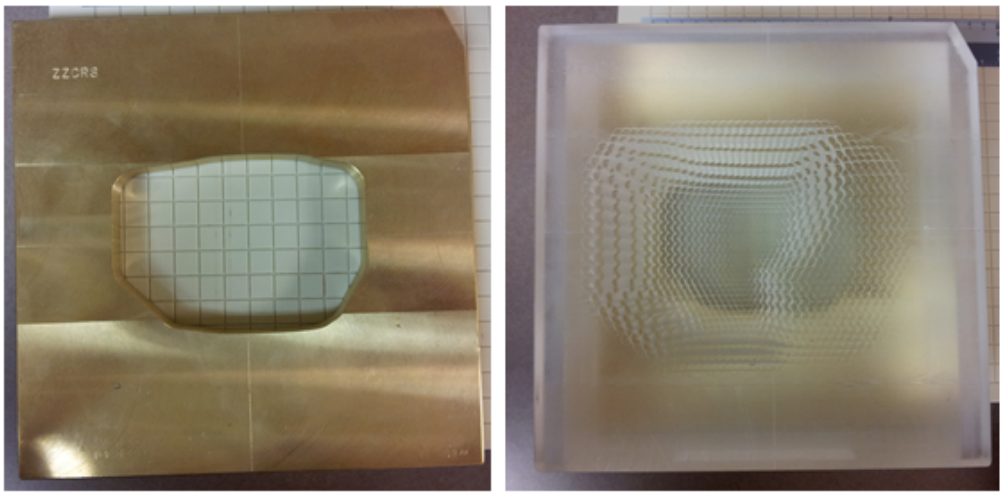

Figure 1-8 An aperture (left) and a compensator (right).

In order to account for the geometrical miss of a target volume due to setup or internal motion of a target, the aperture block can be cut-out further to extent the isodose line laterally from the CTV. The inherent range uncertainty is accounted for by adding extra depth in protons range during compensator design (i.e. to add margins distally, the compensator thickness is lessened to increase proton range in patient). Furthermore, in order to account for the range error caused by the change in local tissue density distribution, the thickness of compensator is lessened further by the process called "compensator smearing" (34). A compensator that is appropriately smeared can account for the change in the WET along the beam path due to setup and internal motion error, thereby maintaining sufficient dose coverage.

Despite its effectiveness in dealing with both setup and range uncertainties, there are two major problems with this current method. First, this method cannot be used for proton therapy using scanning beam delivery because scanning beam delivery does not require apertures or compensators. The lateral spread of dose distribution is achieved by steering a small pencil beam using steering magnets so it typically does not require an aperture. Also, for scanning beam delivery method, the compensator is not required as the range proton is controlled at the level of accelerator by changing its initial kinetic energy. Second, in the absences of the PTV it is harder to evaluate the CTV coverage under uncertainties. Another important role of the PTV in conventional photon therapy is that it acts as a surrogate volume of CTV under the worst-case scenario: the PTV coverage is related to the CTV coverage under assumed geometrical error. For this reason, typically, a dose is prescribed and reported using the PTV instead of the CTV itself. Despite these known limitations of the PTV in proton therapy, it is still used to

prescribe and report dose in proton therapy treatment plans as there are no readily available alternatives. Therefore, in this study, we propose to adapt the conventional PTV to fit better with proton therapy in terms target coverage and also suggest different uncertainty analysis method to evaluate CTV coverage under treatment uncertainties.

B. Objectives

The main objective of this research is to develop methods and tools to account for the setup and range uncertainties in proton therapy that can apply to both passively scattered and scanning beam delivery. First, we need to develop a treatment planning method that ensures prescription dose is delivered to a target volume. Second, we need a method to evaluate if a given treatment plan is indeed delivering the intended prescription dose to a target as well as if dose limits for organs at risk are satisfied under the influence of uncertainties.

B.1. Treatment plan designing method adapted to proton therapy

In this research we propose to modify the conventional PTV used in external beam photon therapy to better account for the uncertainties related to proton therapy. This will be achieved by considering beam by beam, ray by ray margin specific PTV or beam-specific PTV.

B.2. Treatment plan evaluation method adapted to proton therapy

In this research we propose to add uncertainty analysis into the conventional treatment planning assessment parameters such as dose objectives and dose-volume histograms. This will be achieved by comprehensive statistical sampling methods to

quantify both expectation value and standard deviation of interested dose related parameters.

C. Hypotheses

We propose the following hypotheses in this research:

Hypothesis 1: A plan designed with a Beam-specific planning target volume (bsPTV) can minimize the loss of target coverage due to setup and range uncertainties when compared to a plan treated to a conventional planning target volume (PTV).

Hypothesis 2: Statistical method can be used to quantify the variation in dose distribution and dose-volume histograms (DVHs) due to setup and range uncertainties.

D. Specific Aims

In order to resolve technical difficulties in testing our hypotheses, we propose following specific aims.

Specific Aim 1: Develop and validate the concept of bsPTV and its ability to maintain target coverage under setup and range uncertainties.

Specific Aim 2: Develop a robust plan analysis tool using statistical parameters and quantify the effect of setup and range uncertainties on proton plans.

CHAPTER 2: BEAM-SPECIFIC PLANNING TARGET VOLUME

Chapter2 is based on the material that was published in the International Journal of Radiation Oncology and Biology and Physics in Feb, 2012 by the author of this dissertation. [Int. J. Radiat. Oncol. Biol. Phys. 2012:82(2):e329-336. Written permission has been obtained from the publisher for use of these materials in this dissertation.

A. Introduction

As discussed in chapter 1, the greatest challenge in proton therapy treatment planning is accounting for various uncertainties associated with actual dose delivery, such as patient setup uncertainty, organ motion and proton beam range calculation. For external beam radiotherapy using high-energy photon, some of these issues can be addressed by using geometrical concepts, such as the planning target volume (PTV) as introduced in the International Commission on Radiation Units and Measurements reports (36, 37, 38). In general, the PTV is created by adding geometric margins to the clinical target volume (CTV). The CTV to PTV margins are determined by considering uncertainties that arise during the treatment beam delivery process. The magnitude of errors resulting from hardware performance uncertainties, patient setup errors, and internal organ motion and external patient motion is specific to the type of radiation being used. Therefore, unlike the CTV, the PTV should be treatmentmodality and beam delivery method dependent. For example, size of the PTV can be significantly minimized under the guidance of image-guided or adoptive re-planning strategy whereas the CTV does not depends on the actual beam delivery process. For external-beam photon treatments, it is assumed that the spatial dose distribution from the photon plan may not be noticeably affected by the geometric change in the target or patient's anatomy (39, 40). Cho et al (41) conducted a study showing that, for the majority of clinical cases, change in photon dose distribution due to a small misplacement error of the target is negligible and that simple uniform expansions of the CTV are adequate. The fact that the dose distribution given by photons is insensitive to small perturbation in CT density gave a rise to the term dose cloud. However, studies of treatment margins for proton therapy have found that simple geometric expansions of the CTV are inadequate for proton therapy treatment planning (42, 43). The difficulty of applying a geometric concept of the PTV to proton therapy is due to the fact that proton dose distribution can vary substantially when patient's anatomy in the beam path is changed. In particular, misalignment of the proton beam with the patient can cause significant cold spots or hot spots

within the target volume in the presence of tissue heterogeneities, such as air pockets, dense bone, or skin surface irregularities, near the beam path. We have described this type of error that is unique to proton therapy as setup or internal motion error being coupled to range error (i.e. it should be noted that setup error induced range error is different from inherent range error discussed in chapter 1). Due to setup error, these tissue heterogeneities may move into the beam path, causing cold spots or hot spots. When using a simple geometric expansion of the CTV,unanticipated changes in proton range can result in insufficient dose coverage to the target (43-45). The magnitude of error that can be caused by tissue heterogeneities misalignment is expected to be greater for treatment sites with dramatic change in tissue density such as in lung and soft tissue boundary (See figure 2-1).

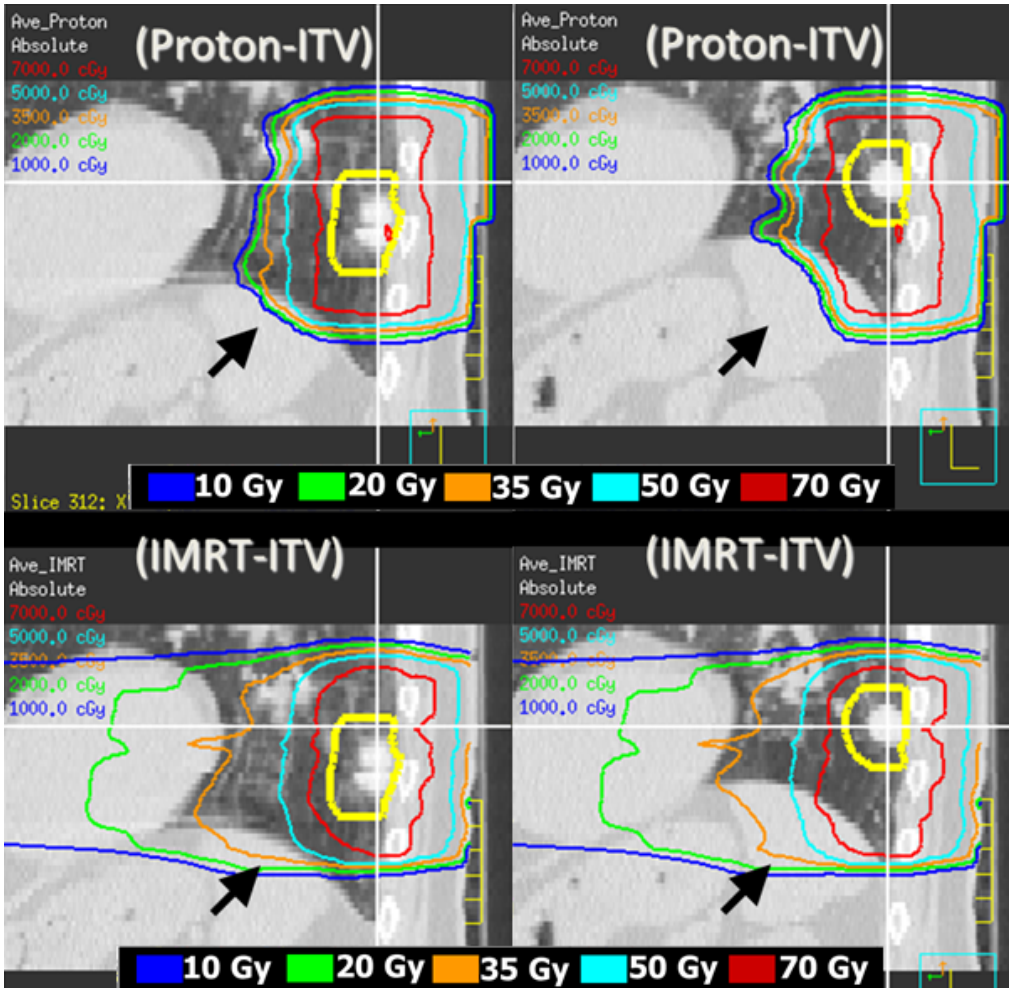

Figure 2-1 Dose distribution re-calculated on inhale (right column) and exhale (left column) is compared for Proton (top row) and IMRT (bottom row).The arrow shows the boundary between liver and lung where dose distribution changes significantly for proton while remains roughly the same for IMRT. (Courtesy of Lei Dong Ph.D. Scripps Health)

Moyers *et al.* (42) proposed abandoning the PTV concept and suggested corrections be made by adjusting the beam-specific hardware, such as the aperture and range compensator, in passively scattered proton treatments. However, a scanning beam system can steer a small proton pencil beam to paint large target while controlling the proton range directly by adjusting the initial kinetic energy of protons extracted from accelerator, therefore, proton therapy delivered using a scanning beam system does not use hardware beam shaping devices. Therefore, most treatment planners using scanning beam proton therapy use a conventionally derived geometric PTV concept to define the treatment target (46, 47, 48, 49,50), which may not be ideal.

In this chapter, we investigate a PTV design method for proton treatment planning using single-field optimization (SFO) via a beam-specific PTV (bsPTV). The bsPTV concept will also apply for both passively scattered proton plans and scanning beam proton plans, especially in the evaluation of such plans to confirm adequate compensator designs. This method provides a significant advantage over the conventional method using a single PTV for all beams because the magnitude of each margin can be individualized for each field. For passively scattered beam delivery method, the uncertainty caused by tissue misalignment can be compensated by the compensator smearing technique as proposed by Urie*et al.* (52). We will demonstrate a similar concept can be used for constructing the bsPTV without a physical compensator. One unique contribution in our implementation is that we converted the margin calculated using the water equivalent thickness (WET) into a local distance (i.e. physical distance in space) based on local density near the target region, which proves important for evaluating target coverage in heterogeneous tissues, such as lung or head & neck cancers.

B. Methods

B.1. Design of bsPTV

Our proposed method of designing a bsPTV, we primarily focused on three types of uncertainties. First, a "geometrical miss" of the CTV due to lateral setup error was accounted for by a lateral (in beam's eye view) expansion of the CTV. Second, inherent range uncertainties due to uncertainties in relative stopping power ratio (rsp) were accounted for by adding distal margins (DMs) and proximal margins (PMs) for each ray trace from the beam source to the distal and proximal surfaces of the CTV. Third, range error due to misaligned tissue heterogeneity was accounted for by adding extra margins from a density correction kernel that mimics the function of compensator smearing.

B.1.1 Lateral margin calculation

Foremost, it is important to cover the extent of target motion geometrically as position of spots (i.e. where monitor unit of from a pencil beam is defined) must be assigned to account for a "geometrical miss" of the CTV due

to setup and internal target motion error. For this reason, the first step in creating bsPTV is to expand the CTV laterally from the beam's eye view using margins that encompassed the typical setup error margin (SM) and internal motion margin (IM). This step is similar to the aperture expansion step used in passively scattered proton therapy treatment planning in the sense that the margins are expanded laterally away from the beam axis rather than the patient axes. Thus, lateral margins (LM) can be defined as

$$LM = IM_{CTV} + SM \qquad (1).$$

The magnitude of IM can be determined for each patient using four-dimensional CT (4DCT). The magnitude of SM depends on the confidence level based on experience of therapist, institutional history, immobilization, and image-guidance procedure.

B.1.2 Distal and proximal margin calculation

The second step in designing the bsPTV was to account for the range error; the combination of errors resulting from the uncertainties in the calibration curve used to convert the computed tomography (CT)number (in Hounsfield units [HU]) to the proton stopping power and from the uncertainties in the HU values themselves that may appear during CT acquisition (*i.e.,* due to artifacts in the CT images). Accurate estimation of range uncertainty due to CT HU to stopping power conversion still remains a challenge (53-55). In this study, we used 3.5% of the WET to the target as the range error,following the current protocol used at our institution for passively scattered treatment field design. In order to account for range calculation error more precisely,the magnitude of the DMs was specific to each ray directed through the target volume (i.e. the laterally expanded CTV). First, we computed a "range matrix" whose pixel value representedtheWET of protons in a 1x1 x 2.5 mm grid (i.e. or equivalent to the CT grid space) perpendicular to the beam direction. For example, the relative radiological path lengths for distal ($D_{i,j}$) and proximal ($P_{i,j}$) rays representing the index (i, j) of the range matrix were calculated by integrating the line segments $\overline{sc}$ and $\overline{sb}$ as follows (see figure 2-2):

$$D_{i,j} = \int_{s}^{c} rsp(i, j, z)\, dz \qquad (2)$$

$$P_{i,j} = \int_{s}^{b} rsp(i, j, z)\, dz \qquad (3)$$

where $rsp(i, j, z)$ is the relative stopping power ratio function of the given CT data; that is, each CT number along the line segment is converted to its corresponding relative stopping power ratio from the previously measured calibration curve (56). Both the $DM_{i,j}$ and $PM_{i,j}$ for a given ray were found by

taking 3.5% of the radiological path length that was calculated usingEqs. (2) and (3).

$$DM_{i,j} = D_{i,j} \times 3.5\% \qquad (4)$$

$$PM_{i,j} = P_{i,j} \times 3.5\% \qquad (5)$$

All the rays and their corresponding PMs and DMs were calculated accordingly. All margins were measured in WET.This step is illustrated in figure 2-3 (c).

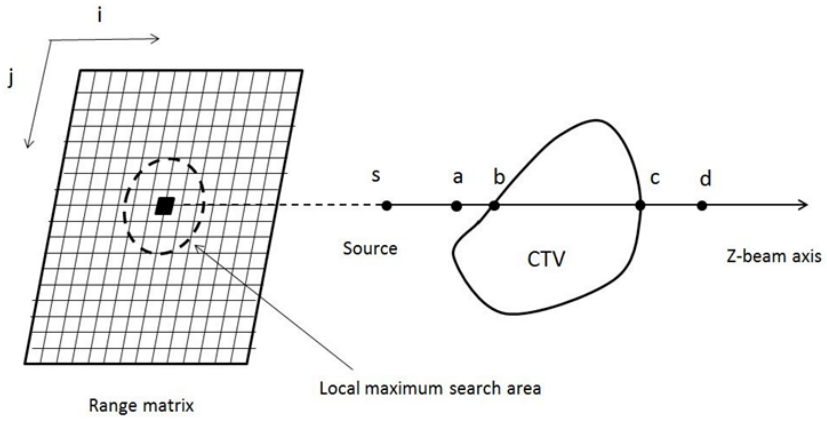

Figure 2-2A schematic illustration of the method used to calculate the range matrix and relevant margin of a ray. Radiological path length is calculated per ray, and a kernel is applied to replace the radiological path length of a given ray with the local maximum within a distance (the lateral setup error and organ motion) of the range matrix. 3.5% of the assigned path length is used to convert to physical depth to form a margin (distal $\overline{cd}$, proximal $\overline{ab}$). [Permission to publish this figure was obtained from the *Int J OncolBiolPhys*]

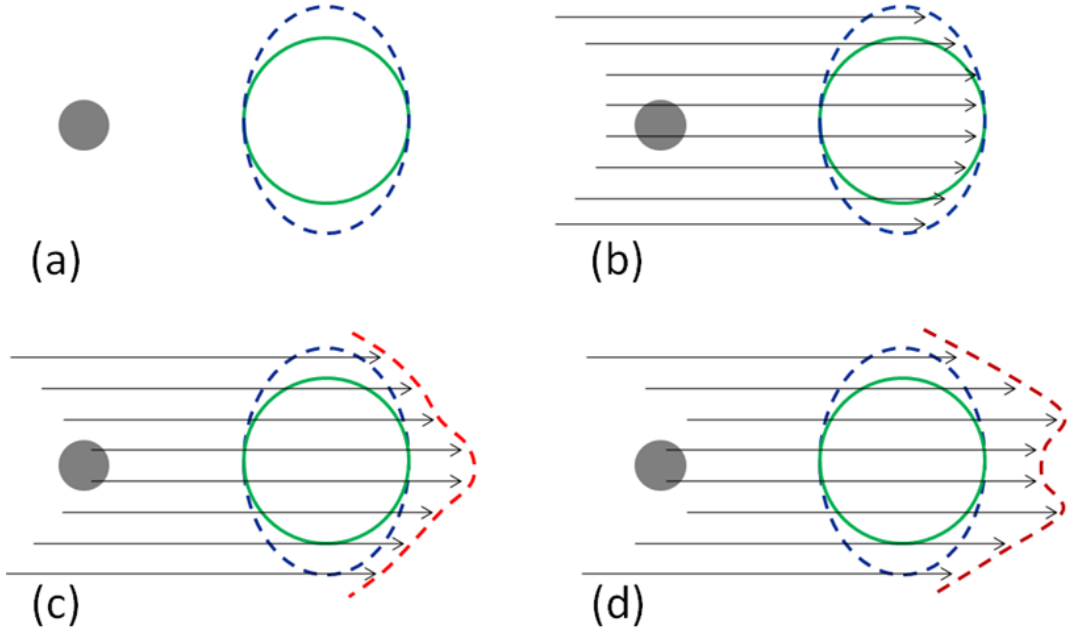

Figure 2-3 An illustration of the four essential steps in creating the bsPTV (red contour) from a CTV (green contour)with a dense object (grey sphere) along the beam path. (a) The CTV is expanded laterally away from the beam axis using the expectedmotion margin (IM) and setup margin (SM). (b) From a given beam angle, ray tracing is performed to calculate the radiological path length of each ray from the source to the both distal and proximal surface of the laterally expanded CTV (blue contour). (c) The fraction of the total radiological range calculated in previous step is used to the distal margins per ray. (d) Correction for interplay effect of setup and range error is accounted by applying the correction kernel and the radiological path length margins are converted to physical depth margins. [Permission to publish this figure was obtained from the *Int J OncolBiolPhys*]

B.1.3 Correction for tissue density misalignment

So far margins treated in this method concerns only with setup and range error independently. However, it is clear, that the setup error is coupled to a further range error as they are bounded by the line integral in Eq. (2 and 3). This type of error is described as the misalignment of tissue heterogeneity as it only occurs in inhomogeneous medium. In order to account for the misalignment of tissue heterogeneity, we replaced $D_{i,j}$ for a given ray with the WET ($D_{Max(i,j)}$) found within a distance defined by the lateral setup error and organ motion perpendicular to the ray line: this is done by applying local maximum filter kernel in the range matrix that was pre-calculated. This maximum WET is then

used to compute $DM_{i,j}$. Similarly, the same operation was applied to proximal side by replacing $P_{i,j}$ with the minimum (rather than the maximum) WET($D_{Min(i,j)}$). This process was repeated for all rays. This process is conceptually equivalent to the physical range compensator smearing technique.

B.1.4 Conversion to physical depth margin

The margins calculated above are defined in terms of the WET. However, surrounding tissues of CTV where bsPTV is expanded may be heterogeneous with different density. In such case, the margin based on WET calculation must be re-converted back to the physical distance according to the local density in order to visualize bsPTV and overlay onto the image of patient and compare the isodose lines with PTV volume directly. Therefore, in the final step, we converted the water-equivalent bsPTV to a physical bsPTV with identical radiological path length using the local density information from the CT data. Thus, we expressed the resulting physical depth margins of a given ray line as follow:

$$DM_{i,j}^{Physical} = d - c \tag{6}$$

$$PM_{i,j}^{Physical} = b - a \tag{7}$$

where the points c and d (a and b for proximal) are the limits of the following integral:

$$D_{Max(i,j)} \times 3.5\% = \int_{c}^{d} rsp(i, j, z)dz \tag{8}$$

$$P_{Min(i,j)} \times 3.5\% = -\int_{a}^{b} rsp(i, j, z)dz \tag{9}$$

Figure 2-3 shows a step-by-step illustration of bsPTV formation using the method described here.

B.1.5 Software Implementation

Because existing treatment planning system could not produce the bsPTV, we implemented the calculation in standalone software written in Matlab (Mathworks, Natick, MA). The software takes DICOM CT images, structure set, and RT plan as input. The software allows the selections of a target (CTV), a beam angle, and various parameters related to setup errors and range uncertainties. The software will calculate and create the bsPTV as a DICOM RT structure contour, which can be imported back to the treatment planning system (See figure 2-4).

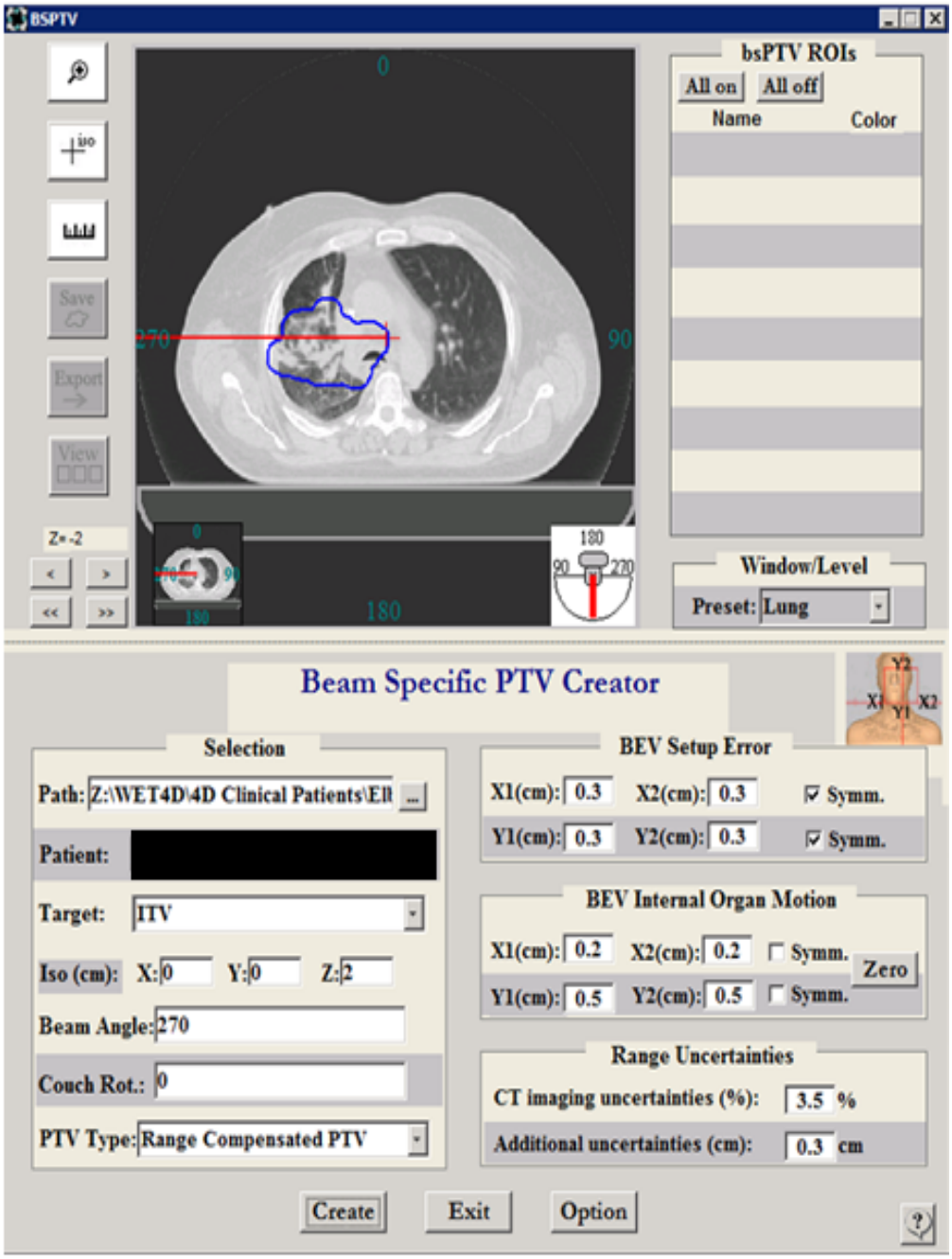

Figure 2-4 Final implementation of bsPTV software. It takes DICOM images and structure file of patient, expected setup and internal motion margin, and range uncertainties, and selected beam angle, in order to compute beam-specific planning target volume that can be exported as another DICOM structure file.

B.1.6 Validation Study

In order to validate the design method and its software implementation we designed an experiment based on a phantom.A virtual CT phantom with a water-equivalent body, a CTV, and a high-density object was created. The CTV (50 Hounsfield unit [HU]; volume = 50.4 cm^3) was placed at the center of the body of water-equivalent material (0 Hounsfield unit [HU]), and the high-density object (1800 HU; volume = 1.9 cm^3) was placed approximately 5cm upstream of the proximal surface of the CTV in order to create heterogeneity that can contribute as a source of added range uncertainty in case of misalignment. The conventional PTV was constructed in order to compare the results with bsPTV. The PTV was derived by expandingtheCTV as follow: 8-mm margin was used to expand the CTV laterally in the beam's eye view to create the PTV. The 8-mm LM was carefully selected to make sure the magnitude of simulated setup error (i.e. 6 mm) does not exceed this bound.For the sake of simplicity, we wanted to make sure that in case under dosage to CTV occur during our simulation, it should occur at the distal and proximal surface of the target volume rather than from lateral geometrical "hit or miss". DM and PMvaluesof8.5mm and 7.5mm, respectively, were calculated using the following equations:

$$DM = 3.5\% \times (distal\ CTV\ depth) + 3mm \quad (10)$$

$$PM = 3.5\% \times (proximal\ CTV\ depth) + 3mm \quad (11)$$

The extra 3mm margins from the above equations are used to account for inaccuracies in dose calculation algorithm to handle large angle scatter and nuclear interactions in the proton beam as well as the inaccuracy in manufacturing compensators. It should be noted that for scanning beam proton therapy where compensator and aperture that adds uncertainty in our ability to calculate range is missing, the addition of 3mm can be lessened or completely ignored. Similarly, for the bsPTV, the same 8-mm LM was used to expand the CTV. The method described in the previous section was used to expand the CTV in the distal and proximal directions with a uniform setup error of 6mm, which resulted in a non-uniform expansion of the CTV for both the distal and proximal surfaces. It should be noted that in creating PTV and bsPTV, there is not lateral margin bias but difference is in proximal and distal margin.

A treatment plan using a single field with a gantry angle of 270° (directed from the patient's right to his/her left) that passed through the high-density object was created using SFUD to give a uniform dose of 200cGy to the PTV and likewise to the bsPTV. Other than the primary target volume, all other treatment planning parameters were the same for both PTV and bsPTV plans. To compare the robustness of the plans based on the PTV and bsPTV, we applied the original treatment beam data to CT data sets under different combinations of errors and recalculated doses for each simulation. Setup error

was simulated by shifting the entire CT data set from its original isocenter from 0mm to 6mm in increments of 2mm perpendicular to the beam axis. Internal motion was simulated by moving the high-density object from 0mm to 8mm in increments of 2mm with respect to the center of the CTV along the same direction of the body shift. Systematic proton range error was introduced into the simulation by increasing the HU values of the entire CT data set by 3% which is close to 2.1% of radiological range error in the soft tissue region (i.e. this is according to the CT to stopping power ration calibration curve we used). Different combinations of setup, motion, and range errors resulted in 40 unique dose distributions for each plan using the PTV and bsPTV.

C. Result

The resultant bsPTV closely conformed to the PTV except for the area where the smearing operation had the greatest impact. The final bsPTV was slightly larger than the PTV owing to the "horn-like" expansion asshownin figure 2-3 (d). The measured volume of PTV and bsPTV were 126 cm^3 and 161 cm^3, respectively. Figure 2-5 shows examples of the dose distributions for some of the conditions used in the PTV and bsPTV treatment plan comparisons.

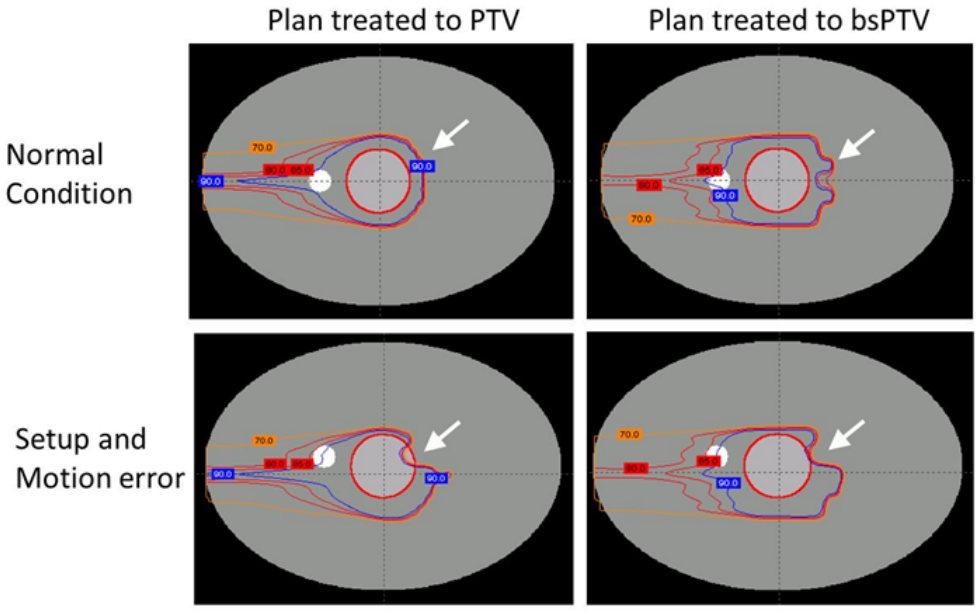

Figure 2-5 Dose distributions when conforming dose to the CTV (inner circular contour) using plans based on the PTV and bsPTV. From outside to inside, the isodose lines of 90% (blue), 85% and 80% (red), and 70% (orange) are shown. [Permission to publish this figure was obtained from the *Int J OncolBiolPhys*]

The left column shows the dose distribution of plans designed using the PTV, and the right column shows the bsPTV as described in the previous section. The top figures show the dose distribution under normal conditions and no setup or motion uncertainties, while the bottom figures show the dose distribution with

CT data with 3% increase in the CT number and a 6-mm setup error and an 8mm shift of the high-density object. As one expects, when there is no introduced error, both plans dose distribution conforms well to the CTV and no cold spot within the CTV is observed.

The minimum percent dose which is the minimum dose found within the ROI as a percentage of the prescribed dose was used to measure the performance of both PTV and bsPTV. For the plans using the PTV as the primary target, with the normal CT data set, the minimum percent dose coverage to the CTV dropped from 99% to 95% with a 6-mm setup error, to 94% with an8-mm motion, and to 88% when both setup error and motion were applied (see Figure 2-6 a). The modest drop in PTV coverage here is from the margins calculated for both the proximal and distal edges using Eqs. (10) and (11) were meant to account for the systematic range calculation error. To take this systematic range calculation error into consideration in conjunction with both setup error and motion, we increased the CT number by 3% of its original value and recalculated dose distributions using the original beam data. Using this range uncertainty imbedded CT set, the minimum percent dose coverage to the CTV dropped from 99% to 92% with a 6-mm setup error, to 83% with an 8-mm motion, and to 67% when both setup error and motion were applied (see Figure 2-6 b). Despite using PTV margins that exceeded the simulated uncertainties, dose coverage to the CTV was not maintained owing to the misplacedhigh-density object. Most of the underdosage occurred at the distal surface of the CTV along the lines passing through the high-density object.

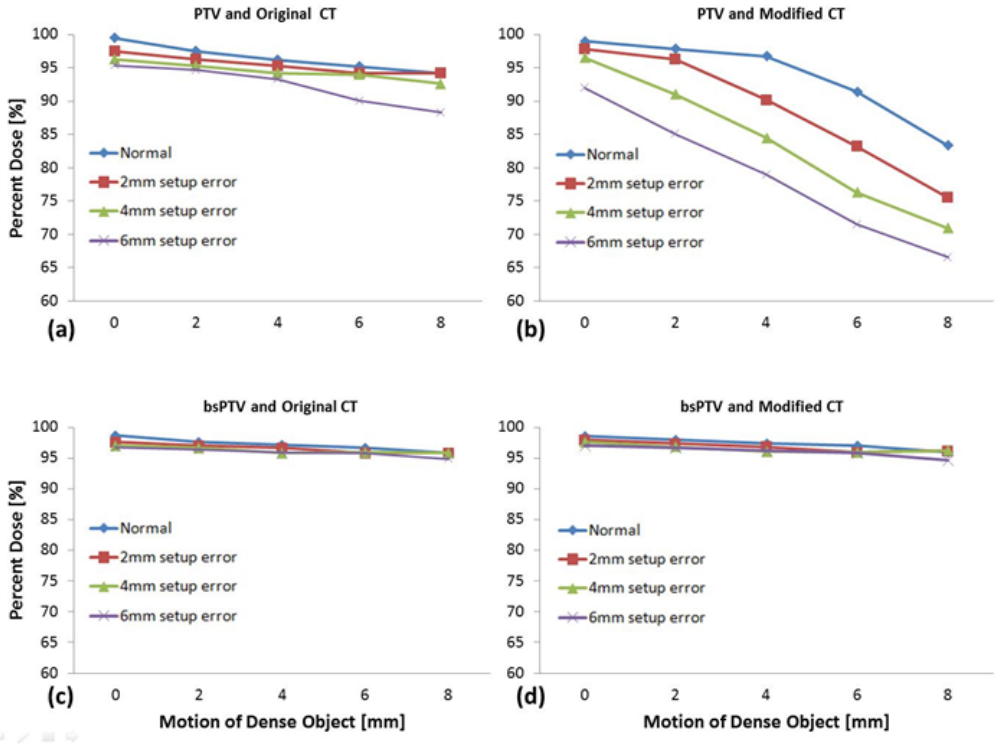

Figure 2-6 The minimum percentage ofprescribeddoseto the CTV for (a) plans using PTV simulated with original CT data, (b) plans using PTV with 3% up-scaled CT data, (c) plans using the bsPTV with original CT data, and (d) plans using bsPTV with 3% up-scaled CT data. The lines represent different setup errors ranging from 0mm to 6mm while the horizontal axis represents increasing motion errors of the dense object from 0mm to 8mm. [Permission to publish this figure was obtained from the *Int J OncolBiolPhys*]

The right-hand images infigure 2-5 show the dose distributions for plans that were designed using the bsPTV, which was derived from the CTV using an 8-mm LMplusPM and DM calculated as described above. For this plan, using the normalCT data set, the minimum percent dose coverage to the CTV dropped from 99% to 95% when both 6mm of setup error and 8mm of motion were introduced. Unlike the plansusing the PTV, plans using the bsPTV showed little change in the minimum dose coverage to the CTV when using the modified CT data set. Under conditions of the largest simulated treatment uncertainty using the modified CT data, the dose coverage of the CTV dropped to 94% (see figure 2-6d). The range calculation error introduced by scaling up the CT numbers by 3% did not affect the dose coverage to the CTV when using the bsPTV as the primary target volume.

D. Discussion

In this chapter we developed and showed our implantation of the beam-specific PTV concept in order to account for the setup and range uncertainties in proton therapy. The results of the simulation study support the appropriateness of using bsPTV to calculate adequate margins to guarantee dose to CTV coverage for charged particle therapy. Previous studies have shown thatthe magnitude of required target margins depends on the beam's direction in proton therapy(50, 57) but specific designing methods to create such bsPTV have not beenpublished in open literature. Thus, this study fills an important gap in the goal of creating robust and yet practical target volumes particularly for scanning beam proton therapy system that relies on the conventional PTV method currently. The fundamental difference between the bsPTV design we have describedin this paper and the conventional PTV is that the bsPTV method createsDMs and PMsthatare varied along different rays according to their radiological path lengths. Furthermore, the bsPTV adds extra margins to account for possible range errors due to the misalignments of heterogeneous tissues traditionally done by compensator smearing. In addition, the final bsPTV takes into account local density variations of anatomical objects in the patient. The final shape of bsPTV is not intuitive in as it depends on the local density heterogeneity. In figure 2-7 we demonstrated the beam angle dependent characteristics of bsPTVs for one prostate and one thoracic case.

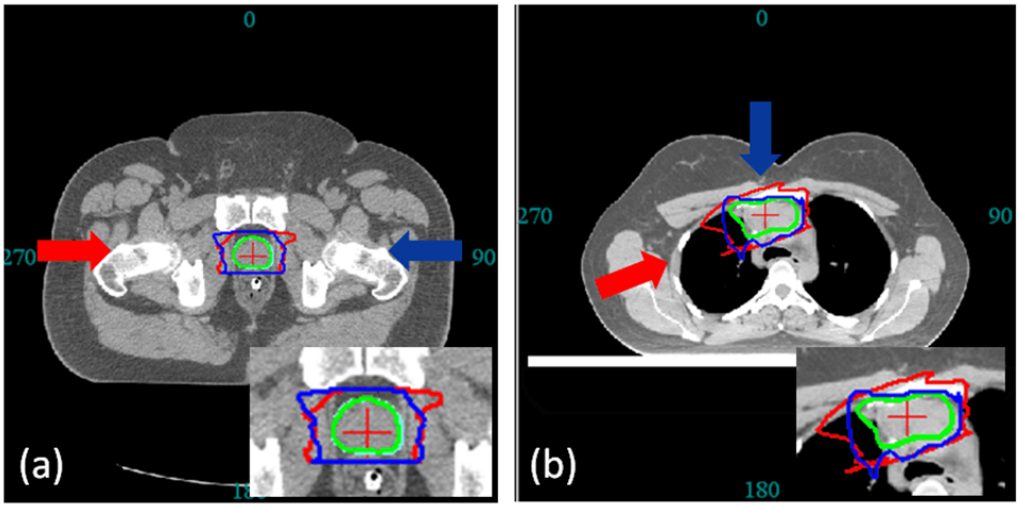

Figure 2-7 The CTV (green contour) is used to derive two bsPTVs (red and blue contours) under same specification (setup and range error) at different angles. (a) For prostate site, both bsPTV shows characteristic horn like distal shape to account for the misalignment of highly dense femur and femoral head. (b) For thoracic site, the two bsPTVs are significantly different in its shape and volume due to the difference in tissue density along their beam paths. [Permission to publish this figure was obtained from the *Int J OncolBiolPhys*]

It is evident that the bsPTVs look different for different beam angle. In fact, in certain case the sheer size of the bsPTV can be obviously bigger than the other beam angle that it can help avoid beam angle that requires large margins in order to spare dose to normal tissue. However,forahomogeneous medium, the bsPTV should be similar to that of the conventional PTV, provided the PTV expansion is along the beam direction. In general, the size of the bsPTV will increase with increasing radiological path length to the target, setup error and the range of organ motion.

Although the focus of this study was the utility of bsPTV as a robust proton planning tool, it is worth mentioning that defining the bsPTV may also be useful in plan evaluation. In conventional photon therapy, the dose-volume histogram (DVH) of the PTV is compared to the DVH of the CTV in order to judge the robustness of a given plan. In a way, the PTV coverage is a surrogate of the CTV coverage under uncertainty. This comparison assumes the PTV is large enough to contain the CTV of uncertain position during the course of treatments. Therefore, the DVH of the PTV is typically seen as the worst-case representation of CTV coverage in photon therapy. In proton therapy, however, such an interpretation of the DVH of the PTV does not work wellbecause of the sensitivity of proton dose distribution to tissue heterogeneity and setup error. Currently there is no readily accepted method to evaluate a proton plan other than performing multiple dose calculations withsimulated isocenter shifts. In

figure 2-8, the DVH of the PTV and the DVH of the bsPTV under original conditions from our phantom study are shown separately along with all the DVHs of the CTV under the different simulation conditions.

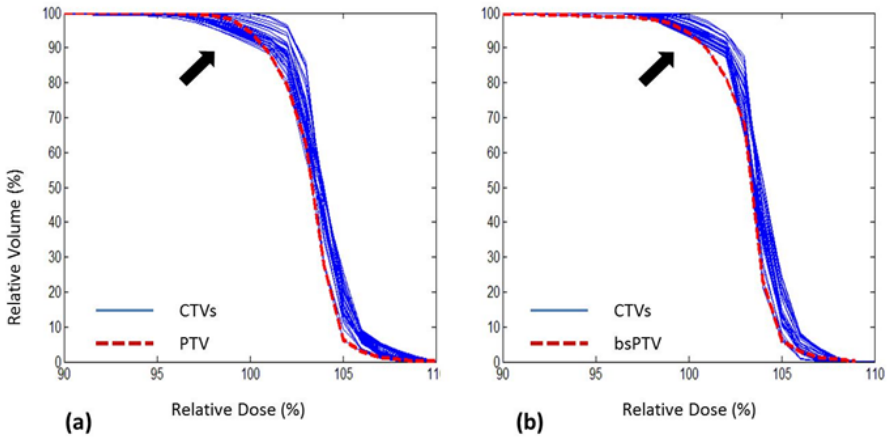

Figure 2-8. The DVHs of the CTV (blue lines) under simulated setup error and motion. (a) Plan using PTV, also shown here is DVH of PTV (red dotted line). (b) Plan using bsPTV, also shown here is DVH of bsPTV itself (red dotted line). [Permission to publish this figure was obtained from the *Int J OncolBiolPhys*]

The arrow on figure 2-8 points to the area where some of the DVH curves reflect much worse coverage of the CTV than of the PTV itself, indicating that the DVH of the PTV does not necessarily represent the worse-case scenario for CTV coverage despite the fact that the PTV is derived by adding margins to the CTV that exceed the simulated geometrical uncertainty. In contrast, the DVH of the bsPTV curve conforms closely to the DVH curves of the CTV in this area, indicating that the coverage to the bsPTV closely represents the worst-case coverage for the CTV. Thus, it should be possible to use the difference in coveragebetween the bsPTV and CTV as a heuristic technique for evaluating the robustness of the proton treatment plan.

The fundamental assumption used to derive the method of generating the bsPTV is that a uniformhomogeneous dose is delivered to the volume being defined. When multiple beams are used and each beam is used to deliver uniform dose to the target, the bsPTV should be evaluated for each individual beam. It will be difficult to assess the overall target coverage because the inter-relationship of different bsPTVs is difficult to combine into one PTV. The method presented in this paper will not be applicable to multi-beam, simultaneously optimized proton plan, such as the intensity- and energy-modulated proton therapy (IMPT) (58).

E. Conclusion

In this chapter, we investigated a practical method to create beam-specific PTV (bsPTV) for treatment planning and evaluation of proton beams. In current practice, scanning beam proton therapy using single-field optimization lacks a well-defined way of dealing with treatment uncertainties. The bsPTV takes into account both setup errors and range calculation uncertainties for the specific beam angle. The bsPTV can be used to directly design and evaluate a proton treatment plan similar to the geometric PTV concept used in the photon treatment planning. We demonstratedthatthe conventional (geometry-based) PTV concept in photon therapy failed to guarantee the prescribed dose coverage of the target in proton therapy because the dose distribution of protons is influenced by tissue heterogeneity along the beam's path. We demonstrated that the proton plan designed based on bsPTV concept provided better target coveragein the presence of setup error and range uncertainties.

F. Appendix

In this chapter we described the method of generating beam-specific PTV (bsPTV) that is robust against setup uncertainty, internal target motion, and range error of proton beam. However, the discussion regarding the determination of input parameters needed to generate bsPTV was omitted. In this appendix, we will briefly discuss how bsPTV margin parameters can be determined in clinical practice. In our validation study, we designed PTV and bsPTV using same lateral margins (i.e. 8mm). The rational of choosing 8mm lateral margin comes from the design of our validation study: we intended to simulate setup and internal motion error up to 8mm therefore having that 8mm lateral margin would provide just enough coverage on the lateral region of our target volume. For the purpose of our validation study, the 8mm margin was an arbitrary choice (i.e. we could have easily shown the similar result with different margins)and its choice wasn't important as long as the same lateral margin is applied to both PTV and bsPTV to create fair comparison.

In clinical practice, the determination of margins or the parameters that are needed to generate bsPTV would be of a significant importance. For PTV, margins are typically derived by considering all the geometric uncertainties (i.e. setup error, organ motion, and target delineation). According to the ICRU report No 78, the systematic and random portion of such errors can be added in quadrature to derive overall margin as follow.

$$\Sigma = (\Sigma_{set-up}^2 + \Sigma_{organ\ motion}^2 + \Sigma_{delineation}^2)^{1/2} \quad (12)$$

$$\sigma = (\sigma_{set-up}^2 + \sigma_{organ\ motion}^2)^{1/2} \quad (13)$$

Once the above overall systematic and random errors are determined, one can follow a model based margin determination formalism to determine the magnitude of geometrical margin sizes. In general, the sizes of such margin will depend on the desired target coverage in certain proportion of population.For example, Stroom*et al*(39) suggested that to ensure at least 95 percent of the dose is delivered to 99 percent of the CTV in 95% of patient population, one needs to derive margin by summing systematic and random error with following weights:

$$CTV - PTV\ margin = 2\Sigma + 0.7\sigma \quad (14)$$

In this formalism, the systematic error is weighted twice more heavily than the random error. Van Herk*et al*(59) and McKenzie*et al*(60) formulated similar margin recipe for different clinical sites. The method of determining these weights go beyond the scope of our discussion but it should be noted that the precise determination of such weights are difficult as they are dependent on patient setup procedure, tumor location, and beam

penumbra. Although these margin recipes provide ways to determine PTV margins without ambiguity, in most clinical practice, the margins are defined based on the experience and confidence of clinical staffs involving patient setup and treatment planning.

For bsPTV, lateral expansion (i.e. respect to beam's eye view) of original CTV volume can be considered identical to the expansion in the conventional PTV. In terms of lateral coverage, there's no conceptual difference between the conventional PTV and bsPTV since the purpose of lateral margin is to cover the geometrical misplacement of CTV volume with respect to beam's eye view. However, for bsPTV, both proximal and distal margins are determined uniquely for different field direction for different patient. Furthermore, the magnitude of required margins is not geometric and must be determined through ray-tracing of patient body along the beam direction. For these reasons, in bsPTV creation, both proximal and distal margins are determined not by population based generic formula as was done for PTV using equation (14). Therefore, to describe bsPTV margins in terms of the objective of covering certain percentage of patient population is not suitable. In our implementation of bsPTV software, we let user input both the magnitude of setup error and internal motion error as well as the expected range uncertainty. Based on these numbers, and by incorporating the ray-tracing algorithm and conversion of water-equivalent thickness (WET) to the physical distance, proximal and distal margins are determined. The magnitude of setup error and internal motion error should be determined based on the clinical experience and confidence in patient setup and simulation procedure. For example, if treatment planning incorporates 4DCT to acquire internal target volume (ITV), the internal motion error can be set to

zero. The range error is specified as the percentage of the total WET from the skin to the distal surface of the target volume. Currently, based on the study performed by Yang *et al*(20) and Moyer *et al*(22), this number is estimated approximately 3-3.5% two standard deviations.

In summary, in creating bsPTV, its lateral margin should be determined similar to the way PTV lateral margin is determined. However, for both proximal and distal margins, a geometric and population based generic formalism should not be used, instead, the margins should be determined for each patient for each selected beam angle.

CHAPTER 3: Application of Beam-Specific PTV in Beam Angle Optimization

A. Introduction

In chapter 2, we developed and implemented the beam-specific planning target volume (bsPTV) for creating a proton therapy plan with built-in robustness in target coverage under setup and range uncertainties. In this chapter we show another application of bsPTV: bsPTV as an objective function in beam angle optimization for lung cancer proton therapy. In the discussion of chapter 1, we briefly discussed that the size and shape of bsPTV is different for different beam angle selected, in some cases it can be used as an evaluation tool of a selected beam angle simply by visually assessing the size and shape of the bsPTV (61). The beam angle optimization problem is unresolved problem that is currently under extensive investigation and research for both photon and proton therapy (62, 63, 64, 65). Beam angle selection is one of the most important decision making steps in radiotherapy treatment planning. Once a beam angle is selected, a treatment field is tailored respect to the beam angle to shape a dose distribution to meet overall plan objectives. The magnitude of which the selected beam angle effects the overall dose distribution is inversely proportional to the total number of beam angles used. As there are more treatment fields, the weight of monitor unit from each field is decreased. Therefore, it can be argued that for a typical lung cancer case, beam angle selection is more important for proton therapy than the conventional photon based intensity modulated radiation therapy (IMRT) since a number of fields used for proton therapy is two to three times less than a number of fields used in IMRT (i.e. typically, proton plan employs 2 to 3 fields while IMRT employs 5 to 9 fields (see figure 3-1).

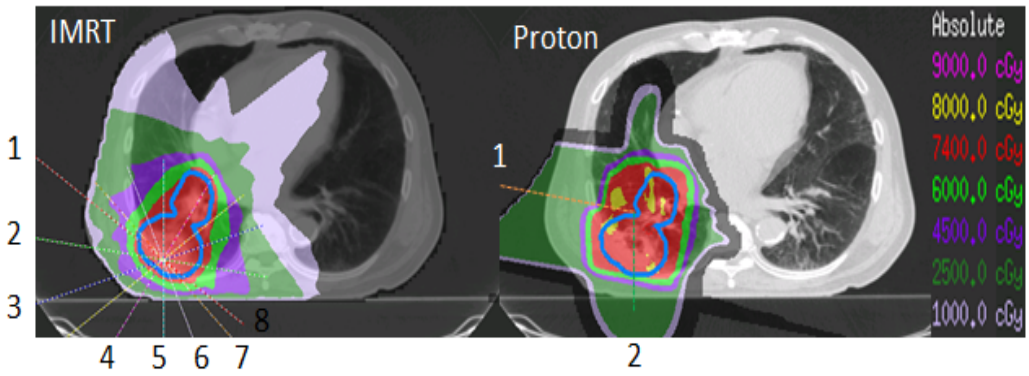

Figure 3-1 An example of typical field arrangement for IMRT (left) and proton therapy (right) of lung cancer. In IMRT, 5 to 9 fields are selected while for proton therapy only 2 to 3 fields are typically required.

Furthermore, due to the physical characteristics of proton beam, overall plan quality is much more sensitive to a given beam angle for proton than IMRT. As discussed in chapter 1, when accounting for the inherent proton range uncertainty the conventional 3.5% water equivalent thickness (WET) of the radiological path length varies significantly over the span of available beam angles. There are two factors contributing to this. First, the depth of target is different for different beam angle. When we account for the range error by taking 3.5% of the total depth in WET, the distal margins of a beam angle with deeper depth would be necessarily larger than other beam angles resulting increased dose to normal tissue surrounding the tumor volume. Furthermore, when creating a spread-out Bragg peak (SOBP), both entrance dose and proximal dose can change for different beam angles because for different angle both target depth and the required width of SOBP is different. In general, entrance and proximal dose increases as depth and width of SOBP increases. We showed the magnitude of such

increases in figure 3-2 where the SOBP with varying depth and width were simulated using an analytical functions of proton depth dose (66, 67).

In this simulation, we found that the entrance dose can rise about 30% of the dose in plateau region of the SOBP when increasing the width of SOBP from 3cm to 5cm at 10cm depth. Secondly, another significant factor to be considered in beam angle selection process is the local tissue density. Because the local tissue density near the tumor volume can vary along the beam direction, when a calculated distal and proximal margins in WET is converted back to a physical depth distance, the final margin can change as much as in the order of three times when going from soft tissue (i.e. tumor) to lung tissue (see figure 3-3).

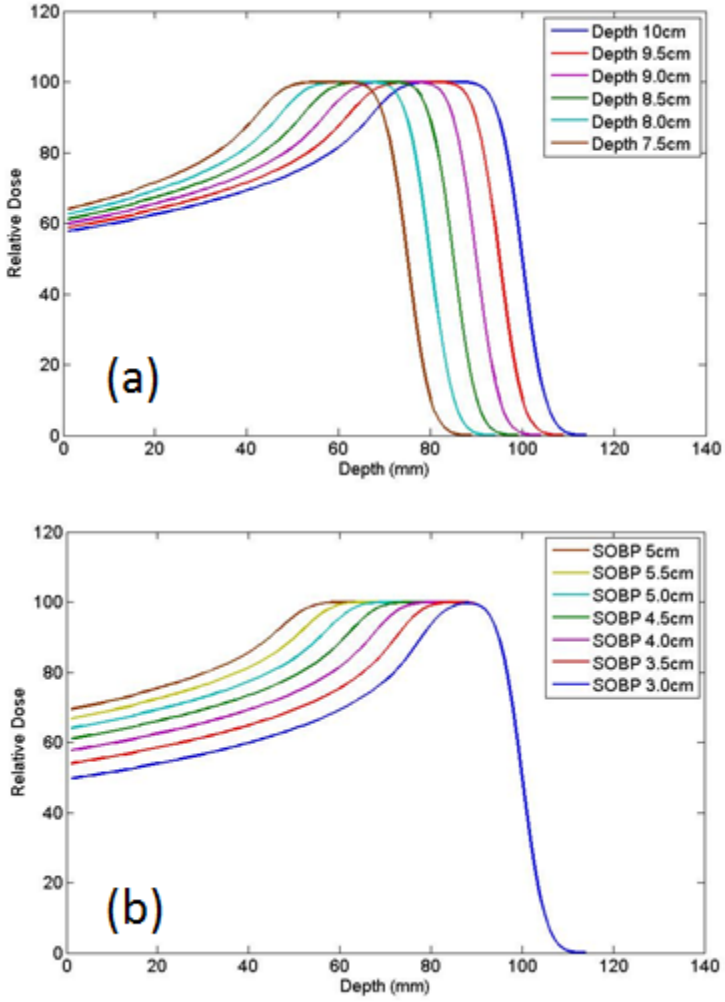

Figure 3-2 Proximal dose as a function of target depth (a) and varying width of SOBP (b) simulated with analytical functions. The proximal dose is larger for a beam angle with deeper target depth and larger width of the SOBP.

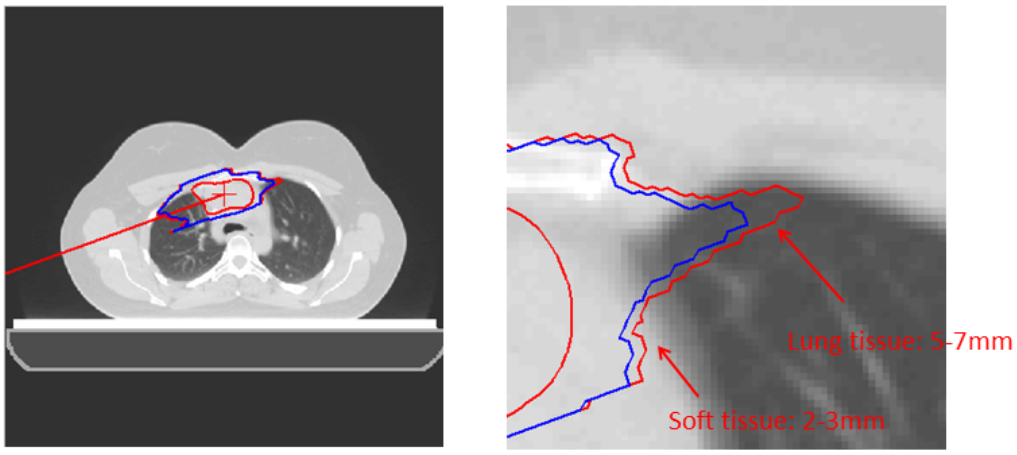

Figure 3-3 An example of bsPTV for the selected beam angle (red straight line). Both blue and red bsPTV contours are shown in magnified view (right) that were generated using constant 3.5% and 3.0% WET margins. Distal to the PTV, the physically converted margin extends up to 3mm in soft tissue, where it extends to 7 mm in lung tissue.

In general, when designing a treatment plan for proton therapy, different margins that account for uncertainties in beam delivery process are added to each fields (i.e. lateral aperture margin, distal and proximal margin, and compensator smearing margin). The addition of these margins to the beam shaping devices usually enlarges irradiated volume, ultimately increasing the dose to normal tissue surrounding the tumor volume. It is difficult to visualize the effect of added margins on the final dose distribution before a full dose calculation is performed. The iterative process of calculating dose and modifying a beam angle configuration is a time consuming process. On the other hand, in chapter 2, we pointed out that the bsPTV can be used as an evaluation target volume because its contour represents the necessary area to be irradiated at the full prescription dose level in order to achieve the desired target coverage under the assumed uncertainties (see figure 3-4).

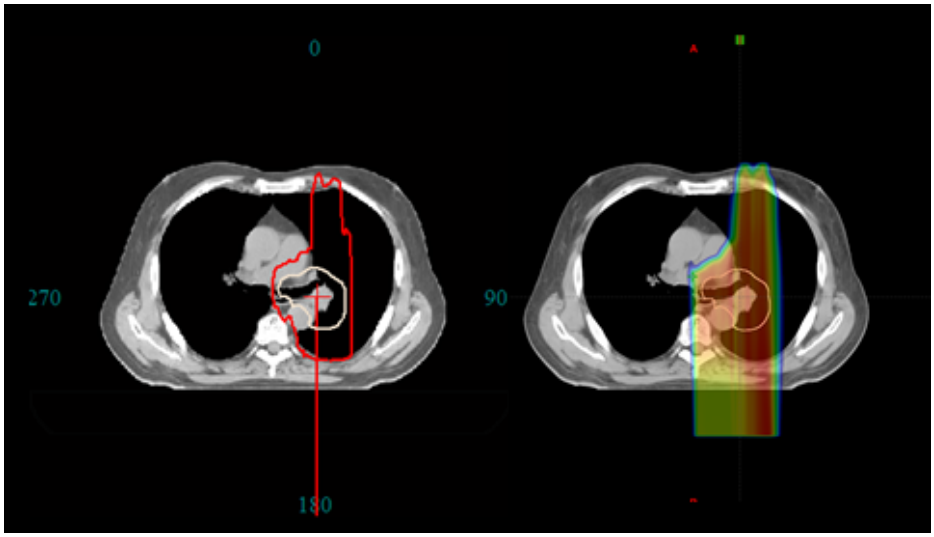

Figure 3-4 A comparison between the bsPTV (left) and planned dose distribution (right). The bsPTV mimics the isodose line of prescription dose level very closely.

Our goal in this study was to optimize beam angle configuration of lung cancer proton plan by using volume of bsPTV as an objective function to be minimized (i.e. inter- or union of volumes of bsPTV). The rational for proposing to use the bsPTV as an objective function are:

1. Beam angle that requires larger distal and proximal margin will have larger volume of bsPTV and should be avoided.
2. Beam angle that requires larger depth and width of SOBP will have larger volume of bsPTV and should be avoided.
3. Beam angle with beam passing through greater amount of tissue heterogeneity will have larger volume of bsPTV and should be avoided.

It should be noted that fully applicable beam angle selection method should consider other equally important objectives such as dose limit to the organs at risk (OAR) that

cannot be directly assessed through the volume of bsPTV alone. Ultimately, incorporating more objectives would require a full dose calculation for every combination of beam angles that requires very expensive computing power that is not readily available in clinics. A full development of such a tool for proton therapy is a beyond the scope of this dissertation therefore, the purpose of this chapter is limited to showing the feasibility of using bsPTV as one of the objective function to be optimized when selecting beam angle for a lung cancer patient.

B. Method

A lung cancer patient who was recently treated using passively-scattered beam proton therapy at our institution was randomly selected for this study. The patient was prescribed receive 74Gy to the clinical target volume (CTV) with dose limiting requirement to total lung $V_{20Gy} \leq 37\%$; mean lung dose (MLD) ≤ 22Gy; and as low as achievable to esophagus $V_{65Gy}$and V_{45Gy}; heart $V_{60Gy}$and V_{30Gy}; and maximum spinal cord dose ≤ 50Gy. The two-field (i.e. two beam angles) plan was designed by a certified dosimetric and approved for treatment by a certified physician. The treatment plan information and patient CT image set and structure set was exported from treatment planning system (TPS) as DICOM formatted files. These files were imported to the bsPTV software (see chapter 2, figure 2-4). The bsPTV was created with setup error parameter set to 5mm and internal motion error 0mm (i.e. the patient showed insignificant breathing motion and the integrated growth tumor volume was painted with constant CT Hounsfield number when calculating dose using average 4DCT in order to compensate for the slight change in tissue density). The inherent range uncertainty of 3% was incorporated into the bsPTV calculation. The smearing kernel

with 5mm smearing distance was also applied to account for the misalignment of local tissue heterogeneity. The volume bsPTV generated under these parameters were recorded for angle spanning from 0 degrees to 360 degrees in 10 degrees interval. Furthermore, the volume of overlap and the volume of intersection between two bsPTVs for a pair of beam angles with every possible combination were computed and displayed as 2D hot-map. The final two fields beam angle configuration was selected based on the combination of beam angle pair that gave the minimum of linear sum of the volume of overlap and the volume of intersection. A treatment plan with new beam angle configuration was created in TPS with identical treatment planning parameters of the original clinical plan. The dose distributions and dose-volume histograms (DVHs) calculated from TPS for both plans were compared.

C. Results

Figure 3-5 shows the resulted bsPTVs for selected beam angles. A significant difference in both shape and volume of bsPTVs for different beam angles are observed. In general, the most significant factor contributing to the increase in volume of bsPTV was the amount of lung tissue present in the distal end of the selected beam path. This was because the relative stopping power ratio of the lung tissue was about 3 times less than the relative stopping power ratio of the tumor tissue, resulting in increased physical distal margin to account for the inherent range errors.

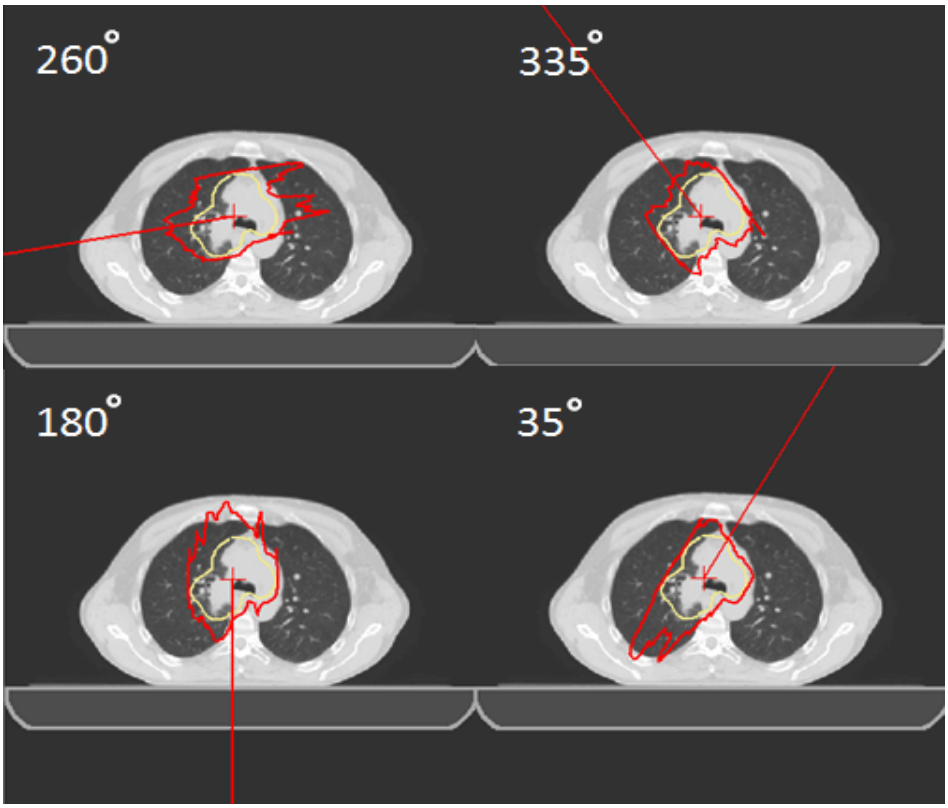

Figure 3-5 bsPTVs (red contour) for different beam angles (red line) computed to account for 5mm setup and 3% inherent range uncertainties.

The overall influence of each sources of uncertainty (i.e. setup and range uncertainty) on the volume of bsPTVs can be seen in figure 3-6. Once can see from the figure 3-5 that the volume of bsPTV computed based on the range error alone is larger than the volume of bsPTV computed based on the setup error alone, indicating that the range uncertainty is contributing slightly larger to the overall treatment volumes. When only one beam angle is considered, the optimum beam angle that has the lowest required volume of bsPTV was found to be at 0 degrees or the anterior-posterior field.

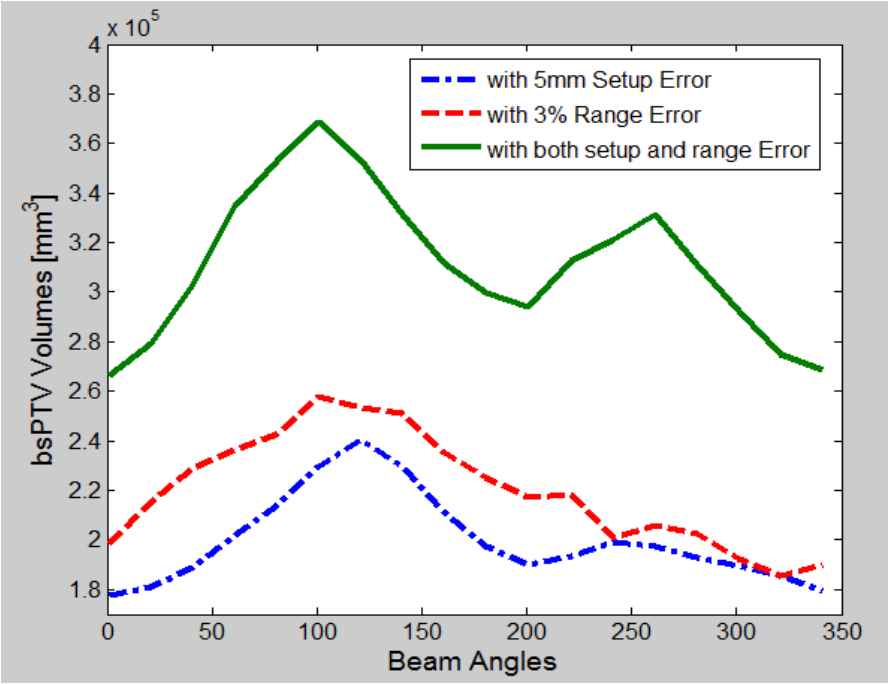

Figure 3-6 Figure of merit showing the variation of the volume of bsPTV over the span of beam angles. The computed volumes of bsPTVs vs. beam anlgle under the effect of setup error only (blue), range error (red), and both combined (green) are shown here separately.

The volume of intersection and the volume of union of multiple a pair of bsPTVs of all possible configurations (i.e. 630 pairs) were computed as shown in figure 3-7 and the linear sum of the volume of union and intersection that was to be used as the one final objective function to be minimized was represented in color map as shown in figure 3-8.

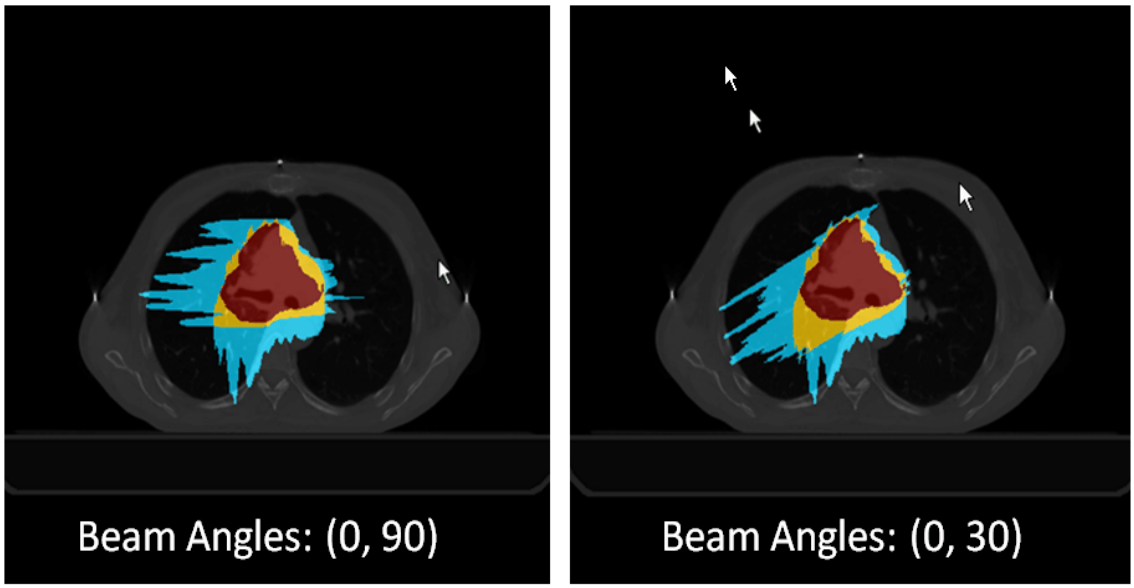

Figure 3-7 The volume of intersection (yellow) and the volume of union (blue) of two bsPTVs are shown for a few selected beam angle configurations. The red colored region represents the original CTV that is used to expand bsPTVs.

Our objective function leads us to find the optimum beam angle configuration of 110 and 130 degrees as supposed to 30 and 90 degrees used in clinical plan. Figure 3-9 and figure 3-10 shows the dose distribution resulted from the plan with optimized beam angles vs. clinical plan was compared visually and the DVHs of lung, esophagus, hear, and integrated-clinical target volume (ICTV) respectively. Our results show a significant reduction in lower dose region of lung. However, we also observed slight increases in heart dose while both dose to esophagus and ICTV remained the same.

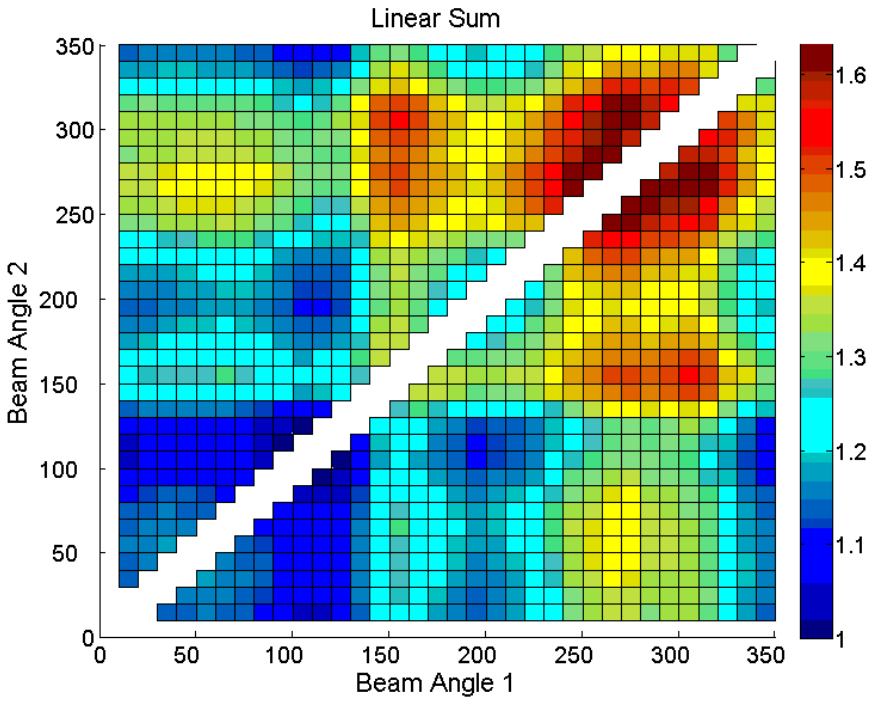

Figure 3-8 The color map of values representing linear sum of the volume intersection and the volume of union of a bsPTV pair. The optimum beam angle configuration was found by search for the minimum (i.e. 110 and 130 degrees).

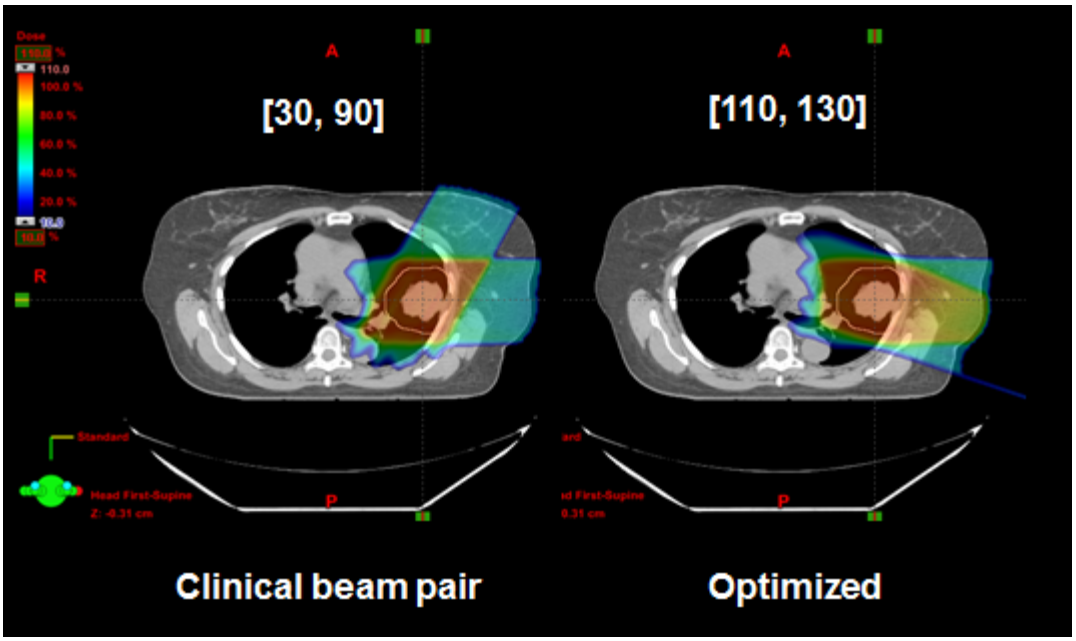

Figure 3-9 A comparison of dose distribution of the clinical plan (left) and the beam angle optimized plan (right).

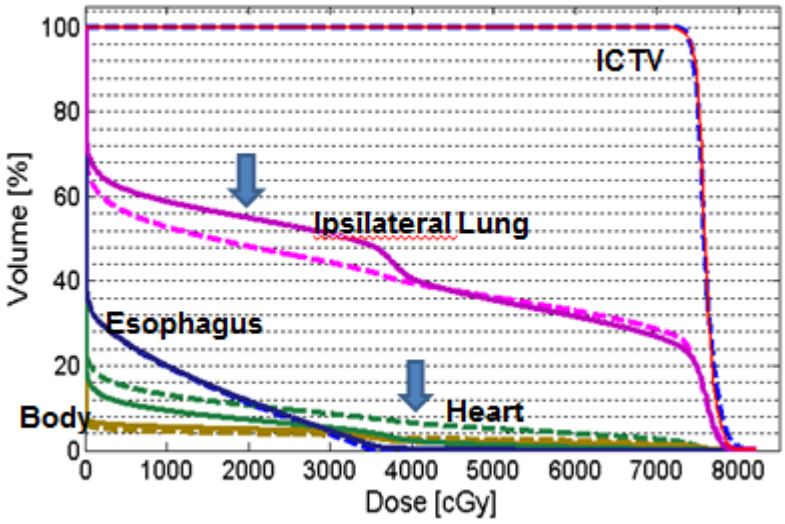

Figure 3-10 The resulted DVHs of clinical plan (solid line) and optimized plan (dash line)

D. Discussion

The volume of bsPTV was most sensitive to the amount of lung tissue present in the beam path. The WET margins accounting for both setup and range uncertainties in lung tissue dramatically increased the physical depth dose requirement which in turn resulted in irradiating a large portion of normal lung tissue both distal and proximal to the tumor volume. As a result, when we optimized the beam angle configuration of the given plan purely based on the minimum volume of bsPTV, we were able to lower dose to the lung significantly as shown in figure 3-10. However, our optimization ignores other dosimetric goals such as dose to the heart, esophagus, and etc. We observed an increase in heart dose in the optimized plan. It can be expected that for lung cancer cases, beam angle configuration optimized based on bsPTV volumes only, would minimize dose to lung while dose to other organs at risks can either increase or decrease.

E. Conclusion

In this chapter we showed that the bsPTV developed in chapter 2 for the robust planning of proton therapy can be used for the purpose of beam angle evaluation and beam angle optimization by minimizing the volume of a bsPTV for a single field plan or a combination of intersection and union volumes for multi-fields plan. The rational for using bsPTV as the objective in beam angle optimization problem is based on the fact that a large volume of bsPTV is required if the given beam angle is more vulnerable to the uncertainties that were considered in creating the bsPTV (i.e. setup and range uncertainties). By reducing the margin required to create bsPTV, we can reduce dose to normal tissue as shown in this chapter for the selected patient case. However, a full

optimization must involve dosimetric objectives that correctly reflect other equally important dose limit criteria.

CHAPTER 4: FAST PROTON DOSE APPROXIMATION FOR ROBUST PLAN EVALUATION

Chapter4 is based on the material that was published in the Physics in Medicine and Biology in Jun, 2012 by the author of this dissertation. [Phys. Med. Biol. 2012 57(11):3555-3569. Written permission has been obtained from the publisher for use of these materials in this dissertation.]

A. Introduction

In this chapter we describe and show our validation of the fast proton dose approximation method that will be used to develop out robust plan evaluation tool in chapter 5. Understanding and inclusion of various effects of treatment uncertainties during treatment planning procedure is of significant importance to reach desired clinical outcome. Careful assessment of treatment uncertainties by accounting those into a treatment plan design in terms of increases in treatment margin or modification of beam shaping devices (e.g. aperture, compensator, and etc.) is essential in creating a robust plan. A robust plan by definition is robust in terms of its ability to deliver prescription dose to a target and to maintain dose constraint to critical structures under uncertainties. The treatment planning dose distribution is only a snapshot of the dose based on the assumed setting at the time of calculation and is therefore subject to variations under different conditions, including patient setup and anatomical changes. As was discussed earlier in chapter 2 and 3, the difference in what was planned and what was actually delivered to a patient due to such changes is expected to be greater for proton therapy than the conventional photon therapy because proton beam ranges depend heavily on the tissue density along its path. Any changes that can influence the given water equivalent thickness (WET) of the proton beam can potentially result in differences between the delivered and planned dose distributions, thereby making proton plan inherently less robust than the photon counterpart.

Uncertainties in setup and range error can cause differences between the value of WET from the treatment plan and actual WET at the time of beam delivery (68, 69, 70, 71). For example, respiratory motion can cause lung and thoracic tissues and the tumor to move during treatment such that the WET along the beam's path can change in any given breathing cycle (72). Also, in multi-fractionated radiotherapy, as tumor response to radiation, a significant deformation or volume shrinkage as well as the patient weight loss can alter the intended dose distribution (73). For the conventional external beam radiotherapy using high-energy photon beam, geometrically expanded volume such as the planning target volume (PTV) or planning organ-at-risk volume (PRV) are

routinely used for robust treatment planning and evaluation (74, 75, 76). Under the assumption that the dose distribution given by photon beam is static, if PTV that encompasses the clinical target volume (CTV) is sufficiently covered by the prescription dose, then as long as CTV resides within the volume bounded by the PTV, we can expect that the coverage of CTV is guaranteed. In terms of treatment evaluation, dose coverage to PTV and PRV acts as surrogate volume of CTV and OAR to be evaluated under uncertainties. However, this is based on the assumption that the dose distribution is not altered in anyway by the motion of CTV or patient body. While this static dose assumption is fairly accurate for photon beam (77) it is not true for proton beam (78, 79).

Ideally, in order to gauge the robustness of a given proton treatment plan under various situations, multiple dose calculations are required in order to simulate different setup errors. Recently, researchers have developed methods which incorporate multiple dose distributions under different setup and range errors to derive dose volume histograms (DVHs) or its derivatives in order to evaluate treatment robustness (80, 81, 82). Similarly, researchers have shown that multiple dose distributions can be incorporated into treatment planning for robust plan optimization (83, 84, 85, and 86). All of these methods rely on, in some way, extremely boundary condition. In order to save computation time, it was suggested that they only calculate dose under extreme condition and create theoretical worst-case dose distribution by sampling the worst possible dose for individualized voxel and combining them later to give full dose distribution. However, when we only rely on the worst case dose distributions or any deviation resulted from it, we tend to over-estimate the true impact of uncertainties in our ability to deliver intended dose distribution. While such method would be acceptable for the purpose of comparing two different plans in order to determine which plan is more robust, it does not provide any insightful information as to whether or not the plan itself is an acceptable what would be the most likely dose distribution under the assumed uncertainties. In order to realistically assesse and quantify the impact of the uncertainties on planned dose distribution, it requires to look at, not only at the extreme condition, but almost all possible scenarios as dictated by their statistical nature. However, due to the computational cost of calculating proton dose distributions under various circumstances, the clinical feasibility of robust evaluation and optimization are difficult to implement. For example, if we wish to simulate setup errors of up to 8mm at 2mm intervals isocentrically, this would require a total of 729 dose calculations. At our institution, for a typical lung plan, this would require well over 15 hours of computation time. Therefore, robust optimization and verification can potentially benefit from a fast dose calculation method in order to include more information.

In this study, we describe a fast range-corrected dose approximation method. Our method is different from full dose calculation in that we take advantage of pre-calculated dose distribution in order to predict new dose distribution when patient tissue density or WET undergoes slight change. This is motivated by the heuristic observation that perturbation of the WET along the

beam path pulls the dose profile proximally or distally from the nominal setting without significantly changing its overall shape. The new dose distribution can be created by simply shifting the dose profile based on the "iso-WET"along the beam direction. This equivalent-WEPL based dose correction strategy reduces both computational time and computer memory requirements and extends its applicability to include anatomical deformations. We will benchmark the fast range-corrected dose approximation method against the full dose calculation using a commercial treatment planning system that is based on the 3D pencil beam convolution method (87, 88). Furthermore, we will assess the ability of the dose approximation method to estimate DVH curves.

B. Methods

In principle, the dose to a point can be calculated by summing up all contributions of doses from individual beamlets. For the sake of computational efficiency and our purpose, calculation of individual beam is not done again; rather, we make the assumption that the scattered dose from small changes in the patient's anatomy will remain constant and the dose effect is only caused by the change in the cumulative WET at each voxel along the beam path. Taking advantage of the full dose calculation at the nominal position, we can approximate the new dose distribution by shifting dose along the beam path based on the equivalent WET from the original plan. This process of remapping the dose based on the change in WET can be think of pulling protons range in and out of the beam direction. This requires that a single full dose calculation is performed using the planning CT images under the nominal setting.

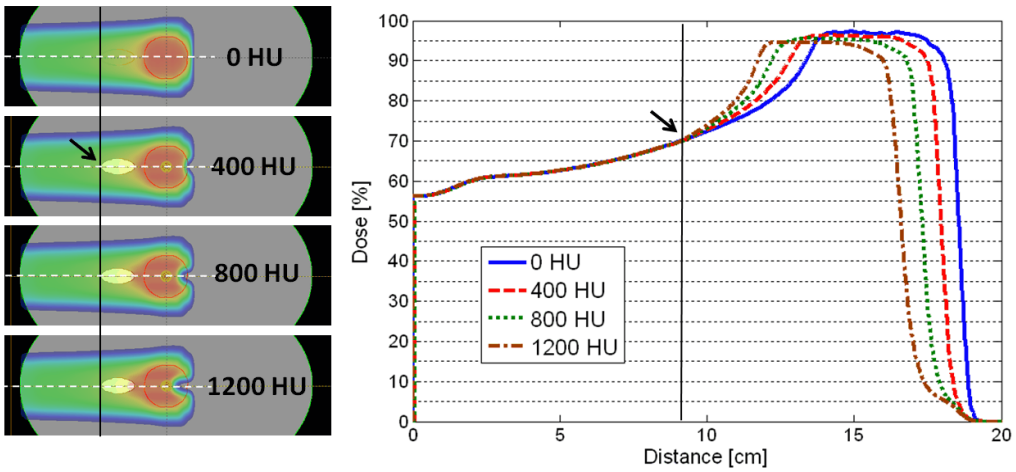

Figure 4-1 An oval shaped heterogeneity was inserted in the beam path to simulate anatomical changes. The density of the object varied from 0 HU to 1200 HU in increments of 400 HU. The line dose profiles beyond the start location of heterogeneity (indicated by the arrow) are pulled proximally towards the source as the density of the hetergeneity increases according to the effective change in the WEPL while the rest of the profile proximal to the heterogeneity remains approximately the same. [Permission to publish this figure was obtained from the *Phys Med Biol*]

In this study, we used the clinically commissioned proton treatment planning system (Eclipse™, Varian Medical Systems, Inc., Palo Alto, CA, USA). This dose distribution is referred as the nominal dose distribution (D) while the dose under the testingsituation is referred as realized dose distribution (d). D will be used as a template when we approximate d under the influence of both setup error and anatomical change. It is essential that we define our coordinate system in beam's eye view in order as it is most natural way to think about how proton's range change in perspective of that traveling protons. We make the z-axis be the depth along the beam's axis. A point dose at an arbitrary coordinate of (x, y, z), with (0,0,0) being defined at the isocenter, under nominal setting can be written as$D_{x,y,z}$.The realized dose to that point can be written as a function of the patient shift error$(\Delta x, \Delta y, \Delta z)$ and change in physical depth (z'), giving $d_{x,y,z}(\Delta x, \Delta y, \Delta z, z')$. It should be noted that that $z'$is a fundamentally different quantity than Δz: Δz is simple the patient setup deviation whereas $z'$is the location in depth under nominal setting which corresponds to the same WET for the depth at z under the realized or testing setting.

For the case of the static dose distribution (i.e. for photon beam), we can immediately approximate the realized dose to a point as follows:

$$d_{x,y,z}(\Delta x, \Delta y, \Delta z) = D_{x+\Delta x, y+\Delta y, z+\Delta z} \quad (1)$$

That is essentially same as sampling the adjacent dose as if the whole dose cloud is shifted according to the setup error. To account for the variant dose distribution, we assume that the perturbation in WET moves point doses in physical space according to their WET values in the original plan.

B.1 Approximation under setup error

If setup error occurs, there will be a change in WET due to the misaligned tissue density along the plane that is perpendicular to the beam's axis. This will lead to a difference in WET between the line segments tracing different locations in space. Therefore, one can write:

$$d_{x,y,z}(\Delta x, \Delta y, z') = D_{x+\Delta x, y+\Delta y, z'} \times INV(z, z'), \quad (2)$$

where$z'$is given by the following line integral relation

$$\int_s^z rsp(x, y, z)dz = \int_s^{z'} rsp(x + \Delta x, y + \Delta y, z)dz. \quad (3)$$

The function $rsp(x, y, z)$ is the relative stopping power ratio from the given CT data and $s$is the effective source position. Simply put, equation (2) approximates the realized point dose by shifting the ray line geometrically (in the BEV coordinate) while adjusting the longitudinal dose profile given by that shifted ray line according to the effective change WEPL from equation (3). In equation

(2), $INV(z,z') = \left(\frac{z'+VSAD}{z+VSAD}\right)^2$ is the inverse square factor to compensate for the loss in protons in a divergent beam with the effective source-to-axis distance (VSAD).Here, the effect of a patient shift along the direction of the beam axis (Δz) is ignored (except for the inverse square factor)because physical shift of patient along the beam direction dose not influence WET.

In general, z'in equation (3) must be solved by iteratively, and therefore is the most time consuming process of this method. The computational time can be decreased by saving the line integral values at different depth with the corresponding D values in computer memory and referencing them as a look up table for later uses.

B.2 Approximation under anatomical change

For anatomical deformation without considering the setup error (assuming the images have been registered together), we can approximate the realized dose as

$$d_{x,y,z}(z') = D_{x,y,z'} \times INV(z,z'), \quad (4)$$

where z' is given by the limit of the following integrals

$$\int_s^z rsp(x,y,z)dz = \int_s^{z'} rsp^{New}(x,y,z)dz. \quad (5)$$

In this case, the realized dose will be a function of the effective change in WET caused by the anatomical deformation which can be tracked using the new images (i.e. daily or weekly CT images), which gives the function rsp^{New}. For the above formula, the location of the line being integrated is identical since no setup error is assumed but $rsp^{New}(x,y,z)$ is used on the right side of the equation (4) to account for the anatomical deformation given by the new images. Finally, the approximation method under setup error and anatomical deformation can be combined to give a general formulation

$$d_{x,y,z}(\Delta x, \Delta y, z') = D_{x+\Delta x,y+\Delta y,z'} \times INV(z,z'), \quad (6)$$

where again, z' is given by the limit of the following integrals

$$\int_s^z rsp(x,y,z)dz = \int_s^{z'} rsp^{New}(x+\Delta x, y+\Delta y, z)dz. \quad (5)$$

Below step generalize the algorithm for program implementation described in this method:

Step 1.Calculate the WEPL to a point along the beam path under the nominal setting.

Step 2.Translate beam's isocenter according to the setup error or introduce new CT images.
Step 3. Calculate WEPL along the corresponding line segment and locate the physical point along the depth which has the same WEPL as calculated in Step 1.
Step 4. Correct for inverse square factor based on the original physical location found in Step 3.
Step 5.Repeat steps 1-4 for all points in the image.

B.3 Validation for selected patient cases

In order to validate our dose approximation method, we compared the dose distributions calculated using a static dose approximation, our proposed range-corrected dose approximation, and a full 3D pencil beam convolution method from our clinical treatment planning system (TPS). In this case, we consider the TPS calculation to be the gold data. All dose calculations were performed using a dose grid resolution of $2 \times 2 \times 2.5\, mm^3$. First, a lung cancer patient was selected. The patient received 4-dimensional computed tomography (4DCT) scans for treatment planning and weekly over the course of treatment with a 1mm pixel size and 2.5mm slice thickness over the first 6 weeks (denoted week0 to week6) of treatments. Only the time averaged 4DCT data set is used for all dose calculations. Treatment plan under nominal setting and all consequent dose calculations were done on these averaged CT data sets following the clinical protocol used at our institution (89). In order to subject our method to the extreme case, the PTV was defined as 5mm uniform expansion of CTV and we deliberately simulated setup error up to 8mm, exceeding the margin bound. . For anatomical deformation simulation, the volumes of interest were contoured by a physician on the planning CT and were deformed to weekly CT data sets using an in-house developed deformable image registration software (90, 91).The nominal dose was calculated using the planning CT data set with no assumed setup error via the spot scanning beam delivery method with single-field optimization (92). The setup error was simulated by shifting the planning CT images along the Anterior-Posterior direction ±8mm in 2mm intervals. At each interval, doses were calculated using all three different methods: static dose approximation, our proposed range-corrected dose approximation, and a full recalculation with the TPS. For the weekly CT data sets, doses were calculated using all three different methods after manual alignment of beam's isocenter based on the bony anatomy to separate the effect of setup error.

Similarly, we validated the proposed method on a prostate and a head & neck (HN) patient case with inter-fractional anatomic changes to show the applicability of the proposed method to these sites as well. The prostate case was chosen due to a change in the femur position on the day of treatment. The HN case was chosen because of a substantial change in the nasal air cavity in the beam path on week 6 of treatment, which was partially due to a head rotation

and tissue/fluid variation in the nasal cavity. We used a 270° beam angle for the prostate case, and a 0° beam angle for the HN case.

The overall accuracy of both approximation methods were quantified through the use of a 3D gamma analysis tool developed in-house with 3% dose and 3mm distance criteria (93). Furthermore, we quantify the accuracy of the cDVHs derived using the range-corrected method (The difference is denoted as ΔcDVH).

C. Results

C.1 Dose distribution comparison and 3D gamma analysis

For all cases observed, the magnitude of dose variation increased as setup error increased in all direction. Also for the lung case, the dose variation was gradually increased from week0 to week6. But both prostate and HN cases showed no obvious increment in dose variation over the weeks. Table 4-1 shows % volume change of the tumor related volume (i.e. integrated gross tumor volume and clinical target volume (IGTV and ICTV), and GTV-50 and CTV-50, the volumes for the exhale phase of the breathing cycle) for the lung patient over the course of treatment. The largest variation of the planned dose distribution amongst all of the simulations was observed when we recalculated dose using the 6^{th} treatment week's CT images for both lung and HN cases and the 1^{st} week CT images for the prostate case.

The difference in dose distribution due to both setup and anatomical change were noted. Figure 4-2 (a) and (b) compares planned dose distribution and the realized dose distribution using full dose calculation. The most significant contributing factor to the change in dose distributions for the lung case was the patient weight loss and tumor shrinkage. The realized dose distribution given by the static approximation (Figure 4-2 (c)) fails to adjust for such a change and thereby significantly underestimates the dose to contralateral lung. However, the realized dose distribution computed using the range-corrected method (Figure 4-2(d)) is able to estimate the change in depth penetration of the proton beam with a reasonable accuracy, displaying visually similar to the result given by the TPS dose calculation

Table 4-1 The measured volume change of the target volumes of interest observed in the weekly CT images for the lung case. The structures were contoured on the planning CT and deformed to the weekly CT images using in-house deformable image registration software. For the selected patient case, a reduction of 41% of the gross tumor volume (GTV-T50 and IGTV) and 21% of the clinical target volume (CTV-T50 and ICTV) was observed.[Permission to publish this figure was obtained from the *Phys Med Biol*]

	Volume [cc] (% Volume change)			
Site (week)	GTV-T50	CTV-T50	IGTV	ICTV
Lung (week 0)	128 (0%)	323 (0%)	148 (0%)	331 (0%)
Lung (week 1)	110 (−14%)	300 (−7%)	126 (−15%)	307 (−7%)
Lung (week 2)	96 (−25%)	277 (−14%)	110 (−25%)	286 (−14%)
Lung (week 3)	90 (−30%)	275 (−15%)	104 (−29%)	282 (−15%)
Lung (week 4)	82 (−36%)	264 (−18%)	96 (−35%)	272 (−18%)
Lung (week 5)	77 (−40%)	257 (−20%)	90 (−39%)	264 (−20%)
Lung (week 6)	76 (−41%)	254 (−21%)	88 (−40%)	262 (−21%)

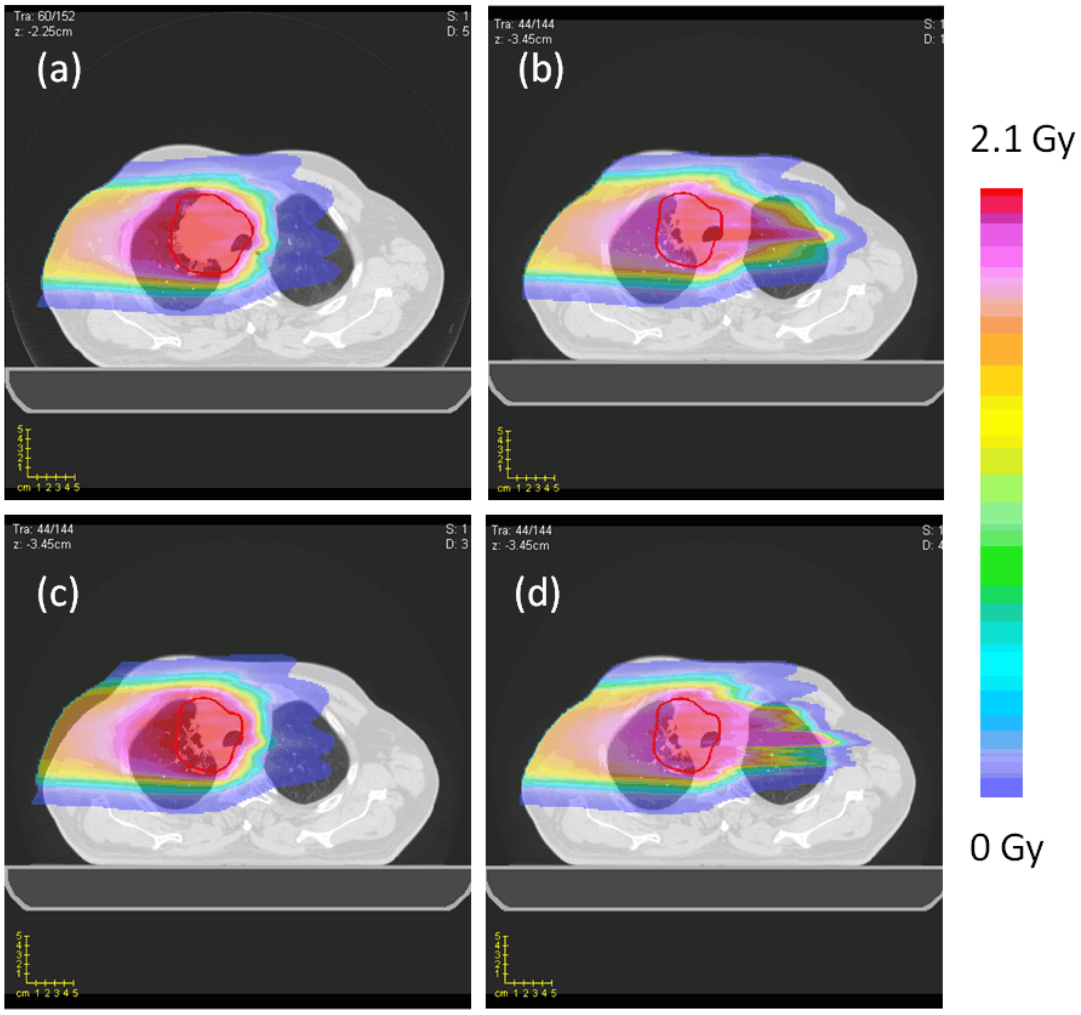

Figure 4-2 The dose distributions for the lung case. (a) The full dose (TPS) calculation on the lung planning CT (planned dose distribution). (b) The full dose (TPS) calculation on the lung week6 CT (realized dose distribution). (c) The static dose approximation on the lung week6 CT. (d) The range corrected dose approximation on the lung week6 CT.[Permission to publish this figure was obtained from the *Phys Med Biol*]

Figure 4-3 shows percentage dose difference maps of the dose distributions between the full dose recalculation and the static dose approximation, and the full dose and the range corrected dose approximation. From this figure it is obvious that the static dose distribution can underestimate (i.e. or does not account at all) the overshoot of proton beam. But our approximation method was able to predict the change reasonably well. The result of the gamma analysis is presented in Table 4-2. The lowest passing rate was observed at the limit of our simulation ranges (8mm setup errors and lung 6th week). Under the chosen criteria (3% dose and 3mm distance), the range-

corrected method achieved a 93% passing rate for an 8mm setup error while the static dose approximation method achieved only an 81% passing rate. For the weekly CT simulation, the range-corrected method achieved a 86% passing rate for the 6th week CT while the static dose approximation method achieved only 36% passing rate.The worst passing rate found for the 3D gamma analysis of the prostate case was 89% and 83% for the range corrected and the static approximation methods, respectively. Similarly, the worst passing rate found for the HN case showed 84% and 70% passing rates for range corrected approximation and static approximation methods respectively.

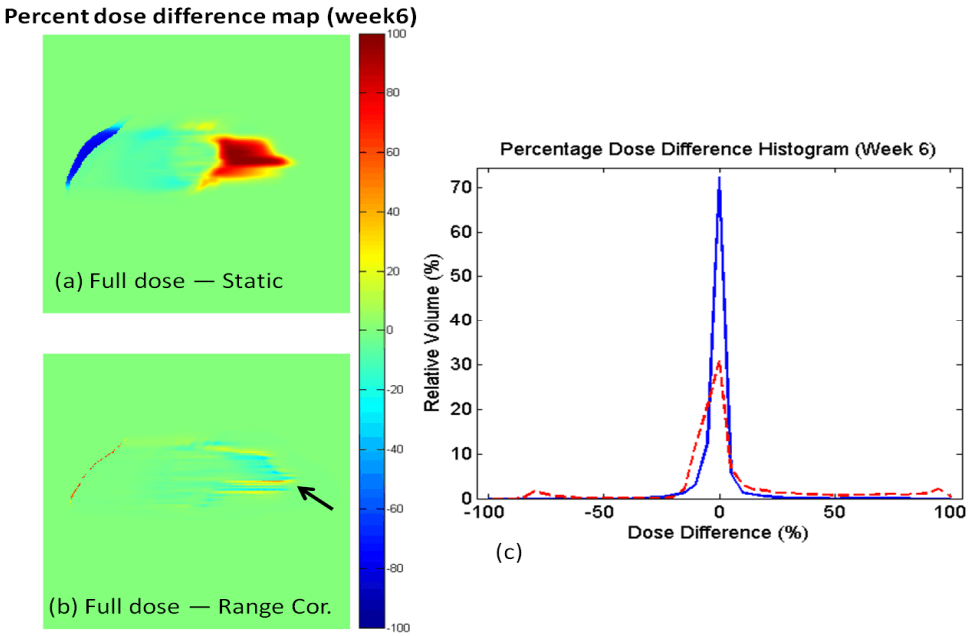

Figure 4-3 The percent dose difference map on the lung week6 CT between dose distribution using full calculation and dose distribution using (a) static dose approximation, (b) range corrected approximation, and (c) the percentage dose difference histograms for the two difference maps. Red dashed line in the histogram is derived from (a) while blue solid line is derived from (b).[Permission to publish this figure was obtained from the *Phys Med Biol*]

Table 4-2. The result of the 3D gamma analysis on both the ranged-corrected approximation and static dose approximation with respect to the full dose (TPS) calculation under setup error and weekly CT simulations. A passing criteria of 3% dose difference and 3mm distance-to-distance agreement was used. For the sake of simplicity, for both prostate and HN cases, only the worst passing rate observed during weekly simulation is shown (week1 for prostate and week6 for HN). [Permission to publish this figure was obtained from the *Phys Med Biol*]

	3D gamma (% passing)			3D gamma (% passing)	
Lung AP Setup error (mm)	(3%, 3 mm) Range corrected	(3%, 3 mm) Static	Site (week)	(3%, 3 mm) Range corrected	(3%, 3 mm) Static
−8	94%	81%	Lung (0)	100%	100%
−6	95%	87%	Lung (1)	89%	75%
−4	97%	93%	Lung (2)	89%	74%
−2	98%	98%	Lung (3)	91%	66%
0	100%	100%	Lung (4)	89%	54%
2	98%	98%	Lung (5)	86%	43%
4	96%	93%	Lung (6)	86%	36%
6	95%	88%	Prostate (1)	89%	83%
8	93%	83%	HN (6)	84%	70%

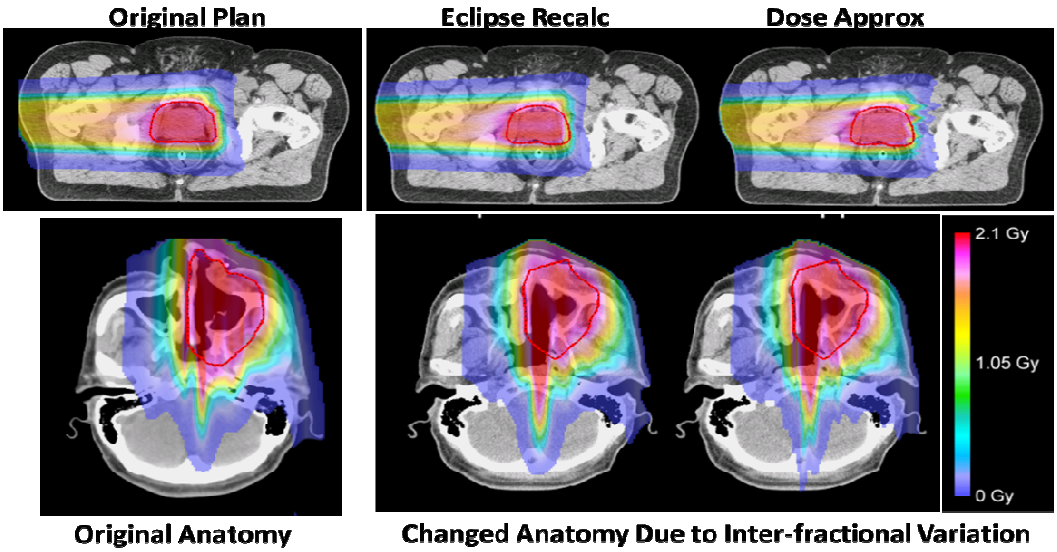

Figure 4-4 A comparison of the dose calculation results in the presence of inter-fraction anatomical changes. The original plan and original anatomy for a prostate case (top row) and a HN case (bottom row) are shown to the left column. The dose distributions for the changed anatomy calculated by the commercial treatment planning system (Eclipse, Varian Medical Systems) are shown in the middle column, and the dose distributions calculated by the range-corrected dose approximate method are shown to the right, respectively. [Permission to publish this figure was obtained from the *Phys Med Biol*]

Figure 4-4 shows the comparison visually. The original plan calculated for the anatomy in the treatment planning CT image is shown in the left column for each case; the dose distributions in the changed anatomy (due to inter-fractional variations) are calculated by the TPS and the dose approximation method in the right column, respectively. It can be seen that the range-corrected dose approximation method did a reasonable job overall. Most differences are seen in regions with sharp change in WET. In these regions, more accurate modeling of lateral scatter appears to be important.

C.2 DVHs comparisons

The change in the planned dose distribution due to both setup and anatomical deformation resulted in variation of cDVHs derived from realized dose distributions. Figure 4-5 compares the DVH-bands (the area enclosed by the envelope of the cDVHs) of various structures using full dose calculation and different dose approximation methods. The overall shape of the DVH-bands derived using range-corrected method closely resembled the DVH-bands derived using the full dose calculation while the DVH-bands derived using static method mostly under estimated the thickness of the bands for the CTV and other structures (except for the esophagus under setup error simulation). It is clearly

shown that the static dose approximation completely failed to account for the decrease in dose to the target volume and increase in dose to the left lung and esophagus. Table 4-3 lists the RMS and the maximum difference from the ΔcDVH. Overall, the RMS deviation and maximum difference were larger for the CTV and esophagus than for other structures due to their small volume size and their position near the high dose gradient. For the lung case, the largest of the RMS deviation found were within 2% for both the setup and weekly simulation. The largest of the maximum differences were found to be within 4% and 8% for setup and weekly simulation, respectively. The average of the maximum differences over all simulations was found to be 1.5% and 2.6% for setup and weekly simulation, respectively for the lung case.

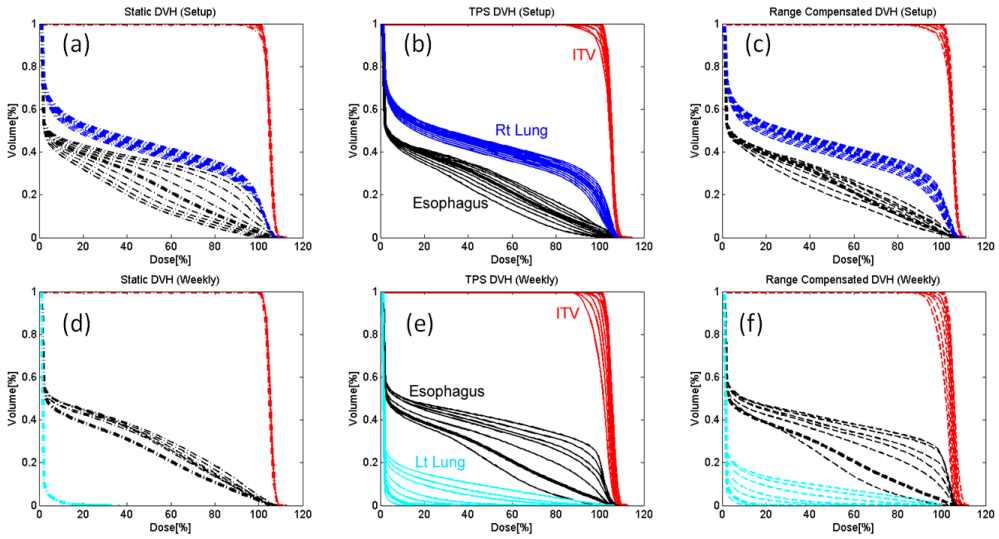

Figure 4-5 ThecDVHs of the CTV (red), involved lung (dark blue), contralateral lung (light blue), and esophagus (black) derived from realized dose distributions under various setup error (top row) and weekly imaging (bottom row) using static approximation (a, d), full dose calculation (b, e), and range-corrected approximation methods (c, f). The thicker lines indicate original DVHs derived from the planned dose distribution. [Permission to publish this figure was obtained from the *Phys Med Biol*]

Table 4-3 The root mean square (RMS) deviations between the cumulative DVHs derived using a full dose (TPS) calculation and range-corrected dose approximation method under various simulations. The first two tables are from setup error (in Anterior-Posterior direction) and weekly simulations of lung patient. For the sake of simplicity, for both prostate and HN cases, only the worst passing rate observed during weekly simulation is shown (week1 for prostate and week6 for HN). [Permission to publish this figure was obtained from the *Phys Med Biol*]

Lung	CTV Δ cDVH (% vol)		Lung (R) Δ cDVH (% vol)		Esophagus Δ cDVH (% vol)		Lung (L) Δ cDVH (% vol)		Cord Δ cDVH (% vol)	
Setup error (mm)	RMS (%)	Max (%)	RMS (%)	Max (%)	RMS (%)	Max (%)	RMS (%)	Max (%)	RMS (%)	Max (%)
−8	0.4	1.9	0.3	0.6	1.9	3.4	0.4	1.4	1.1	2.5
−6	0.3	1.5	0.3	0.6	1.5	2.3	0.5	1.2	0.9	2.2
−4	0.4	2.2	0.3	0.6	1.1	2.0	0.4	0.9	0.8	1.8
−2	0.4	2.1	0.2	0.7	0.9	1.6	0.3	0.6	0.5	1.3
0	0.0	0.0	0.0	0.0	0.0	0.0	0.0	0.0	0.0	0.0
2	0.6	3.3	0.2	1.0	0.4	0.8	0.3	0.6	0.2	0.5
4	0.7	3.5	0.3	1.4	1.4	2.5	0.4	1.0	0.3	0.4
6	0.6	3.7	0.3	1.6	2.0	3.3	0.5	1.2	0.3	0.6
8	0.7	4.0	0.4	1.6	1.8	3.1	0.6	1.5	0.3	0.7
	CTV Δ cDVH (% vol)		Lung (right) Δ cDVH (% vol)		Esophagus Δ cDVH (% vol)		Lung (left) Δ cDVH (% vol)		Cord Δ cDVH (%vol)	
Site (week)	RMS (%)	Max (%)	RMS (%)	Max (%)	RMS (%)	Max (%)	RMS (%)	Max (%)	RMS (%)	Max (%)
Lung (0)	0.0	0.0	0.0	0.0	0.0	0.0	0.0	0.0	0.0	0.0
Lung (1)	0.5	2.8	0.2	1.2	1.0	2.3	0.4	1.0	1.0	1.6
Lung (2)	1.0	6.1	0.4	1.3	1.6	3.3	0.5	0.7	0.2	0.5
Lung (3)	1.0	6.8	0.6	0.9	0.8	3.0	0.4	0.6	0.3	0.7
Lung (4)	1.0	6.0	0.4	0.6	1.4	5.7	0.4	0.8	0.1	0.3
Lung (5)	1.0	6.6	0.6	1.2	1.9	7.6	0.9	1.4	0.3	0.7
Lung (6)	1.4	5.0	0.6	1.0	1.2	5.9	0.8	1.4	0.4	0.8
	STV		Bladder		Rectum		Ant rectal wall		Femoral heads	
Prostate (1)	1.1	7.2	1.0	1.7	0.6	0.9	0.7	1.8	0.2	0.5
	CTV1		Brain stem		Left optic nerve		Right optic nerve		Left parotid	
HN (6)	0.8	4.8	1.6	6.4	1.6	4.2	2.9	6.2	3.8	7.9

D. Discussion

The main purpose of this fast proton dose approximation was to be able to roughly estimate the realize dose distribution under the influence of both setup and range uncertainties caused either by the inherent range or anatomical deformation in patient. In chapter 4, we demonstrated how statistical mean or standard deviation can be used to show robustness of a given plan. When computing such parameters that are computed based on the large number average (i.e. order of couple hundreds), each sampled calculation does not need to be so accurate to compute the averaged quantity accurately: standard deviation of sampled mean is inversely proportional to the square root of the sample numbers. While the proposed method does not give a sufficient accuracy for treatment planning and quality assurance, it can be used for gauging a plan's sensitivity to setup and range error, for intermediate dose calculations during plan optimization, or for on-line assessment of major dosimetric impacts. For this reason, it may be sufficient for such important applications.

Our choice to use the 3D gamma analysiswas to demonstrate that the approximated dose distribution is spatially comparable to the full dose calculation. The overall accuracy in terms of percentage passing rate presented in table 4-2 depends heavily on the choice of passing criteria. In this work, we selected a 3% dose difference and 3mm distance-to-agreement criteria and found that the average passing rate was 93% and 89% for setup errors and anatomical change. The 3% dose 3mm criteria was chosen arbitrarily and the question of what criteria to be used and what the minimum passing rate should be considered acceptable would depend on the nature of applications.

Aside from the actual dose distribution itself, we also measured the accuracy of DVHs derived using the approximated dose. This is highly relevant to the application of the proposed method since when evaluating the robustness of a plan or the dose on the day of treatment, it is necessary to summarize the multiple 3D dose distributions into 2D dosimetric information such as DVH-bands. Previously, Cho et al. (10) discussed the clinical recommendations on accuracy of DVH curves. Based on the assumption that the point dose accuracy of 2-4% is clinically tolerable, the RMS of the difference in relative dose between two cDVH should be less than 1-2%. This RMS criterion measures overall accuracy of the cDVH curve and permits certain dose bins to deviate more than the 2%, while still being clinically acceptable. From our experience, this can happen if the OAR is small or is situated near the beam penumbra and high dose gradient. For the proposed method, table 4-3 shows that RMS deviation is well within 2% for all simulations considered except for the right-optic nerve and left parotid from H&N case.

It's worth mentioning that our test cases were should be considered the worst case scenario. In the lung case, the choice of the single lateral beam arrangement maximized the dosimetric effect of anatomical changes. We selected this case to test if our dose approximation method can do well in the presence of significant anatomical changes. In a typical clinical plan where multiple beam arrangement is used, the magnitude of error in inaccuracy of our approximation method would scale down. We also challenged the proposed method using a prostate and a HN case. Both cases had a relatively large change in anatomy that would affect the proton beam delivery for these sites. The results were similar to the ones found for the lung case (See table4-2 and table 4-3).

In our current implementation, we only used a single CPU for dose calculation, which already can achieve the calculation speed of around one second. Further reduction of computation time can be realized because the proposed method allows for parallel calculation of using independent beamlets or ray-tracing lines. We expect that the implementation of this application in multi-core environment would increase the computation time greatly.

One of the limitations of the proposed method is that it does not consider change in scattered dose separately from the primary dose when mapping the pre-calculated nominal dose. Also, the ray-casting of proton tracks are done in parallel rather than divergence. The errors resulting from this simplification will be more pronounced for greater displacement of setup error and near regions with a sharp gradient of tissue density change lateral to the beam direction. The pencil-beam based dose calculation algorithm used in Eclipse treatment planning system is also not perfect in modeling the lateral scatter under complex geometries or heterogeneities. A montecarlo based dose calculation would produce more accurate assessment of the proposed method.

E. Conclusion

In order to expedite robust plan evaluation or optimization process, a simple and fast proton dose approximation method was introduced. The proposed method takes advantage of the pre-calculated planned dose distribution when approximating a new dose distribution by correcting the difference in proton range under setup error or anatomical deformation given by the new set of CT images. The accuracy of the range-corrected method was shown to be superior to the static dose approximation method. The proposed method could be used for robust evaluation, robust optimization, and on-line treatment assessment.

CHAPTER 5: STATISTICAL ROBUST PLAN EVALUATION

A. Introduction

In radiotherapy, once a treatment plan has been determined, it must be carefully assessed beforetreatment can be approved. Conventional plan assessment includes checking dose distribution quality (e.g., conformity, homogeneity, and cold or hot spots) by overlaying the 3D dose distribution on patient anatomical images. The information contained in the 3D data is too complex and voluminous for the practical purposes of prescribing, reporting, and checking the plan. To mitigate this problem, current clinical practice includes, in addition to 3D dose distribution confirmation, theuse of volume-specific metrics,such as the mean dose of a volume of interest (VOI)andits dose-volume histogram (DVH)or derived quantities (e.g.,V_D: the volume receiving at least dose D). However, the dose distribution and DVHrepresent a nominal situation that does not account for the uncertainties associated with the beam delivery process. Dose uncertainty can be caused by dose calculation inaccuracy(94), estimated stopping poweruncertainty(95), daily patient set-up fluctuation(96),and interfractionalandintrafractional anatomy and motion changes(97).These uncertaintiesmake it difficult to accurately assess plan robustnessin proton and conventional photon therapy.Thus, a geometrically expanded volume that is used for beam design, such as a planning target volume (PTV),is used for treatment evaluation.For example, under the assumption that dose distribution is static in space and the extent of motion of the clinical target volume (CTV) is contained within the margin added to create the PTV, PTV coverage can be considered an underestimate of CTV coverage(98). For this reason, PTV is often usedin prescribing and reporting rather

than the CTV itself(98). The assumption that dose distribution is static in space is crucial for such interpretation. However, a previous study revealed that this assumption does not apply to protons because of their sensitivity in range to the density variationin the beam path(99).Therefore, the paradigm of using PTV as a surrogate for CTV under uncertainty does not translate well to proton therapy.

Recently, researchers reported evaluation methods that account for both set-up and range uncertainty in an effort to assess robustness directly. Lomax *et al.*(100)proposed the useof worst-case dose distribution and DVHs that are derived from dose distributionscalculatedunderextreme conditions. Albertini*etal.*(101)proposed the use of an error-volume histogram that describes the variation in the point dose of 3D information as simpler 2Dinformation.Trofimov*etal.*(102)proposed the use the DVHbands to visualize the range of DVH variation under uncertainties.However, these methods rely on dose distributions calculated under a handful of extreme conditions (i.e., 6 calculations for set-up errors and2 calculations for underestimated and overestimated range errors). Although these methods are fast and convenientmeans of comparing the robustness of two different plans, the metrics used are generally too conservative or even unrealistic and lacks statistical interpretations. On the other hand, Maleike*et al.* (103) and Henriquez*et al.*(104)proposed methods that fully characterize the probability density function (PDF)of individual point dose distributions.However, their studieswere limited to dose variations caused by predefined organ motionmodels (103) anddosecalculationinaccuracies (104).Using statistical methods to characterize dose uncertaintiescaused by set-up and proton range errors is difficult because the PDF of a point dose distribution under such uncertainties is not known. To our knowledge, no

studieshaveperformedacomprehensive statistical analysis of the effectsof set-up and range uncertainties on proton plans.Therefore, in this study, we proposed and implemented a practical method to evaluateproton plan robustnessthat is based onwell-known statistical parameters such as expectation values and sampled standard deviations.

B. Methods

B.1 Patient selection and treatment planning

We retrospectively evaluated the passively scattered beam proton therapy plans of 15 lung cancer patients who were randomly selected from the randomized trial protocol group of patients who had been treated in the past year at our institution. Their treatment plans had been developed usingthe following planning objectives: ≥ 99% of the PTV receiving ≥ 95% of the prescribed dose (i.e., 14 patients prescribed to 74Gy and 1 patient to 60Gy); total lung $V_{20Gy}$of ≤ 37%; mean lung dose of≤ 22Gy; as low as possible doses to the esophagus $V_{65Gy}$and$V_{45Gy}$and heart $V_{60Gy}$and V_{30Gy}; and maximum spinal cord dose of≤ 50Gy. It should be noted that 3 out of 15 treatment plans were not met with the PTV coverage criteria due to the limit imposed by other organs at risk but approved for treatment under physician's discretion. On the basis of the 4DCT data, each gross tumor volume at individual phases was used to develop the integrated gross tumor volume, and this was further expanded to become the integratedCTV (ICTV).The uncertainty in the proton range was addressed by adding a margin equivalent to 3.5% of the total water equivalent path length to both the proximal and distalICTV surfaces along the beam path. The uncertainty in the set-up position was considered by expanding the beam-specific aperture laterally with respect to the ICTV in the beam's

eye view.The tissue density change along the beam path as a result of the set-up error was accounted by smearing the local depth of the compensator. A nominal dose was calculated on an averaged 4DCT image set. For the purpose of conventional plan evaluation, a PTV was created by expanding ICTV with 5-mm margins. A more detailed description of the treatment planning procedure used at our institution and in this study can be found elsewhere(105).

B.2 Statistics and simulation

A VOI consisted of smaller volume elements or voxels (total number, n). A dose to the ithvoxel(v_i)was considered a random variable (d_i). If thePDF of d_i(PDF_i) for all n is known, the expectation value of DVH or $E[DVH]$ can be derived by the weighted sum of the probability of a given voxel receiving a certain dose level.For the sake of convenience, the framework and definition used in (104) are repeated here in brief. DVH is defined as $DVH(k) = \sum_{i=1}^{n} T_i^k v_i$, where T_i^k is 1 if$d_i \geq k$; otherwise, it is 0. When we use an expectation value operator, we get$E[DVH\ (k)] = E\left[\sum_{i=1}^{n} T_i^k v_i\right] = \sum_{i=1}^{n} E[T_i^k]\ v_i$. Because T_i^k can be considered a Bernoulli random variable,$E[T_i^k]$ is equal to $P[d_i \geq$k], which turns the above equation into

$$E[DVH(k)] = \sum_{i=1}^{n} P[\ d_i \geq\ k]\ v_i = \sum_{i=1}^{n} \left\{ \int_k^{\infty} PDF_i(x)\ dx \right\} v_i. \qquad (1)$$

To proceed further,we must determinethePDF_i.Even thoughthePDF_i isunknown, it can be closely approximated from extensive sampling of point dose values.Acumulative dose of a treatment course that consists of multiple fractions is considered one sample dose distribution. To archive the samples, systematic setup errors ($\Delta x_s, \Delta y_s, \Delta z_s$) were randomly drawn from a Gaussian distribution function with the mean at the planning isocenter and the standard deviation equal to 2mm in all $x, y,$ and z directions. Similarly,

random setup errors ($\Delta x_r, \Delta y_r, \Delta z_r$) were randomly drawn from Gaussian distribution function but with its mean at the shifted error position given by ($\Delta x_s, \Delta y_s, \Delta z_s$). The systematic error varied over the courses but was fixed over the fractions within a course.The random set-up error varied over all fractions. Asystematic range error that varied over the courses was alsodrawn from the Gaussian function, with a standard deviation equal to 1.5% of the nominal CT number-to-stopping power ratio calibration curve.In this study, 60 treatment courses (i.e. a course is composed of multiple fractions) are simulated for each patient; each treatment course consists of 10 daily fractions that comprise 600 dose distributions. Although, the actual treatment course consisted of 37 fractions, in our preliminary study,in which we evaluated the convergence of the $E[DVH]$ as a function of the number of simulations of treatment courses and fractions, we found that the influence of the uncertainty over the fractions converged when 60 treatment courses comprised of 10 fractions are simulated. (See figure 5-1).

Despite the imposed limit on simulation counts, 600 dose calculations per given plan is too time consuming and computationally expansive forpractical settings.Therefore, dose distributions were approximated using a validatedfast dose calculation method(106). The fast dose calculation method approximates proton dose from original dose distribution under perturbation of radiological path length caused by set-up isocenter and CT image change. For the sake of continuity of this chapter, we postpone the detail description of the fast proton dose calculation used in this method to next chapter (see Chapter 4).

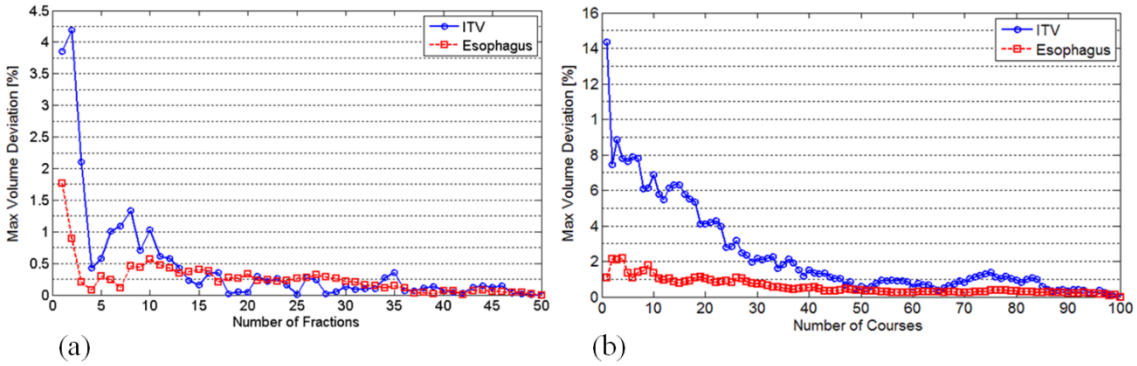

Figure 5-1 A selected case was pre-evaluated to determine the appropriate number of courses andfractions. The $E[DVH]$ was computed while increasing the number of simulations counts, and the maximum difference from the previously calculated $E[DVH]$ was recorded. (a) After approximately 10fractions the maximum deviation was contained within 1%. (b) Similarly, after approximately 60 fractions (i.e. each fraction consisted of 10 fractions) the maximum deviation was contained within 1%. To give a conservative estimate, the ICTV and esophagus were chosen because the DVHs of both structures are sensitive to the considered uncertainty;its position near high dose gradient and its smaller volume size respectively.

On the basis of these sample dose distributions, the integration of PDF_i in equation (1) was closely approximated to computethe$E[DVH]$ of various VOIs. The standard deviation of DVH or $SD[DVH]$ was estimated using the following definition of sample standard deviation:

$$SD[DVH(k)] = \sqrt{\frac{1}{N-1}\sum_{i=1}^{N}(DVH_i(k) - E[DVH(k)])^2}, \qquad (2)$$

Where$N$ is the number of sampled dose distributions over the courses ($N = 60$).We compared the DVH under nominal setting ($N[DVH]$) against $E[DVH]$ to assess if what you see on the treatment plan is what you would get under the influence of uncertainties. Furthermore, we plotted the area extended by all DVHs from 60 simulated treatment courses ($C[DVH]$) and from 600 simulated fractions ($F[DVH]$) to gauge the difference between the variation of realizable DVHs over treatment courses against the variance of

DVHs over single daily fractions. A sample distribution of both setup errors in 3D scatter plot and randomly generated CT calibration curve is shown in figure 5-2.

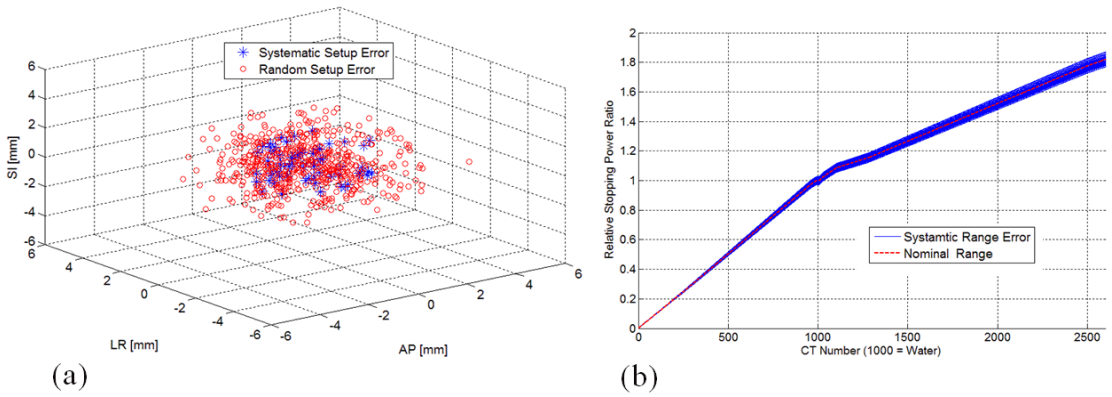

Figure 5-2 (a) The scattered plot of random and systematic setup errors and (b) systematic range error calibration curves randomly sampled from Gaussian distributions.

B.2 Probability map of risk

Above method predominantly addresses uncertainties in DVHs or volumetric parameters.However, a thorough plan assessment involves spatially confirming dose distribution.To spatially visualize dose uncertainty, we implemented a similar method,described by Maleike*et al* (103). We visualized the probability of a given voxel not meeting the clinical goal (i.e. risk). For example, the probability map of risk can show precisely which voxels in the ICTV willnot likely meet the prescription dose under uncertainties;these probabilities can be displayed as a heat map, overlaid on the CT images.The probability of risk for voxel v_i is calculated using the PDF_i which was approximated from 600 sampled dose distributions (see figure 5-7). For example, the probability of risk for a voxel within an organ is calculated by integrating the

approximated PDF with its limit of integral defined by the dosimetric objectives of that organ.

The plan robustness evaluation software, which comprised all the methods mentioned in this section, was implemented as a plug-in module to the CERR treatment planning system (107) (version 4.0,beta 2) on an Intel Xeon X5680 3.33 GHz CPU-based computer. The computation time for one patient was approximately 15-20 minutes.

C. Results

C.1 DVH and volumetric parameter assessment

For each patient, we visualized and quantified the variation in DVHs that resultedfrom set-up and range uncertainties. In all cases, the area extended by the $F[DVH]$was much larger than that covered by the $C[DVH]$ as shownin figure 5-3 through 5-5 for the ITV, both lungs, and other organs at risk respectively.This was expected because over the treatment course, errors from random set-up uncertainties tend to averageout and when the cumulative dose is calculated by summing over the fractional doses, the extent of the random setup error was significantly reduced.

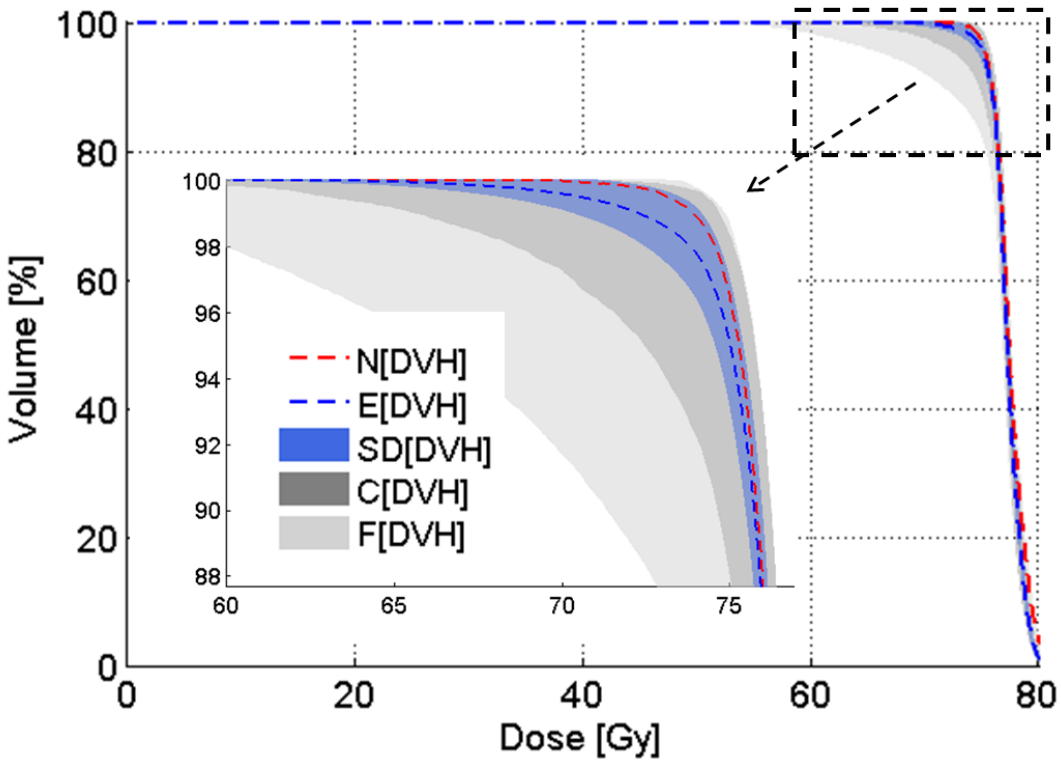

Figure 5-3 Overall robustness of the treatment plan under uncertainty was assessed by comparing the DVH under nominal setting ($N[DVH]$ or dash red line) with its expectation value ($E[DVH]$ or dash blue line) or standard deviation ($SD[DVH]$ or blue band). The area extended by DVH variations over the realizable treatment courses ($C[DVH]$ or dark gray area) and the area extended by DVH of single fractional cases whose lower bound closely approximates the worst-case scenario ($F[DVH]$ or lighter gray area) are also compared.

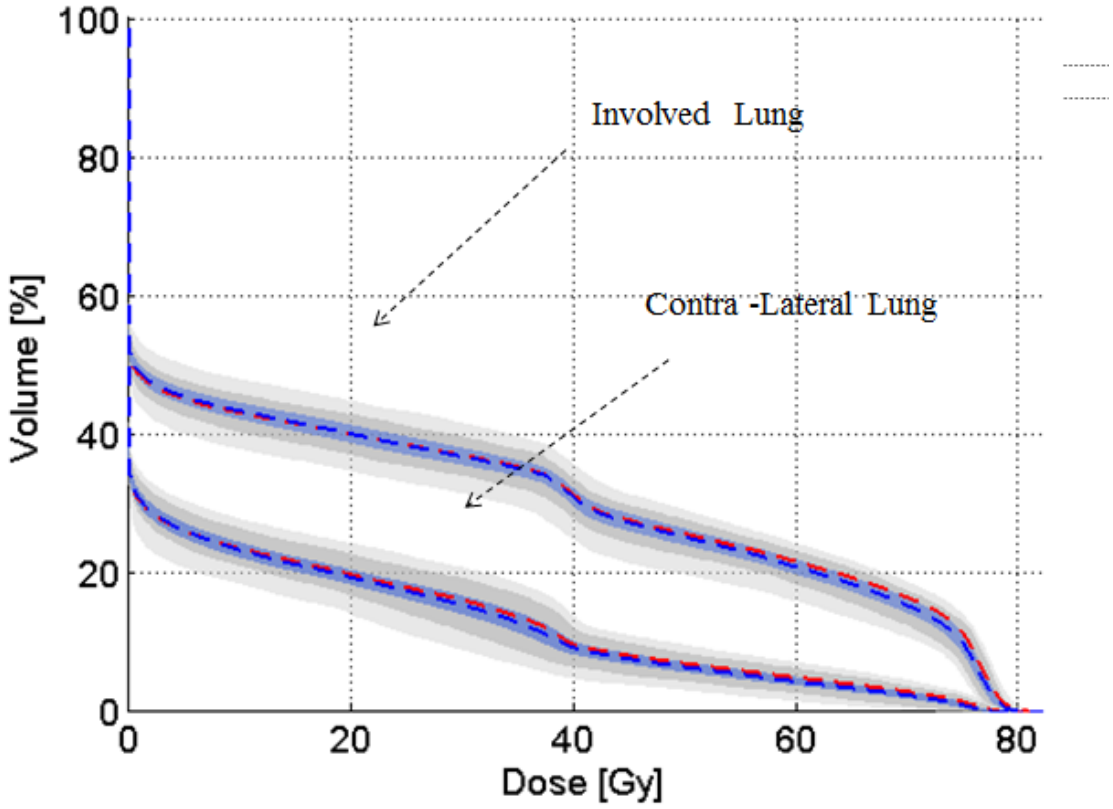

Figure 5-4 See the legend from figure 4-3. Shown here are the two lungs.

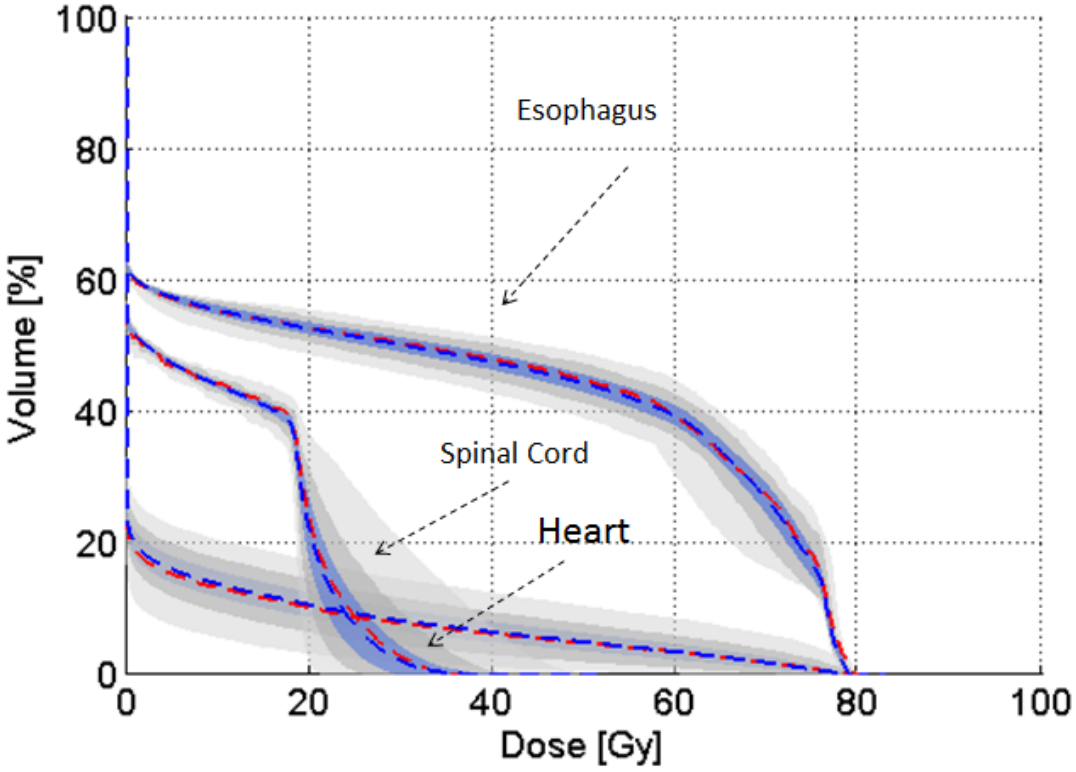

Figure 5-5 See the legend from figure 4-3. Shown here are the esophagus, spinal cord, and heart.

Furthermore, $E[DVH]$, which represents the best possible estimateof the true DVH, was comparedwith the DVH computed under the nominal setting. Figure 4-6 shows the boxplots of volumetric parameters that were used as constraints during treatment planning.

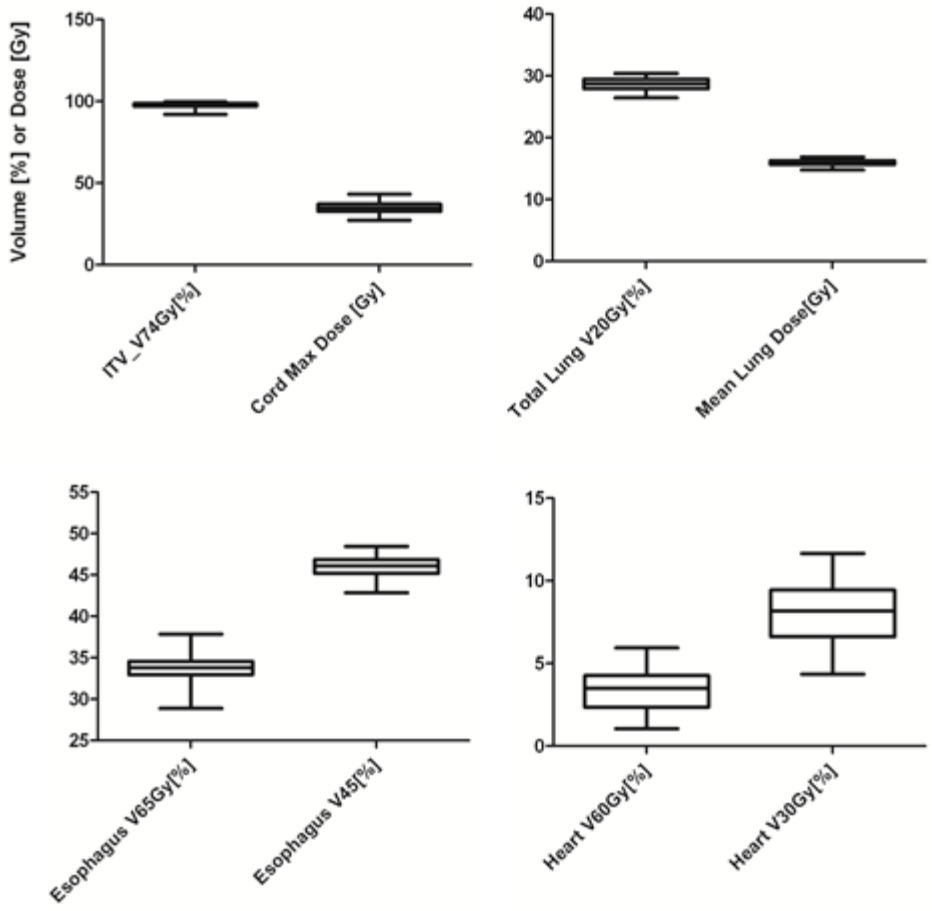

Figure 5-6 The effect of uncertainties on the planning parameters (i.e., constraints) were visualized using box plots that display the smallest, lower quartile, median, upper quartile, and the largest values observed.

The statistical assessment of volumetric parameters used during treatment planning for all 15 patients is summarized in table 5-1. The mean ICTV V_{74Gy}coverage under uncertainties was only 1.1% lower than that calculated under the nominal plan. In cases in which one standard deviation lower than the expected value occurred (i.e., corresponding to a 16% chance under the normality assumption), 9 of 15 patientscan be estimated to receive2% less than in the nominal plan V_{74Gy}. In particular, patient 1,whohad the largest standard deviation value,would receive approximately 5% less than in the nominal plan. For the total lung dose, the V_{20Gy} and mean lung dose fluctuationswere less than 1% on average,whereas the esophagus and spinal cord dosesexperienced substantial fluctuations, with a maximum standard deviation of up to 5% and 5.5Gy for the esophagus V_{45Gy} and maximum spinal cord dose, respectively.

C.2 Probability map of risk

Probability map of risk was visualized at all slice locations of VOIs. Figure 5-7 shows the utility of a probability map of risk,which is intended to evaluate the effect of uncertainties on the plan's dose distribution, in terms of clinically relevant dosimetric goals for each VOI.

Table 5-1 Statistical Analysis of Plan Robustness on 15 Lung Cancer Proton Treatment Plans

	ICTV		**Total lung**				**Esophagus**				**Heart**				**Spinal cord**	
	$V_{74Gy}[\%]$		V_{20Gy} [%]		MLD [Gy]		V_{65Gy} [%]		V_{45Gy} [%]		V_{60Gy} [%]		V_{30Gy} [%]		Max dose [Gy]	
	$N-E$	SD	$N-E$	SD	$N-E$	SD	$N-E$	SD	$N-E$	SD	$N-E$	SD	$N-E$	SD	$N-E$	SD
1	1.7	3.1	0.6	1.0	-0.3	0.4	-5.0	3.2	0.2	1.4	0.0	0.0	0.0	0.0	0.3	5.3
2	0.9	1.2	-0.3	0.7	-0.4	0.3	-2.7	3.4	1.1	2.1	0.0	0.0	0.0	0.4	-0.5	5.2
3	0.2	0.7	0.4	0.6	0.1	0.3	5.8	3.0	6.0	2.0	-0.1	0.6	-0.4	0.7	0.0	2.6
4	0.6	0.6	-0.4	0.9	0.0	0.5	0.6	2.6	0.1	0.7	0.0	0.6	-0.5	1.2	0.5	0.4
5	0.1	0.2	0.1	0.8	0.1	0.4	0.5	1.8	0.6	2.8	0.0	0.0	0.0	0.0	0.8	1.5
6	2.4	1.2	-0.1	1.4	0.0	0.7	0.2	2.1	0.6	2.2	0.0	0.0	0.0	0.0	-1.1	3.2
7	1.2	2.1	0.2	0.9	0.1	0.5	0.2	1.2	0.6	0.8	-0.1	0.4	-0.7	0.9	-4.6	4.2
8	0.9	0.8	-0.6	0.9	-0.4	0.5	0.8	3.0	0.9	2.0	0.0	0.5	-0.1	1.1	0.6	2.9
9	2.2	2.5	0.0	0.7	0.1	0.5	2.0	2.8	1.4	2.1	0.1	0.3	0.0	0.6	0.2	1.6
10	1.2	1.4	0.0	1.0	-0.4	0.3	-0.6	1.8	0.4	1.3	-0.1	1.2	-0.4	1.7	2.5	3.6
11	0.7	0.9	-0.8	1.2	0.4	0.6	1.7	2.8	0.7	2.6	0.0	1.5	-0.4	1.8	1.5	5.8
12	0.6	0.7	-1.0	0.9	0.0	0.3	1.2	2.0	0.6	1.6	0.0	0.5	-0.2	1.0	-2.0	1.9
13	1.0	1.0	0.2	0.4	0.2	0.3	2.5	1.8	0.7	2.0	-0.1	0.6	-0.4	1.2	0.0	5.1
14	1.2	1.5	-0.2	0.9	0.0	0.6	1.9	2.2	3.0	5.0	0.4	0.6	0.2	0.8	-1.0	2.7
15*	1.2	1.3	-3.6	1.2	-1.8	0.6	4.3	0.6	0.2	1.0	0.7	1.6	-0.6	1.7	0.5	4.2
Mean	**1.1**	**1.3**	**-0.4**	**0.9**	**-0.2**	**0.5**	**0.9**	**2.3**	**1.1**	**2.0**	**0.1**	**0.6**	**-0.2**	**0.9**	**-0.2**	**3.3**
Max	**2.4**	**3.1**	**0.6**	**1.4**	**0.4**	**0.7**	**5.8**	**3.4**	**6.0**	**5.0**	**0.7**	**1.6**	**0.2**	**1.8**	**2.5**	**5.8**

Abbreviations: V_{xGy}= percent volume receiving dose greater than $x\ Gy$; $N-E$ = the difference between the value calculated under the nominal setting and its expectation value under uncertainty; MLD = mean lung dose; SD =sample standard deviation of the expected value. *Patient no. 15 was prescribed 60Gy instead of 74Gy.

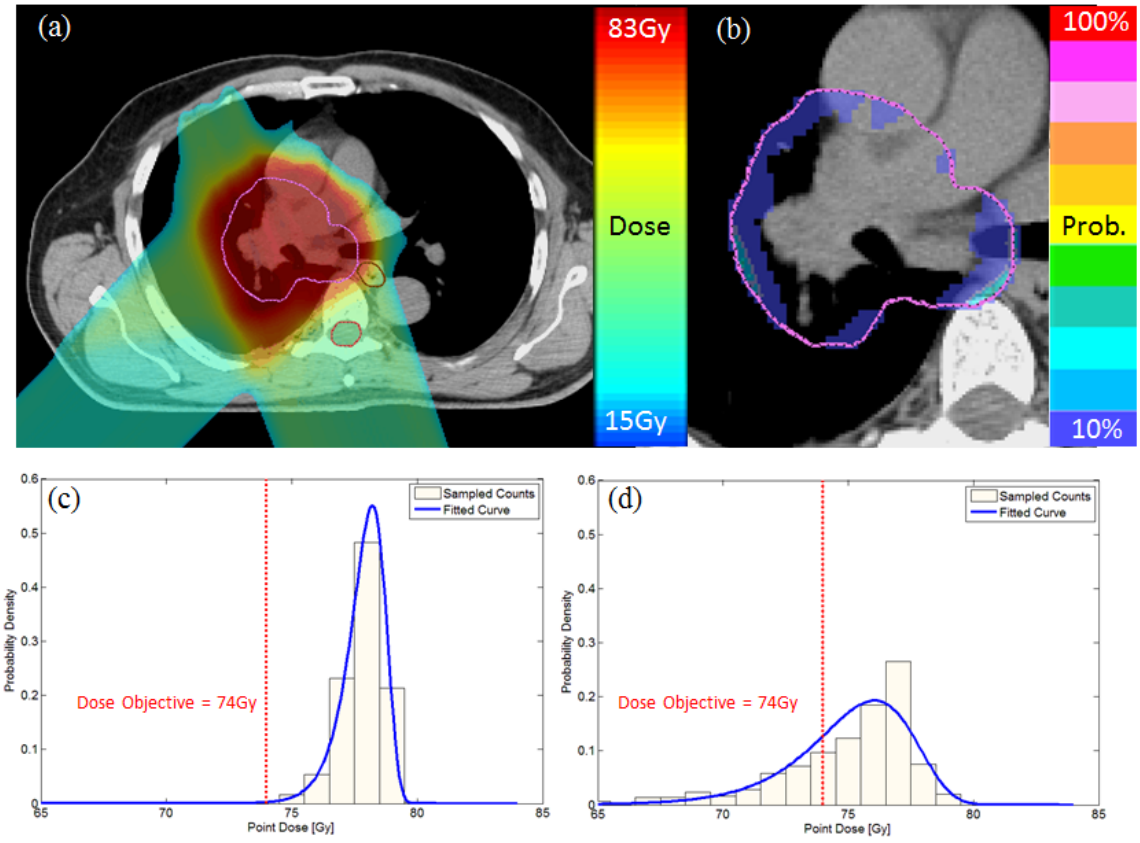

Figure 5-7 (a) Dose distribution under the nominal setting. (b) Probability map of risk of the ITV: The chance of voxels in the ICTV not receiving a dose of more than 74Gy is shown as a color map. The probability of risk for each voxel is calculated by integrating the approximated PDF curve from zero doses to the dose objective (i.e., 74Gy). The PDFofthe voxel located in the center of the ICTV with a 0% chance of receiving a less-than prescription dose is shown in (c), and the voxel at the boundary of the ICTV with the highest chance of receiving a less-than prescription dose is shown in (d).

D. Discussion

D.1 Interpretation of results

The chief advantages of a statistical method for evaluating plan robustness are:first, its prediction is more realistic because it considers all possible range of errors, not just

extreme cases, and use of familiar statistical parameters, such as expectations and standard deviations of doses and DVHs, rather than a new metric for uncertainty assessment such as the worst-case DVH (7). Even though, the theoretical worst-case DVHs were not directly computed in this work, we can consider the lower bound of $F[DVH]$ as the best estimate of the worst-case scenario. For all 15 patients, the lower bound of F[DVH] was out of the bound defined by the 3 times the $SD[DVH]$ indicating that the likelihood of it being realized during actual treatment is very low. The $E[DVH]$ can be interpreted as the most probable DVH under uncertainties; thus,it is more suitable for evaluating and reporting plans than is a DVH generated under a nominal setting. On the other hand, the $SD[DVH]$ can be interpreted as how likely the outcome will deviate from the $E[DVH]$;thusitismore appropriate for evaluating the robustness of the treatment plan. An ideal plan would have$E[DVH]$ value that is close to the clinical goal and a small $SD[DVH]$value. In our study,the overall $E[DVH]$of the ICTV for all patients was close to the prescription dose level, and the standard deviation was mostly acceptable, demonstrating that our treatment planning procedure and margins provide robust target coverage. However, both the esophagus and spinal cord showed significant fluctuation in DVH values under uncertainties. The $SD[DVH]$ ofthe V_{45Gy} of esophagus and maximum spinal cord dose were 5% and 5.8Gy, respectively. Even though, the theoretical worst-case DVHs (7) were not directly computed in this work, we can consider the lower bound of $F[DVH]$ as the best estimate of the worst-case scenario. For all 15 patients, the lower bound of F[DVH] was well out of the bound defined by the 3 times the $SD[DVH]$ meaning that the likelihood of it being realized during actual treatment is less than 1%.

D.2 Geometric PTV and ICTV coverage

Despite the known limitations of PTV,which were discussed in the Introduction, we found that the original PTV coverage ($V_{74Gy}$of PTV)under the nominal setting was a good indicator of how well the ICTV coverage can be retained under uncertainties suggesting that there still is a merit to defining PTV and using it for plan evaluation for proton therapy using passively scattered or single field uniform dose optimized plan. Figure 5-8 shows the relationship between the original PTV coverage and the difference in ICTV coverage under the nominal setting and its expectation value for all 15 patients.

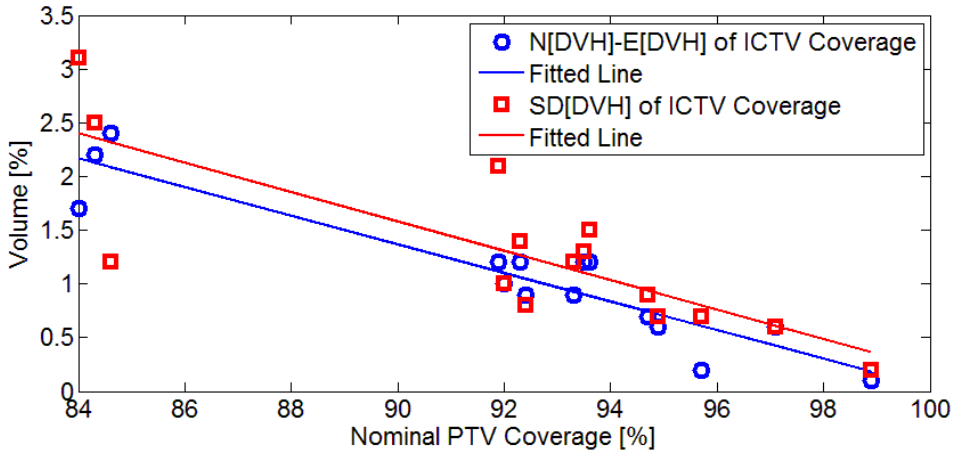

Figure 5-8 The ICTV coverage difference between the nominal plan and its expectation value under uncertaintieswas plotted against the original PTV coverage (blue). Similarly, the standard deviation of the ICTV coverage under uncertaintieswas plotted against the original PTV coverage (red).

A similar relationship was found for the standard deviation of ICTV coverage under uncertainties. As shown in the graph in figure 5-8, 95% PTV coverage under nominal settingsallow a 1% fall-off in ICTV coverage, with a standard deviation of approximately 1% under uncertainties. Negative slopes of the fitted line of both the difference in ICTV coverage and its standard deviation indicate that there is a strong

correlation between the original PTV coverage and the plan robustness.

D.3 Application in head and neck scanning beam proton therapy: a case study

Even though we demonstrated the efficacy of the proposed method using passively scattered beam plans, the method can easily use for single-field uniform dose (SFUD) optimized scanning beam proton therapy, with no modifications. An example of a two-beam intensity-modulated proton therapy plan ofachordoma case is shown in figure 5-9.Of note,because of the high dose-to-CTV conformity, the probability map of risk shows a significant risk of achieving the clinical goal on the boundary between the CTV and the brainstem in terms of its probability.

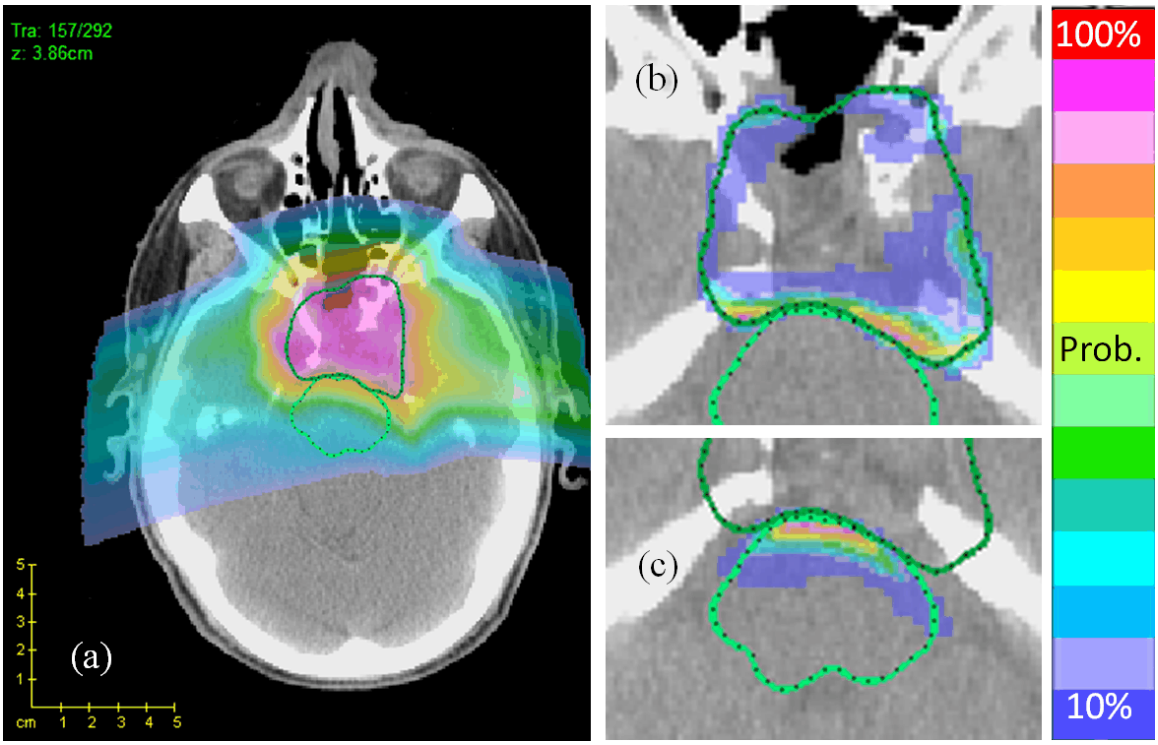

Figure 5-9 (a) Nominal dose distribution of a two-field SFUD plan in which the CTV (dark green) is adjacent to the brainstem (light green). Probability map of risk for the CTV (b) and brainstem (c): the color map shows the chance of the voxel receiving less-than the prescription dose (66Gy) for the CTV and morethan the dose limit (50Gy) for the brainstem.

D.4 Limitation

The limitation of this study was that we did not consider intrafractional and interfractionalchanges in anatomy. The breathing motions and anatomical deformations over the course of treatment, in response to radiotherapy, can lead to deteriorationsin the planned dose distribution. In theory, our method can incorporate the uncertainties associated with breathing motion by using different phases of the 4DCT data set to formulate a more comprehensive $PDF$of point dose distributions. However, anatomical changes over the course of treatment are difficult to predict and remain a challenge for any method of evaluatingtheeffects of uncertaintieson planned dose distribution prior to

treatment.

E. Conclusions

In this study, we demonstrated that our statistical method of evaluating the effectsof uncertainty on DVH and dose distribution is feasible.Our method quantifies the variations in dosimetric parameters in terms of expectation values and standard deviations. In addition, the uncertainty in 3D dose distribution was evaluated using the probability map of risk. The proposed method was used to evaluate 15 lung cancer passively scattered beam proton therapy cases to validate treatment planning procedures and margins. We found that the current treatment planning procedure,using a passively scattered proton beam,was robust in terms of maintaining target coverage under set-up and range uncertainties. However, we also found that the dose to the esophagus and spinal cord variedsignificantly from the planning dose. The information provided by this statistical assessmentofuncertaintieswillhelp us make better clinical decisionsfor plan approval and review.

CHAPTER 6: PLAN ROBUSTNESS COMPARISON: PROTON THERAPY VS. IMRT

A.Introduction

In this chapter we apply the robust plan evaluation method developed in chapter 5 to compare plan robustness of proton therapy and intensity-modulated radiotherapy (IMRT). Currently, comparison study of proton therapy with IMRT is receiving a lot of attention in radiation oncology community. As the number of proton facilities increases there's been a call for more comparison study between proton and IMRT to justify the cost and effectiveness of proton therapy (108, 109, and 110). A fair amount of studies that compares proton and IMRT has been published in recent years (111, 112, 113, 114, 115, 116, and 117). However, it is interesting that most of these studies are purely based on plan comparisons. A plan comparison study is where two treatment plans, ideally of different modality or different method of plan design, are compared side by side in terms of their target coverage, dose conformity, dose uniformity, and dose to critical structures or normal tissue. Although, treatment plan comparison is arguably the most widely accepted form of study when one tries to investigate the superiority of a particular treatment modality over the other, it carries certain risks of not being able to judge the two plans fairly when considering the effect of uncertainties in beam delivery process that are not well represented in the treatment plans at the time of assessment. Such risk is much greater when one tries to compare two modalities that show different sensitivity to the uncertainties as in proton therapy and IMRT. In chapter 2 showed that the sensitivity of proton planned dose distribution to the setup, internal motion, and anatomical change is greater than the conventional photon dose because the range of

proton is essentially determined by the tissue density along the beam path (118). On the other hand, for photon therapy, in most of the time, one can safely assume the planned dose distribution remains static under the small perturbation of tissue density from setup and anatomical deformation (119). This suggests that, when comparing proton plan against IMRT plan, one must account for the fact that the two different modalities behave very differently under the uncertainties. In other words, a fair comparison of proton vs. IMRT study must consist of uncertainty analysis. Up to this point, there is not readily available method to objectively compare the plans from two arms. Most studies however, employee the planning target volume (PTV) coverage as one of the constraint when designing a plan and by matching the PTV coverage to be identical for both arms, it is wrongly assumed that the plans are equally robust to the uncertainties. In this chapter, in order to evaluate plan's robustness for both arms fairly, we propose to use statistical parameters such as expectation value and standard deviation of dose objectives and dose-volume histograms of the clinical target volume (CTV) and other organs at risk (OAR) directly.

B. Methods

For this study, a group of 15 non-small cell lung cancer (NSCLC) patients who were randomly selected from the patient population who are enrolled in IMRT vs. Proton randomized trial at our institution (i.e. in fact, these are the identical patients that were used in chapter 5). For each of these 15 patients, both IRMT and proton plans were created under the identical objectives as follow: : ≥ 99% of the PTV receiving≥ 95% of the prescribed dose (i.e., 14 patients prescribed to 74Gy and 1 patient to 60Gy); total lung $V_{20Gy}$of ≤ 37%; mean lung dose of≤ 22Gy; as low as possible doses to the

esophagus V_{65Gy} and V_{45Gy} and heart V_{60Gy} and V_{30Gy}; and maximum spinal cord dose of≤ 50Gy. The detail description of plan design method based on the 4DCT simulation was described already in chapter 5. For each of these plans, total of 600 dose calculations were performed that simulated 60 virtual courses of treatments with each course having 10 fractions (see figure 6-1). We choose to simulate a treatment course with only 10 fractions even though our clinical protocol has 36 fractions because we found that roughly 10 fractions were enough to estimate the final accumulated dose distribution from the normally distributed random setup errors. A random setup error was introduced over the multiple fractions while a systematic setup error and a systematic range error were introduced over the different courses of treatments. The systematic setup errors were sampled from the assumed Gaussian function with mean position at the isocenter of treatment planning simulation and with standard deviation of 2mm. The random setup errors were also sampled from the assumed Gaussian function but with mean position at the position defined by the systematic setup error and with standard deviation of 2mm. In other words, the random setup error was implied on top of the assumed systematic setup error already in place. The systematic range error was introduced by introducing new relative stopping power to CT Hounsfield calibration curves that are generated by random scaling factor. The random scaling factors were sampled from the assumed Gaussian function with mean at zero and standard deviation of 1.5% of the relative stopping power. Due to the Gaussian nature of these simulation parameters, it can be said that roughly 95% of time, our simulated random and systematic setup errors were within 4mm, while range error were within 3%. This agrees well with our current treatment planning practice (120, 121). In calculating doses

under different simulating parameters, we assumed static dose distribution for IMRT plans. That is, the dose distribution calculated under nominal setting was simply moved in physical space over the patient anatomy as we introduced setup errors. The inherent range error due to the uncertainties in the calibration curve was ignored. Although there is a small effect of CT HU uncertainties on the photon dose distribution, its magnitude is much less than the magnitude caused by setup errors (122, 123). On the other hand, for proton plans, a new dose calculation was performed for every simulation using the fast dose calculation method described in chapter 4 (124). This is because, for proton dose distribution, the uncertainties in the relative stopping power to CT HU calibration curve cannot be ignored. For each simulation data, we computed expectation value of DVHs (E[DVH]) and compare it to the value given under nominal setting (N[DVH]).

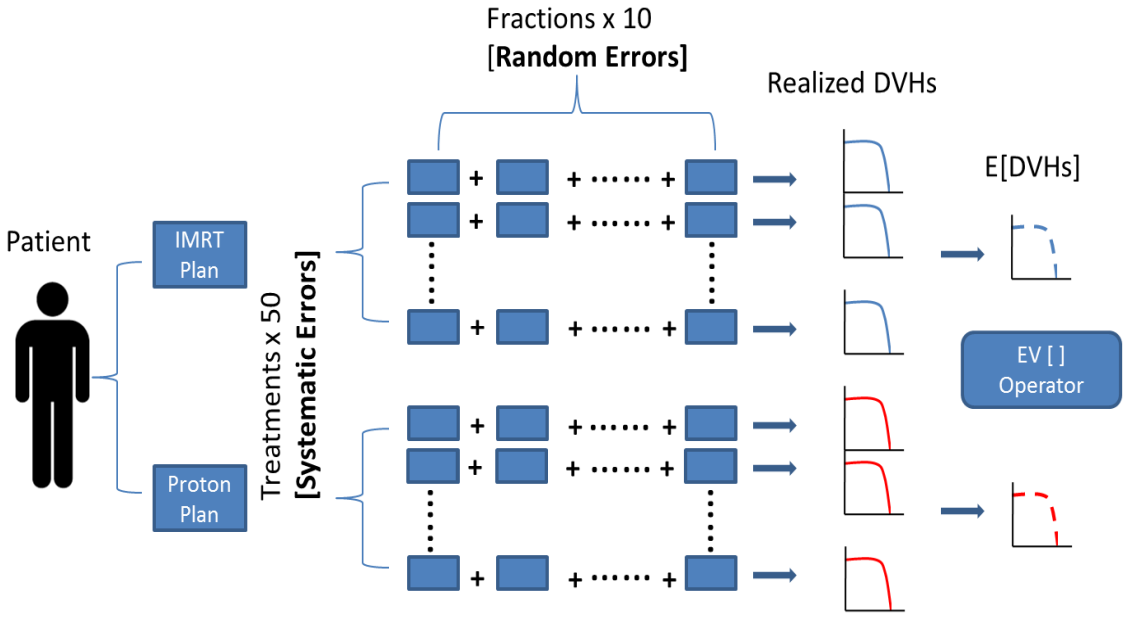

Figure 6-1 Schematics of patient simulation method. Both IMRT and proton plans were created and approved for a selected patient. Each of these plans then was used to calculate dose distributions under varying simulation parameters (i.e. setup position and different calibration curve).

C. Results

Both PTV and ITV coverage under nominal setting were similar between IMRT and proton plans as can be seen from figure 6-2. The average V74Gy for PTV and ITV for IMRT plans were 93% (±2.5%) and 99% (±1%) respectively. The average V74Gy for PTV and ITV for proton plans were 92% (±4.5%) and 99% (±1.7%) respectively. Overall, the difference between the dose objectives calculated under nominal setting and its expectation values were larger for proton plans. All patients regardless of the modalities, the expectation value of V74Gy coverage were lower than the value calculated under nominal setting indicating that the simulated uncertainties always degrades the intended target coverage. Such difference was observed to be bigger for proton plans (p-value = 0.0245). The averaged target coverage fall off (i.e. V74Gy) was -0.4% and -0.1% for proton and IMRT plans respectively. Figure 6-3 through 6-9 compares the variation of the difference observed for all patients between proton and IMRT in box plots. For both V20gy and MLD of lung, there was no significant difference between IMRT and proton plans. For esophagus V65Gy dose objective, there was no significant difference, but for esophagus V45Gy, the difference was observed to be bigger for proton plans (p-value = 0.045). For heart V30Gy, the difference was observed to be bigger for IMRT plans but (p-value = 0.035). For the maximum spinal cord dose, the difference was not statistically significant.

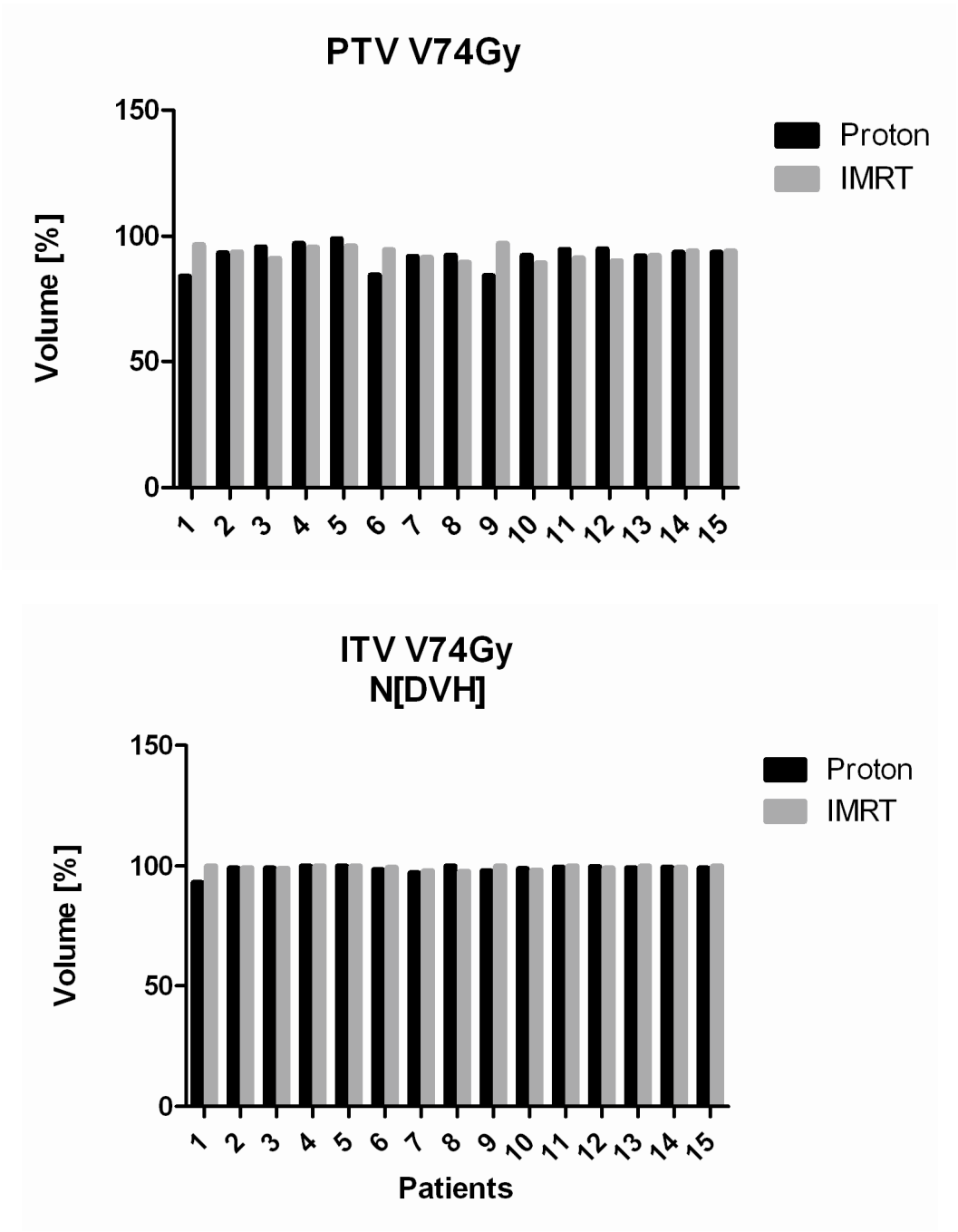

Figure 6-2 The target coverage in terms of percent volume of PTV (top) and ITV (bottom) receiving the prescription dose of 74Gy under nominal setting. Both IMRT and proton plans are fairly identical in terms of planned target coverage.

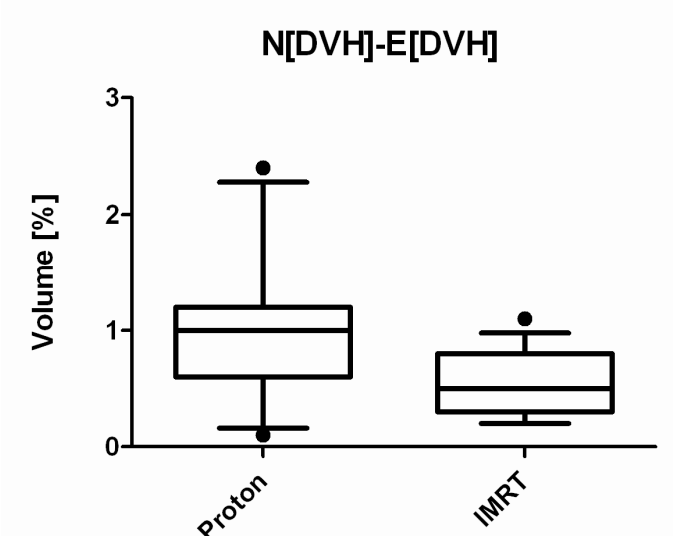

Figure 6-3 Comparison of the boxplot of the difference in ITV V74Gy coverage between the nominal setting and its expectation value sampled from over 600 dose approximations of all 15 patients.

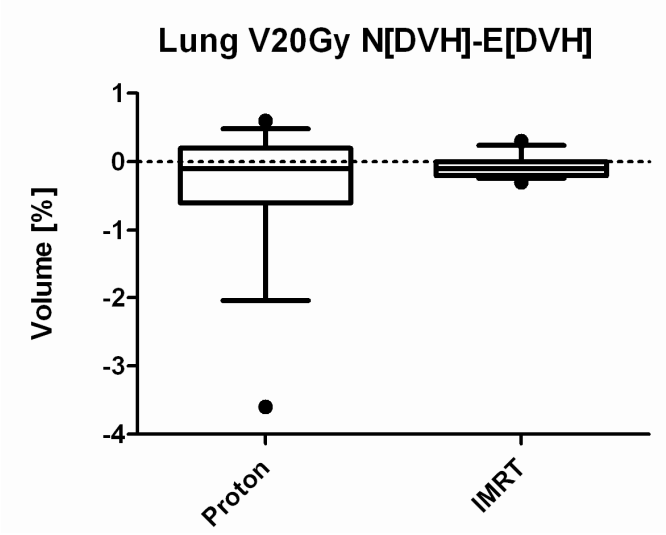

Figure 6-4 Comparison of the boxplot of the difference in Lung V20Gy coverage between the nominal setting and its expectation value sampled from over 600 dose approximations of all 15 patients.

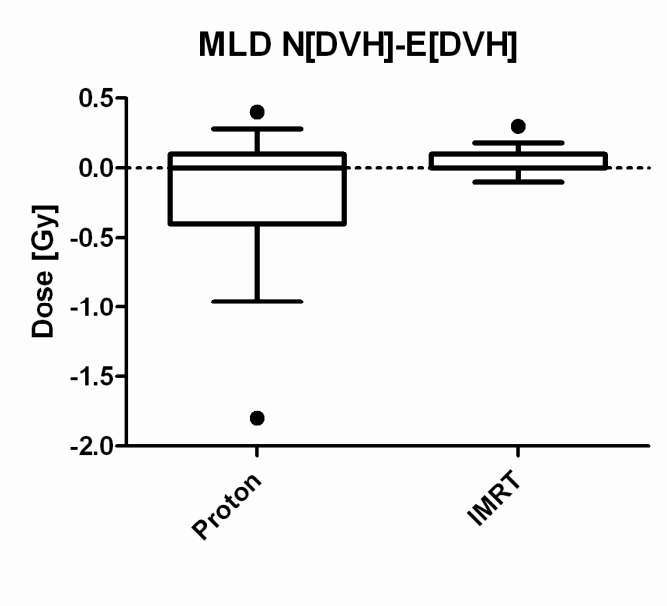

Figure 6-5 Comparison of the boxplot of the difference in mean lung dose (MLD) Gy coverage between the nominal setting and its expectation value sampled from over 600 dose approximations of all 15 patients.

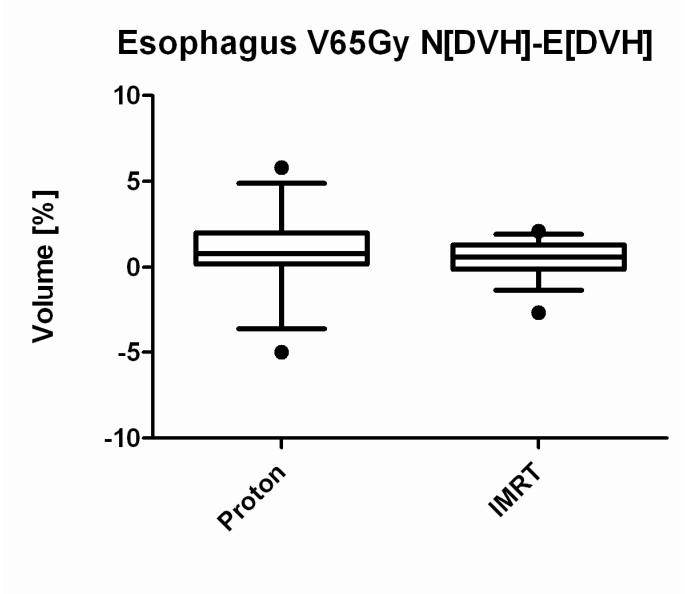

Figure 6-6 Comparison of the boxplot of the difference in Esophagus V65Gy coverage between the nominal setting and its expectation value sampled from over 600 dose approximations of all 15 patients.

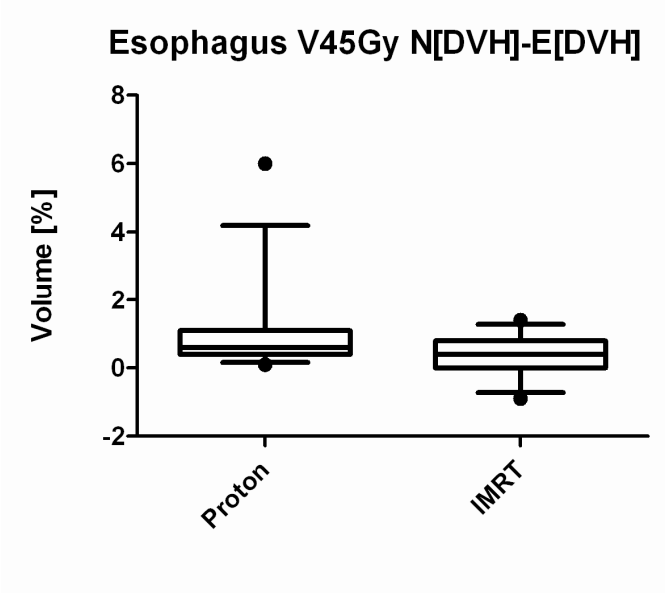

Figure 6-7 Comparison of the boxplot of the difference in Esophagus V45Gy coverage between the nominal setting and its expectation value sampled from over 600 dose approximations of all 15 patients.

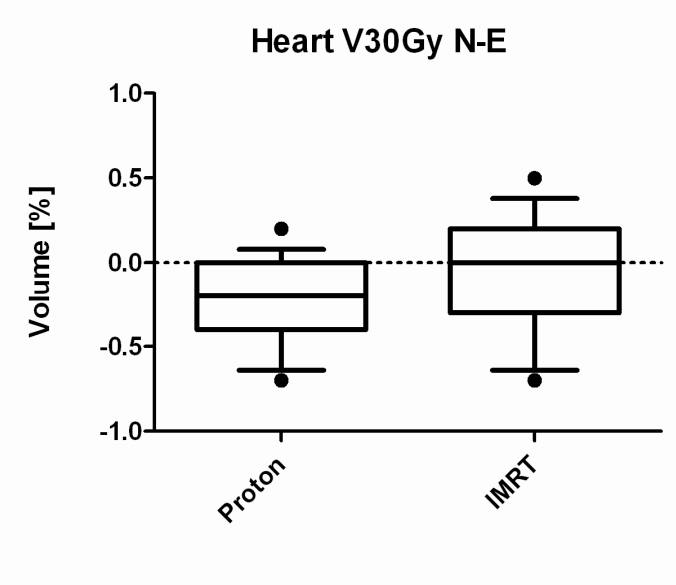

Figure 6-8 Comparison of the boxplot of the difference in Esophagus V65Gy coverage between the nominal setting and its expectation value sampled from over 600 dose approximations of all 15 patients.

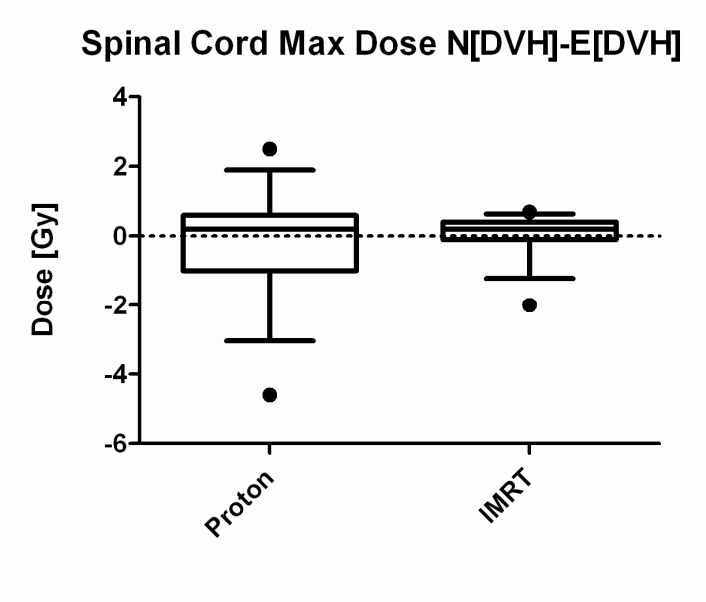

Figure 6-9 Comparison of the boxplot of the difference in Spinal cord max dose Gy coverage between the nominal setting and its expectation value sampled from over 600 dose approximations of all 15 patients.

D. Discussion

Despite the difference in the magnitude of change when we compare the dose objectives under uncertainties, all plans from both arms achieved the initial dose objectives indicating that the current treatment plan design method was adequate enough to account for the simulated uncertainties. However, it was found that proton plans were slightly more sensitive to the uncertainties when compare to IMRT plans.

E. Conclusion

We showed that the statistical parameter such as the expectation value can be used to assess the influence of uncertainties dosimetric parameters. Since this method can apply to both IMRT and proton plans, it was used to assess and compare overall robustness of a given treatment plan for IMRT and proton for 15 lung cancer patients. Except for heart dose, all other dose objectives were better retained in IMRT plans than proton plans.

CHAPTER 7: Conclusions of Dissertation

A. Conclusions of Hypothesis 1

Hypothesis 1: A plan treated to a Beam-specific planning target volume (bsPTV) can minimize the loss of target coverage due to setup and range uncertainties when compared to a plan treated to a conventional planning target volume (PTV).

The concept of bsPTV for accounting setup, internal motion, and inherent range error for proton therapy was proven useful in chapter 3. Our implementation of bsPTV was novel in that it took into account the tissue heterogeneity misalignment into distal margin calculations that was previously only possible with physical compensator smearing. In our carefully designed control experiment, even under the influence of extreme setup and range error, bsPTV retained its initial target coverage up to 94% when the conventional PTV could only retain up to 67%. Therefore, we can conclude that our hypothesis holds its ground within the realm of our experiment. In investigating our hypothesis 1, we have developed and implemented a standalone software that generates bsPTV for a given treatment plan parameters. This software has proven useful for this project and for others as well. The bsPTV awaits more validation in more clinical sites such as prostate, lung, and head and neck area. Also, the design method of bsPTV can be expanded to include the change in tissue density due to breathing motion by incorporating 4DCT data set.

B. Conclusions of Hypothesis 2

Hypothesis 2: Statistical method can be used to accurately quantify the variation in dose distribution and dose-volume histograms (DVHs) due to setup and range uncertainties.

The statistical method of quantifying the impact of uncertainties on planned dose distribution and its DVHs was developed and its application was tested on the selected lung cancer patients in chapter 5. Based on our current proton treatment planning procedures for the lung cancer patient, we quantified the expectations and standard deviationsof volumes of interest for all 15 patients.The mean expectation value of prescription dose of theintegratedclinical target volumewas 1.1%less than that of the original coverage, with a standard deviation of 1.0%. The most sensitive organ at risk was spinal cord with a mean standard deviation of its max dose of 3.3%. Based on the result of our study, we conclude that the proposed statistical method provides a quantitative means of realistically assessing dose and DVH.In investigating our hypothesis 2 we have developed and implemented a standalone software that evaluates the uncertainties of a given treatment plan. Another significant achievement through this project was the development of fast range corrected proton dose approximation method that was discussed in chapter 4. The statistical method of quantifying the treatment uncertainties is new and therefore currently, we lack the ability to interpret the result by matching it to our clinical experience. Future challenge would be to establish the quantification with our previous experience by looking at the relationship between the magnitude of calculated treatment uncertainties and clinical end points such as dose toxicity, recurrence rate, and etc.

References

1. Wilson RR. Radiological Use of Fast Protons.*Radiology* 1946;47:5 487-491.

2. Tobias CA, Lawrence JH, Born JL, McCombs RK, Roberts JE, Anger HO, Low-Beer BV, Huggins CB. Pituitary irradiation with high-energy proton beams: a preliminary report. *Cancer Res*. 1958:18:121.

3. Larsson B, Leksell L, Rexed B, Sourander P, Mair W, Anderson B. The high-energy proton beam as a neurosurgical tool.*Nature* 1958:182:1222.

4. Slater JM, Archambeau JO, Miller DW, Notarus MI, Preston W, Slater JD. The proton treatment center at Loma Linda University Medical Center.*Int. J. Radiat. Oncol Biol. Phys.* 1991:22:383

5. Particle Therapy Co-Operative Group (PTCOG). ptcog.web.psi.ch

6. Paganetti H. Nuclear interactions in proton therapy: dose and relative biological effect distributions originating from primary and secondary particles. *Phys. Med. Biol*. 2002:38:747-764.

7. Attix FH. Introduction to Radiological Physics and Radiation Dosimetry 2004 by *WILEY-VCH Verlag GmbH & Co*.

8. Berger MJ, Seltzer SM. Stopping powers and ranges of electrons and positrons. NBSIR 82-2550-A, *National Bureau of Standards, Washington, DC,* 20234.

9. Koehler AM, Schneider RJ, Sisterson JM. Range modulators for protons and heavy ions. *Nucl.Instrum. Methods* 1975;131;437-40

10. Bonett DE. Current developments in proton therapy: review *Phys. Med. Biol*. 1993:38:1371-1392.

11. Pedroni E, Bacher R, Blattmann H, Bohringer T, Coray A, Lomax A, Lin S, Munkel G, Scheib S, Scneider U, Tourovsky A. The 200 MeV proton therapy project at the Paul scherrer institute: conceptual design and practical realization. *Med. Phys.* 1995:22:37-53.

12. Rasch CR, Steenbackkers R, Van Herk M. Target definition in prostate, head and neck. *SeminRadiatOncol* 2005:15:136-145.

13. Letourneau D, Martinez AA, Lockman D, Yan D, Vargas C, Ivaldi G, Wong J. Assessment of residual error for online cone-beam CT-guided treatment of prostate cancer patients. *Int J. Radiat. Oncol. Biol. Phys*. 2005:4:1239-1246.

14. Vedam S, Docef A, Fix M, Murphy M, Keall P. Dosimetric impact of geometric errors due to respiratory motion prediction on dynamic multileaf collimator-based four-dimensional radiation delivery. *Med Phys*. 2005:32:1607-1620.

15. Wang Y, Efstathiou JA, Sharp GC, Lu HM, Ciernik IF, Trofimov AV. Evaluation of the dosimetric impact of interfractional anatomical variations on prostate proton therapy using daily in-room CT images. *Med. Phys*. 2011:38:4623-4634.

16. Keall PJ, Siebers JV, Jeraj R, Mohan R. The effect of dose calculation uncertainty on the evaluation of radiotherapy plans. *Med Phys.* 2000:27:478-484.

17. Engelsman M, Kooy HM. Target volume dose considerations in proton beam treatment planning for lung tumors. *Med Phys.* 2005:32:3549-3557

18. Wagner MS. Automated range compensation for proton therapy. *Med Phys*. 1983:9:749:759

19. Zhang R, Newhauser WD. Calculation of water equivalent thickness of materials or arbitrary density, elemental composition and thickness in proton beam irradiation. *Phys. Med. Biol*. 2009:54:1383-1395.

20. Yang M. Dual energy computed tomography for proton therapy treatment planning. UT GSBS Dissertations and Theses.Paper 167.*http://digitalcommons.library.tmc.edu/utgsbs_disseration/167*

21. Schneider U, Pedroni E, Lomax A. CT Hounsfield units for radiotherapy treatment planning *Phys. Medi. Biol.* 1996:41:111-124.

22. Moyers MF, Sardesai M, Sun S, Miller DW. Ion stopping powers and CT numbers.*MediDosi*. 2009:35:179-194.

23. YangM, Zhu XR, Park PC, TittUwe, Mohan R, Virshup G, Clayton J, Dong L. Comrephensive analysis of proton range uncertainties related to patient stopping-power-ratio estimation using the stoichiometric calibration. *Phys. Med. Biol.* 2012:52:4095-4115.

24. Robinowitz I, Broomberg J, Goitein M, McCarthy K, Leong J. Accuracy of radiation field alignment in clinical practice. *Int. J. Rad. OncolBiol Phys*. 1985:11:1857-1867.

25. Kang H, Lovelock DM, Yorke ED, Kriminiski S, Lee N, Amols HI. Accurate positioning for head and neck cancer patients using 2D and 3D image guidance.*J. App. Clinic. Med. Phys*. 2011:12:No1

26. Yang J, Garden AS, Zhang Y, Zhang L, Dong L. Variable planning margin approach to account for locoregional variations in setup uncertainties. *Med. Phys.* 2012:39:5136-5144.

27. Li W, Purdie TG, Taremi M, Fung S, Brade A, Cho BC, Hope A, Sun A, Jaffray DA, Bezjak A, Bissonnette JP. Effect of immobilization and performance status on intrafraction motion for stereotactic lung radiotherapy: Analysis of 133 patients. *Int. J. Radiation Oncology Biol. Phys*. 2011:81:1568-1575.

28. Huang K, Palma D, Scott D, McGregor D, Gaede S, Yartsev S, Bauman G, Louie A, Rodrigues G. Inter- and intrafraction uncertainty in prostate bed image-guided radiotherapy. *Int. J. Radiation Oncology Biol. Phys.* 2012 (In Press)

29. Letourneau D, Mrtinez A, Lockman D, Yan D, Vargas C, Ivaldi G, Wong J. Assessment of residual error for online cone-beam CT-guided treatment of prostate cancer patients. *Int. J. Radiat. Oncol. Biol. Phys*. 2005:62:1239-1246.

30. Arjomandy B. Evaluation of patient residual deviation and its impact on dose distribution for proton radiotherapy. *Med. Dosim*. 2011:36:321-329.

31 Engelsman M, Kooy HM. Target volume dose considerations in proton beam treatment planning for lung tumors. *Med. Phys.* 2005:32:3550-3560.

32. ICRU Report 50. Prescribing, recording, and reporting photon beam radiotherapy. International Commission on Radiation Units and Measurements, *Bethesda*, 1999 MD.

33. Moyers MF, Miller DW, Bush DA, Slater JD. Methodologies and tools for proton beam design for lung tumors. *Int. J. Radiat. Oncol. Biol. Phys*. 2001:49:1429-1438.

34. Urie M, Goitein M, Wagner M. Compensating for heterogeneities in proton radiation therapy. *Phys. Med. Biol.* 1984:29(5):553-66.

35. Trofimov A, Nguyen PL, Coen JJ, Doppke KP, Schneider RJ, Adams JA, Bortfeld TR, Zietman AL, Delaney TF, Shipley WU. Radiotherapy treatment of early-stage prostate cancer with IMRT and protons: a treatment planning comparison. *Int. J. Radiat. Oncol. Biol. Phys.* 2007:69:444-453.

36. International Commission on Radiation Units and Measurements 1993. Stopping powers and ranges for protons and alpha particlesICRUReport49 (Bethesda MD: ICRU)

37. International Commission on Radiation Units and Measurements 1999. Prescribing, Recording, and Reporting Photon Beam Therapy ICRU Report 62 (Supplement to ICRU Report 50) (Bethesda MD: ICRU)

38. International Commission on Radiation Units and Measurement 2004. Prescribing, Recording and Reporting Electron Beam Therapy ICRU Report 71 (Oxford: Oxford University Press)

39. Stroom JC, De Boer HCJ, Huizenga H,Visser AG.Inclusion of geometrical uncertainties in radiotherapy treatment planning by means of coverage probability.*Int J RadiatOncolBiolPhys*1999;43(4):905-919,

40. Van Herk M, Remeijer P, Rasch C, Lebesque JV. The probability of correct target dosage: Dose-population histograms for deriving treatment margins in radiotherapy. *Int J RadiatOncolBiolPhys* 2000;47(4):1121-1135.

41. Cho BC, Van Herk M, Mijnheer BJ, Bartelink H. The effect of set-up uncertainties, contour changes, and tissue inhomogeneities on target dose-volume histograms.*Med Phys* 2002;29(10):2305-2318.

42. Moyers MF, Miller DW, Bush DA, Slater JD. Methodologies and tools for proton beam design for lung tumors. *Int J RadiatOncolBiolPhys* 2001;49(5):1429-1438.

43. Engelsman M, Kooy HM. Target volume dose considerations in proton beam treatment planning for lung tumors. *Med Phys*. 2005;32(12):3549-3557.

44. Lomax AJ. Intensity modulated proton therapy and its sensitivity to treatment uncertainties 2: The potential effects of inter-fraction and inter-field motions. *Phys Med Biol* 2008;53(4):1043-1056.

45. Lomax AJ. Intensity modulated proton therapy and its sensitivity to treatment uncertainties 1: The potential effects of calculational uncertainties. *Phys Med Biol* 2008;53(4):1027-1042.

46. Meyer J, Bluett J, Amos R, Levy L, Choi S, Nguyen QN, Zhu XR, Gillin M, Lee A. Spot scanning proton beam therapy for prostate cancer: Treatment planning

technique and analysis of consequences of rotational and translational alignment errors. *Int J RadiatOncolBiolPhys* 2010;78(2):428-434.

47. Yoon M, Shin D, Kwak J, Park S, Lim YK, Kim D, Park SY, Shin KH, Kim TH, Cho KH. Characteristics of movement-induced dose reduction in target volume: A comparison between photon and proton beam treatment. *Medic Dosi*. 2009;34(3):191-201.

48. Trofimov A, Nguyen PL, Coen JJ, Doppke KP, Schneider RJ, Adams JA, Bortfeld TR, Zietman AL, Delaney TF, Shipley WU. Radiotherapy treatment of early-stage prostate cancer with IMRT and protons: A treatment planning comparison. *Int J RadiatOncolBiolPhys* 2007;69(2):444-453.

49. Widesott L, Pierelli A, Fiorino C, Dell'oca I, Broggi S, Cattnaeo GM, Di Muzio N, Fzio F, Calandrino R, Schwarz M. Intensity-modulated proton therapy versus helical tomotherapy in nasopharynx cancer: Planning comparison and NTCP evaluation. *Int J RadiatOncolBiolPhys* 2008;72(2):589-596.

50. Zhang X, Zhao K-, Guerrero TM, McGuire SE, Yaremko B, Komaki R, Cox JD, Hui Z, Li Y, Newhauser WD, Mohan R, Liao Z. Four-dimensional computed tomography-based treatment planning for intensity-modulated radiation therapy and proton therapy for distal esophageal cancer. *Int J RadiatOncolBiolPhys* 2008;72(1):278-287.

51. Rietzel E, Bert C. Respiratory motion management in particle therapy. *Med Phys*2010;37(2):449-160.

52. Urie M, Goitein M, Wagner M. Compensating for heterogeneities in proton radiation therapy. *Plasma Sources SciTechnol* 1984;29(5):553-66.

53. Schaffner B, Pedroni E. The precision of proton range calculations in proton radiotherapy treatment planning: experimental verification of the relation between CT-HU and proton stopping power. *Phys Med Biol*1998;43(6):1579-1592

54. Geithner O, Andreo P, Sobolevsky N, Harmann G, Jakel O. Calculation of stopping power ratios for carbon ion dosimetry. *Phys Med Biol*2006;51(9):2279-2292

55. Moyers MF, Sardesai M, Sun SIon stopping powers and CT numbers. *Medical Dosimetry*2010;35(3):179-194

56. Schneider U, Pedroni, E, Lomax A. The calibration of CT Hounsfield units for radiotherapy treatment planning.*Phys. Med. Biol* 1996;41(1): 111-124

57. Yoon M, Kim D, Shin DH, Park SY, Lee SB, Kim DY, Pyo HR, Cho KH. Inter- and intrafractional movement-induced dose reduction of prostate target volume in proton beam treatment. *Int J OncolBiolPhys* 2008;71(4):1091-1102.

58. Lomax A. Intensity modulation methods for proton radiotherapy. *Phys Med Biol* 1999;44(1):185-205.]

59. van Herk M. Errors and margins in radiotherapy. *Semin.Radiat.Oncol. 14, 52-64.*

60. Mckenzie AL. How should breathing motion be combined with other errors when drawing margins around clinical target volume? *Br. J. Radiol.* 73, 973-977.

61. Park P, Zhu X, Lee A, Sahoo N, Melancon A, Zhang L, Dong L. A beam-specific planning target volume (PTV) design for proton therapy to account for

setup and range uncertainties.*Int. J. Radiat. Oncol. Biol. Phys.* 2012:82(2):e329-336

62. Wang X, Zhang X, Dong L, Liu H, Wu Q, and Mohan R. Development of methods for beam angle optimization for IMRT using an accelerated exhaustive search strategy. *Int. J. Radiat. Oncol. Biol. Phys.* 2004: 60(4):1325-1337

63. Djajaputra D, Wu Q, Wu Y, Mohan R. Algorithm and performance of a clinical IMRT beam-angle optimization nsystem. *Phys. Med. Biol.* 2003:48(19):3191-3212

64. Cao W, Lim G, Lee A, Li y, Liu W, Zhu X, Zhang X. Uncertainty incorporated beam angle optimization for IMPT treatment planning. *Med. Phys.* 2012:39(8):5248:5256

65. Moravek Z, Rickhey M, Hartmann M, Bogner L. Uncertainty reduction in intensity modulated proton therapy by inverse Monte Carlo treatment planning. *Phys. Med. Biol.* 2009:54:4803-4819

66. Bortfeld T, Schlegel W. An analytical approximation of depth-dose distributions for therapeutic proton beams. *Phys. Med. Biol.* 1996:41(8):1331-1339

67. Bortfeld T. An analytical approximation of the Bragg curve for therapeutic proton beams. *Med. Phys.* 1997:24(12):1118-1128

68. Lomax A J 2008a Intensity modulated proton therapy and its sensitivity to treatment uncertainties 1: The potential effects of calculational uncertainties *Physics in Medicine and Biology***53** 1027-42

69. Lomax A J 2008b Intensity modulated proton therapy and its sensitivity to treatment uncertainties 2: The potential effects of inter-fraction and inter-field motions *Physics in Medicine and Biology***53** 1043-56

70. Frank S J, Kudchadker R J, Kuban D A, Crevoisier R D, Lee A K, Cheung R M, Choi S, Tucker S L and Dong L 2010 A volumetric trend analysis of the prostate and seminal vesicles during a course of intensity-modulated radiation therapy *Am. J. Clin. Oncol.***33** 173-5

71. Barker Jr J L, Garden A S, Ang K K, O'Daniel J C, Wang H, Court L E, Morrison W H, Rosenthal D I, Chao K S C, Tucker S L, Mohan R and Dong L 2004 Quantification of volumetric and geometric changes occurring during fractionated radiotherapy for head-and-neck cancer using an integrated CT/linear accelerator system *Int. J. Radiat. Oncol. Biol. Phys.***59** 960-70

72. Zhang X, Zhao K l, Guerrero T M, McGuire S E, Yaremko B, Komaki R, Cox J D, Hui Z, Li Y, Newhauser W D, Mohan R and Liao Z 2008 Four-Dimensional Computed Tomography-Based Treatment Planning for Intensity-Modulated Radiation Therapy and Proton Therapy for Distal Esophageal Cancer *International Journal of Radiation Oncology Biology Physics***72** 278-87

73. Trofimov A, Nguyen P L, Efstathiou J A, Wang Y, Lu H M, Engelsman M, Merrick S, Cheng C W, Wong J R and Zietman A L 2011a Interfractional variations in the setup of pelvic bony anatomy and soft tissue, and their implications on the delivery of proton therapy for localized prostate cancer *International Journal of Radiation Oncology Biology Physics***80** 928-37

74. International Commission on Radiation Units and Measurements 1993. Stopping powers and ranges for protons and alpha particles ICRU Report 49 (Bethesda MD: ICRU)

75. International Commission on Radiation Units and Measurements 1999. Prescribing, Recording, and Reporting Photon Beam Therapy ICRU Report 62 (Supplement to ICRU Report 50) (Bethesda MD: ICRU)

76. International Commission on Radiation Units and Measurement 2004. Prescribing, Recording and Reporting Electron Beam Therapy ICRU Report 71 (Oxford: Oxford University Press)

77. Cho B C J, Van Herk M, Mijnheer B J and Bartelink H 2002 The effect of set-up uncertainties, contour changes, and tissue inhomogeneities on target dose-volume histograms *Medical Physics***29** 2305-18

78. Engelsman M and Kooy H M 2005 Target volume dose considerations in proton beam treatment planning for lung tumors *Medical Physics***32** 3549-57

79. Moyers M F, Miller D W, Bush D A and Slater J D 2001 Methodologies and tools for proton beam design for lung tumors *International Journal of Radiation Oncology Biology Physics***49** 1429-38

80. Albertini F, Hug E B and Lomax A J 2011 Is it necessary to plan with safety margins for actively scanned proton therapy? *Physics in Medicine and Biology***56** 4399-413

81. Lomax A J 2008a Intensity modulated proton therapy and its sensitivity to treatment uncertainties 1: The potential effects of calculational uncertainties *Physics in Medicine and Biology***53** 1027-42

82. Trofimov A, Unkelbach J, DeLaney T F and Bortfeld T 2011b Visualization of a variety of possible dosimetric outcomes in radiation therapy using dose-volume histogram bands *Practical Radiation Oncology*

83. Inaniwa T, Kanematsu N, Furukawa T and Hasegawa A 2011 A robust algorithm of intensity modulated proton therapy for critical tissue sparing and target coverage *Physics in Medicine and Biology***56** 4749-70

84. Unkelbach J, Bortfeld T, Martin B C and Soukup M 2009 Reducing the sensitivity of IMPT treatment plans to setup errors and range uncertainties via probabilistic treatment planning *Medical Physics***36** 149-63

85. Pflugfelder D, Wilkens J J and Oelfke U 2008 Worst case optimization: A method to account for uncertainties in the optimization of intensity modulated proton therapy *Physics in Medicine and Biology***53** 1689-700

86. Unkelbach J, Chan T C Y and Bortfeld T 2007 Accounting for range uncertainties in the optimization of intensity modulated proton therapy *Physics in Medicine and Biology***52**

87. Schaffner B, Pedroni E and Lomax A 1999 Dose calculation models for proton treatment planning using a dynamic beam delivery system: An attempt to include density heterogeneity effects in the analytical dose calculation *Physics in Medicine and Biology***44** 27-41

88. Hong L, Goitein M, Bucciolini M, Comiskey R, Gottschalk B, Rosenthal S, Serago C and Urie M 1996 A pencil beam algorithm for proton dose calculations *Physics in Medicine and Biology***41** 1305-30

89. Kang Y, Zhang X, Chang J Y, Wang H, Wei X, Liao Z, Komaki R, Cox J D, Balter P A, Liu H, Zhu X R, Mohan R and Dong L 2007 4D Proton treatment planning strategy for mobile lung tumors *International Journal of Radiation Oncology Biology Physics***67** 906-14

90. Wang H, Dong L, Lii M F, Lee A L, De Crevoisier R, Mohan R, Cox J D, Kuban D A and Cheung R 2005a Implementation and validation of a three-dimensional deformable registration algorithm for targeted prostate cancer radiotherapy *Int. J. Radiat. Oncol. Biol. Phys.***61** 725-35

91. Wang H, Dong L, O'Daniel J, Mohan R, Garden A S, Kian Ang K, Kuban D A, Bonnen M, Chang J Y and Cheung R 2005b Validation of an accelerated 'demons' algorithm for deformable image registration in radiation therapy *Phys. Med. Biol.***50** 2887-905

92. Smith A, Gillin M, Bues M, Zhu X R, Suzuki K, Mohan R, Woo S, Lee A, Komaki R, Cox J, Hiramoto K, Akiyama H, Ishida T, Sasaki T and Matsuda K 2009 The M. D. Anderson proton therapy system *Medical Physics***36** 4068-83

93. Wendling M, Zijp L J, McDermott L N, Smit E J, Sonke J J, Mijnheer B J and Van Herk M 2007 A fast algorithm for gamma evaluation in 3D *Medical Physics***34** 1647-54

94. Venselaar J, Welleweerd H, Mijnheer B. Tolerances for the accuracy of photon beam dose calculations of treatment planning systems. *Radiotherapy and Oncology* 2001;60:191-201.

95. Moyers MF, Sardesai M, Sun S, Miller DW. Ion stopping powers and CT numbers. *Medical Dosimetry* 2010;35:179-194.

96. Trofimov A, Nguyen PL, Efstathiou JA,Wang Y, Lu HM, Engelsman M, Merrick S, Cheng CW, Wong JR, Zietman AL. Interfractional variations in the setup of pelvic bony anatomy and soft tissue, and their implications on the delivery of proton therapy for localized prostate cancer. *International Journal of Radiation Oncology Biology Physics* 2011;80:928-937.

97. Huang K, Palma DA, Scott D, McGregor D, Gaede S, Yartsev S, Bauman G, Louie AV, Rodrigues G. Inter- and intrafraction uncertainty in prostate bed image-guided radiotherapy. *International Journal of Radiation Oncology, Biology, Physics* 2012.

98. Wambersie A, Jones DTL, Suit HD. Presentation of the ICRU-IAEA joint report "Prescribing, Recording, and Reporting Proton-beam Therapy". *Strahlentherapie Und Onkologie* 2007;183:87-89.

99. Engelsman M, Kooy HM. Target volume dose considerations in proton beam treatment planning for lung tumors. *Medical Physics* 2005;32:3549-3557.

100. Lomax AJ. Intensity modulated proton therapy and its sensitivity to treatment uncertainties 2: the potential effects of inter-fraction and inter-field motions. *Physics in Medicine and Biology* 2008;53:1043-1056.

101. Albertini F, Hug EB, Lomax AJ. Is it necessary to plan with safety margins for actively scanned proton therapy? *Physics in Medicine and Biology* 2011;56:4399-4413.

102. Trofimov A, Unkelbach J, DeLaney TF,Bortfeld T. Visualization of a variety of possible dosimetric outcomes in radiation therapy using dose-volume histogram bands. *Practical Radiation Oncology* 2012;2:164-171.

103. Maleike D, Unkelbach J, Oelfke U. Simulation and visualization of dose uncertainties due to interfractional organ motion. *Physics in Medicine and Biology* 2006;51:2237-2252.

104. Henriquez FC, Castrillon SV. A novel method for the evaluation of uncertainty in dose-volume histogram computation. *International Journal of Radiation Oncology Biology Physics* 2008;70:1263-1271.

105. Kang YX, Zhang XD, Chang JY,Wang H, Wei X, Liao Z, Komaki R, Cox JD, Balter PA, Liu H, Zhu XR, Mohan R, Dong L. 4D proton treatment planning strategy for mobile lung tumors. *International Journal of Radiation Oncology Biology Physics* 2007;67:906-914.

106. Park PC, Cheung J, Zhu XR,Sahoo N, Court L, Dong L. Fast range-corrected proton dose approximation method using prior dose distribution. *Physics in Medicine and Biology* 2012;57:3555-3569.

107. Deasy JO, Blanco AI, Clark VH. CERR: A computational environment for radiotherapy research. *Medical Physics* 2003;30:979-985.

108 Olsen DR, Bruland OS, Frykholm G, Nordehaug IN. Proton therapy - A systematic review of clinical effectiveness. *Radiotherapy and Oncology* 2007;83:123-132.

109. Konski A, Speier W, Hanlon A, Beck JR, Pollack A. Is proton beam therapy cost effective in the treatment of adenocarcinoma of the prostate? *Journal of Clinical Oncology* 2007;25:3603-3608.

110. Lundkvist J, Ekman M, Ericsson SR, Jonsson B, Glimelius B. Proton therapy of cancer: Potential clinical advantages and cost-effectiveness. *Acta Oncologica* 2005;44:850-861.

111. Mock U, Georg D, Bogner J, Auberger T, Potter R. Treatment planning comparison of conventional, 3D conformal, and intensity-modulated photon (IMRT) and proton therapy for paranasal sinus carcinoma. *International Journal of Radiation Oncology Biology Physics* 2004;58:147-154.

112. Yeung D, Malyapa RS, Mendenhall WM, Li Z, Louis D, Liu C, Amdur RJ, Palta JR, Mendenhall NP. Dosimetric comparison of IMRT and proton therapy for head and neck tumors. *International Journal of Radiation Oncology Biology Physics* 2006;66:S412-S412.

113. Lee AK, Kudchadker RJ, Amos RA, Johnson JL, Choi SL, Kuban DA, Cox JD, Mohan R, Gillin M, Dong L. Proton therapy vs. IMRT for prostate cancer: A dosimetric comparison. *International Journal of Radiation Oncology Biology Physics* 2007;69:S342-S342.

114. Berman AT, Ingram M, Both S. Dose-volume comparison of combined IMRT and proton therapy vs. IMRT for pelvis and para-aortic radiotherapy in gynecologic malignancies. *International Journal of Radiation Oncology Biology Physics* 2008;72:S370-S371.

115. Mohan R, Zhang X, Matney J, Bluett J, Dong L, Balter P, Engelsman M, Choi N, Komaki R, Liao Z. IMRT vs. Passively Scattered Proton Therapy (PSPT) for Locally Advanced Non-small Cell Lung CA (LA NSCLC) Randomized Trial -

Is there Equipoise? *International Journal of Radiation Oncology Biology Physics* 2010;78:S201-S202.

116. Nichols RC, Huh SH, Henderson RH*l.* Selective nodal irradiation of regionally advanced non-small-cell lung cancer with proton therapy and IMRT: A dosimetric comparison. *Thoracic Cancer* 2012;3:169-174.

117. Milby AB, Both S, Ingram M*,* Lin LL. Dosimetric Comparison of Combined Intensity-Modulated Radiotherapy (IMRT) and Proton Therapy Versus IMRT Alone for Pelvic and Para-Aortic Radiotherapy in Gynecologic Malignancies. *International Journal of Radiation Oncology Biology Physics* 2012;82:E477-E484.

118. Lomax AJ. Intensity modulated proton therapy and its sensitivity to treatment uncertainties 1: the potential effects of calculational uncertainties. *Physics in Medicine and Biology* 2008;53:1027-1042.

119. Cho BCJ, van Herk M, Mijnheer BJ. The effect of set-up uncertainties, contour changes, and tissue inhomogeneities on target dose-volume histograms. *Medical Physics* 2002;29:2305-2318.

120. Moyers MF, Miller DW, Bush DA*,* Slater JD. Methodologies and tools for proton beam design for lung tumors. *International Journal of Radiation Oncology Biology Physics* 2001;49:1429-1438.

121. Kang YX, Zhang XD, Chang JY*,* Wang H, Wei X, Liao Z, Komaki R, Cox JD, Balter PA, Liu H, Zhu XR, Mohan R, Dong L. 4D proton treatment planning strategy for mobile lung tumors. *International Journal of Radiation Oncology Biology Physics* 2007;67:906-914.

122. Cho KH, Shin D, Cho SJ. The Effect of the CT Number for Each CT on Photon Dose Calculation. *World Congress on Medical Physics and Biomedical Engineering 2006, Vol 14, Pts 1-6* 2007;14:1984-1986.

123. Li JS, Lin T, Chen LL,Price RA, Ma CM. Uncertainties in IMRT dosimetry. *Medical Physics* 2010;37:2491-2500.

124. Park PC, Cheung J, Zhu XR, Sahoo N, Court L, Dong L. Fast range-corrected proton dose approximation method using prior dose distribution. *Physics in Medicine and Biology* 2012;57:3555-3569.

VITA

Peter Park was born on Jan, 21, 1983 in Seoul, S. Korea, as the third child of Ki-Sun Kwon and Chong-Kyu Park. He attended 10 years of pre-college school in S. Korea until his family immigrated to the USA during the depression of S. Korea economy also known as the "IMF-crisis" in 1998. Peter attended the last two years of high school in Orlando, FL. Upon graduation, he then moved to the Bay Area to attend De Anza College to pursue his interest in studying History and Philosophy but soon after having lived with a bunch of physics geeks while attending college he fell in love with the subject of Physics. He transferred to and graduated from University of California in San Diego (UCSD) with Physics and Applied Mathematics degrees in 2008. During his last year of undergraduate study, he joined the MRI research team and worked with Dr. Jiang Du who recommended him to pursue a degree in Medical Physics. Peter started his doctoral study in Medical Physics at the University of Texas Health Science Center in Houston. Because of his interest in proton therapy, he joined a group led by Dr. Lei Dong and started his active participation in proton research at the University of Texas MD Anderson Cancer Center and Houston Proton Therapy Center. Peter completed the requirement for the Doctor of Philosophy in Nov of 2012 under the guidance of Dr. X. Ronald Zhu. Peter currently resides with his wife Patty and son Ron in Houston, Texas.

Permanent address: 2425 Holly Hall St. No.135, Houston, TX 77054